NTNU

Norwegian University of
Science and Technology

Operation Features of a Reduced Matrix Converter for Offshore Wind Power

Mari Røed Hanssen

Master of Science in Energy and Environment
Submission date: January 2011
Supervisor: Marta Molinas, ELKRAFT

Norwegian University of Science and Technology
Department of Electric Power Engineering

Problem Description

The reduced matrix converter will be the object of continued investigation and the focus will be on the losses and the sizing of a converter for a specific wind power application. The impact of modulation techniques will be first analyzed and further the influence of the frequency ratios between different carriers and phase angle relation to it will be investigated in depth to select the optimal solution. Protection of the converter under normal operating conditions will be investigated to evaluate possible impact on losses of the required solution.

Assignment given: 03. September 2010
Supervisor: Marta Molinas, ELKRAFT

Abstract

When a wind park is sited offshore, compact, lightweight and reliable components are important requirements. In this Master's thesis a wind energy conversion system has been proposed, where the objective is to meet the requirements of an offshore environment. The system consists of a permanent magnet generator, a reduced matrix converter, a high frequency transformer and a full-bridge converter. It is the reduced matrix converter which is the main focus of the thesis.

The reduced matrix converter (RMC) provides direct AC-AC conversion without the need of a bulky DC link capacitor, it is thus a compact solution. It is built with six bi-directional switches. Each switch consists of two reverse blocking IGBTs in antiparallel. The reverse blocking IGBT is different from the conventional IGBT because it blocks voltage of both polarities.

Due to the direct AC-AC conversion of the RMC it is necessary to implement a special protection scheme for the circuit. The scheme provides reliable operation of the RMC so the switches are not damaged. This is achieved by the introduction of a clamp circuit. The clamp circuit has been studied during normal operation and the operation during faults has been described.

The entire WECS has been implemented in the simulation program PSIM to simulate behavior of the clamp circuit during normal operation and to calculate switching and clamp circuit losses. Both losses are related to the RMC, and are important for the study of the overall energy efficiency of the converter. Total losses have been compared for two different modulation techniques, these are carrier based modulation and space vector modulation. The simulation results indicated that space vector modulation is the most energy efficient solution for the system.

Preface

This is my Master's thesis in Electric Power Engineering carried out at the Faculty of Information Technology, Mathematics and Electrical Engineering at the Norwegian University of Science and Technology (NTNU) in Trondheim fall 2011.

First, I would like to thank my supervisor, Marta Molinas for providing me with an interesting topic for the thesis, in addition to guidance and feedback during the semester. She encouraged me to submit a paper to a conference, and the experience I gained from the process of writing a scientific paper and presenting it orally in a conference has been very valuable for me.

I will also like to thank the PhD student Alejandro Garces, which is investigating the same topic, for providing me the model of the system in PSIM and answering all the questions I have had during the semester.

The years at NTNU have been fantastic, so many memories and knowledge achieved. It would not be the same without my friends, especially Nathalie. I am also very lucky to have Joan who has made both the good and hard days better.

Thanks to my family.

Contents

List of Figures

List of Tables

Chapter 1

Introduction

Offshore wind farms have today an installed capacity of about 1 % of the total installed wind farm capacity in the world [3]. However, as many power plants around Europe need to be replaced due to high age and the demand for electricity is expected to grow, it is reasonable to expect that the offshore capacity will increase in the following years. A wind farm sited in an offshore environment provides some benefits compared to onshore localization. First of all, there are large available areas, although obstacles such as installation in deep water and other marine activities are limiting factors. Second, when distance to the coast increases, wind conditions are improved while the visual impacts are reduced [4]. According to [5] offshore wind can reach speeds which are 30 - 40 % higher than onshore, in addition to be both less turbulent and more steady.

The main disadvantage with localizing wind farms offshore is mainly related to high costs it represents; it is still 50 % more expensive than onshore wind. Another important disadvantage is the accessibility which strongly depends on the weather conditions [3].

As the distance to shore increases, it has to be considered which of the transmission systems HVAC and HVDC result in the most optimal solution for the offshore wind farm. [6] makes a loss and cost comparison between HVAC and HVDC for different transmission distances. The conclusion is that with distances longer than 50-70 km, HVDC transmission is preferred. Bard Offshore 1 is the first example of an offshore wind farm today connected with HVDC. It is currently being installed in the North sea, 100 km outside the German coast and has a planned capacity of 400 MW [7].

The aim of this Master's thesis is to study a wind energy conversion system (WECS) which meets the demands of the offshore environment, where a compact, reliable and energy efficient solution is required. The proposed WECS consists of a permanent magnet (PM) generator, a reduced matrix converter (RMC), a high frequency transformer (HF trafo) and a full-bridge converter (F-B converter). The transmission of power to shore is performed with HVDC. It is the reduced matrix converter with its switches and protection scheme which is the point of interest for this study. The converter provide voltage and frequency control, in addition to independent control of active and reactive power. The voltage and frequency control in the generator side is especially important due to the variable speed requirements of wind turbines. The proposed WECS is depicted in figure 1.1.

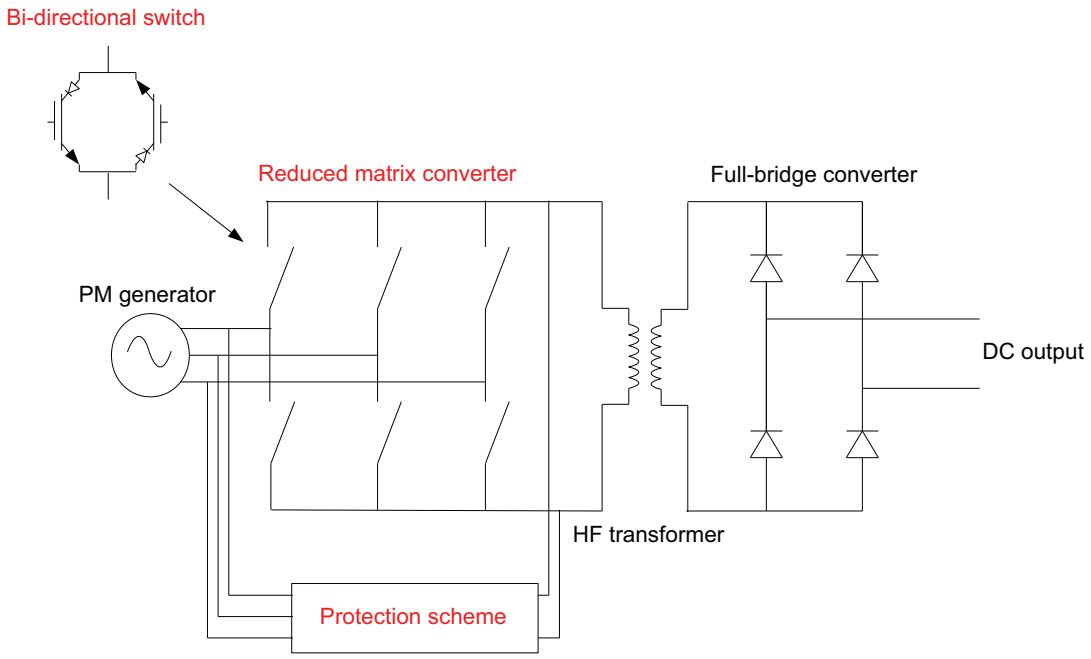

Figure 1.1: The proposed wind energy conversion system.

The study is an extension of the work presented in the specialization project [1] fall 2009. A PhD student is also investigating the same topic. Both the work of this author and the PhD-student is a continuation of the work presented in the Master's thesis with title "New switching pattern for AC/AC converters with RB-IGBTs for offshore wind parks" from [8].

1.1 The layout of the thesis

- **Chapter 1**: The introduction to the Master's thesis.
- **Chapter 2**: The chapter introduces the proposed WECS and discusses its advantages and disadvantages compared to the state of the art for research WECS.
- **Chapter 3**: The theory part which continues in chapter 4, 5 and 6, starts in this chapter. The reduced matrix converter and its operational features are introduced and will be the main topic for the remaining chapters of the thesis.
- **Chapter 4**: The bi-directional switches of the RMC are discussed. The switches consist of reverse blocking IGBTs. The structure and operation of this special semiconductor device are explained. Also the losses they generate during operation are presented.

- **Chapter 5**: In the operation of the reduced matrix converter, two pulse width modulation techniques are implemented. These are carrier based and space vector modulation. The chapter explains the methods to be utilized.
- **Chapter 6**: To provide a reliable operation of the converter, a special protection scheme has to be implemented in the system. In this chapter the schemes developed today are discussed. The one that will be used for further investigation, the clamp circuit, is explained more thoroughly.
- **Chapter 7**: This chapter presents the results which are produced during simulation of the WECS model in PSIM. The first part is dedicated to the operation of the clamp circuit. Some of the theory presented earlier in the thesis is examined through simulations. The second part investigates the losses in the reduced matrix converter. A thorough study of the switching losses will be performed, in addition to a study of the clamp losses. In the end a comparison of the losses and the operation of the reduced matrix converter modulated with CBM and SVM will be given.
- **Chapter 8**: The conclusion of the Master's thesis.

Chapter 2

Background

2.1 Important issues in an offshore environment

When a wind park is sited offshore, operation and maintenance of the wind turbines are considered to be one of the factors that contribute most to higher costs compared to an onshore wind park. The difference in the accessibility between offshore and onshore environment is one of the main reasons to that [9]. The onshore wind park is assumed to have an accessibility of 100 %. This means that each time a fault is detected in the wind turbine, the component which is not working can be repaired or replaced almost immediately, in order to avoid lost power generation. Reliability of components is thus not a crucial element for the availability of the onshore turbines, but rather the time it takes to perform the maintenance.

On the other hand, accessibility of the offshore wind park is fluctuating because it depends strongly on the weather conditions. Horns Rev in Denmark has reported an accessibility of 65 % annual when the transport of personnel is made by vessels [10]. The harsh weather during winter time is one reason to why the accessibility is reduced compared to onshore. Since the vessels are not designed for significant wave heights, the turbines can be impossible to reach from 1-2 months per year in worst case [11]. In some situations helicopters are used, but they are expensive and require turbines that are built with platform for hoisting of personnel. However, they are only restricted by the wind velocity.

The power production of the offshore wind park is dependent on the wind and the availability of each wind turbine. It is therefore most vulnerable for faults during winter time. This is the period when the wind is strongest, and the wind park can deliver the highest amount of electricity. If a turbine experiences a component fault and harsh weather conditions prevent maintenance to be performed, the production loss will cause significant lost revenue.

Due to the low accessibility of the offshore wind park, it is important that the wind turbines are designed with **reliable** components. This will reduce the need of service transport and increase the availability of the park.

Apart from the reliability and availability of the wind turbines, **compact** and **energy**

efficient wind energy conversion systems are important objectives when the wind farm is sited in an offshore environment.

2.2 Wind energy conversion systems

2.2.1 The state of the art for research

The wind energy conversion system which is the state of the art for research is the indirect-drive train where a gearbox increases the rotational speed of the shaft so that it matches the speed requirements of the induction generator (ind.gen.) [12], see figure 2.1. The generator converts mechanical energy from the shaft into electrical energy with variable frequency. In order to keep the frequency at the output of the nacelle constant, a back to back (BTB) converter is implemented. In addition to frequency control of both the generator and the grid side, the converter provides active and reactive power control. The conversion is performed in two stages, the first stage converts the variable frequency AC into DC and the second stage converts DC into constant frequency AC. Due to the ripple in the DC it is necessary to smoothen the signal, this is done by a DC-link capacitor. Due to the high currents produced in the generator a low frequency transformer is implemented as the last stage in the nacelle of this WECS. The transformer increases the voltage, so that losses in the wind park grid are minimized. The output from the wind turbine is connected in cluster formation with other turbines, where the common connection point is the offshore platform. This is where the AC interconnection grid of the wind farm is converted to HVDC, in order to provide an efficient transmission to shore. The platform consists of a low frequency transformer to step up the AC voltage and an AC-DC voltage source converter.

2.2.2 The proposed system

2.2.2.1 From indirect-drive to direct-drive concept

The largest offshore wind turbine manufacturer Siemens has recently launched a direct-drive generator with full power electronics solution for sale [4], [13]. The proposed energy conversion system in figure 2.1 (c) is a modified version of the WECS which was presented in [1] and depicted in figure 2.1 (b). However, in order to follow the tendency of the market, the indirect-drive concept implemented in (b) is replaced with the direct-drive concept. The direct-drive concept makes the gearbox which is used in (a) and (b) redundant in the system. The reason is the permanent magnet generator, which is able to produce voltage with frequency around 50 Hz, even if it is rotating with the same speed as the turbine blades.

Since the gearbox is one of the most vulnerable part of the WECS, the elimination of it is an important improvement for the reliability of the offshore turbine [14].

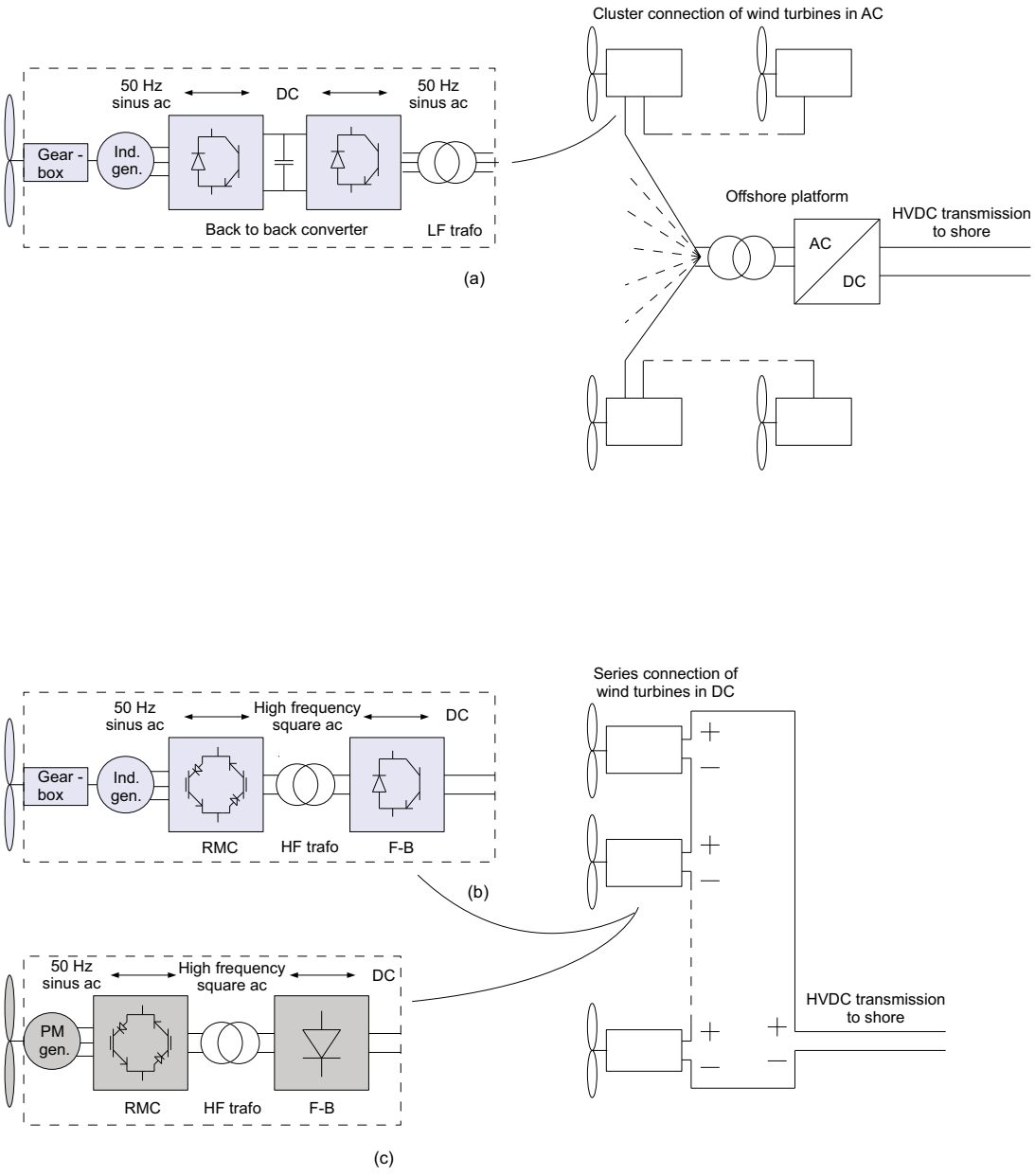

Figure 2.1: WECS: (a) The conventional system in research, (b) Proposed in [1], (c) Investigated in this report.

2.2.2.2 From AC-DC-AC converter to direct AC-AC converter

In (b) and (c) the AC-AC conversion is direct without intermediate stages as in (a). The advantage of making it direct is that the use of the DC link capacitor is avoided and the number of switches is reduced. Thus the converter is both more reliable and compact than the BTB converter. This is true because the capacitor is a large, heavy and expensive part of the power electronics equipment [15]. In addition it contributes to reduced lifetime of the converter, due to its high failure rate. In [16] it is showed that 30 % of the faults in the power electronics equipment occur due to operation of the capacitor.

Another issue of performing direct AC-AC conversion is that the switches have to be of bidirectional type instead of unidirectional type as in (a). This is required for safe operation of the switches. The bidirectional switch blocks voltage of both polarities and allows current in both directions. This is achieved by a composition of either two reverse blocking IGBTs or two diodes and two IGBTs. The RB-IGBTs are not developed for high power applications, but have a maximum capacity of 55 A and 1200 V [17]. Thus the total rating has to be increased by connecting them in series and parallel in order to fit the high power requirements of the wind turbine. However, the RB-IGBTs are still under evolvement and improvement, so it is assumed that the future brings a device with higher capacity.

Despite the fact that the proposed converter consists of less switches than the back to back converter, the total number of semiconductor devices in the two converters are the same if the conventional bidirectional switch with two IGBTS and two diodes is utilized. See table 2.1. Hence the choice of designing the proposed converter with RB-IGBTs is defended by the reduced number of devices required and the special features they represent.

	Diode	IGBT	Total semiconductors
BTB	12	12	24
RMC (RB-IGBTs)	0	12 *	12
RMC (conventional)	12	12	24

Table 2.1: Number of semiconductor devices in BTB, RMC with conventional bidirectional switch and with RB-IGBTs. *RB-IGBT

The disadvantage with direct AC-AC conversion is that the converter is vulnerable for faults because it has a limited ride through capability [18]. The consequence is that a special protection scheme has to be added to the converter in order to assure safe operation of the semiconductor devices. This is not required in the back to back converter since it provides both a natural freewheeling path and energy storage in the DC-link. The protection scheme will contribute to a slight increase in the size of the converter and the losses.

2.2.2.3 From AC to DC interconnection grid of wind turbines

Today wind farms sited far from shore consist of one grid which interconnects the wind turbines by means of cluster connection, and another grid which provides the HVDC

distribution to shore. In order to connect the two grids, an offshore platform is needed. This is an expensive element of the wind farm which can be avoided [19]. The WECS proposed in (b) and (c) represent an alternative solution to the offshore platform. The DC output from the nacelle is connected in series with the other wind turbines so that the voltage increases and reaches the level which is required for direct HVDC transmission to shore, without any transformation stage. The transformer in the nacelle provides the galvanic isolation between the DC grid and the converter and generator. Due to the high frequency in the output of the reduced matrix converter, the transformer has a much more compact design than the low frequency transformer in the BTB solution [20]. Since the output of the RMC is a square wave, the full-bridge converter is implemented to obtain DC in the output of the turbine.

Due to the decision of changing from geared-drive in (b) to direct-drive concept in (c), the topology of the full-bridge converter is changed. The induction generator in (b) requires a bi-directional current flow through the full-bridge. The reason is that the power flow in the startup of the generator is in the opposite direction to when it delivers power because it has to magnetize its windings. The PM generator is designed without this need, thus the IGBTs in the full-bridge are redundant for the operation and can be removed. Although the power flow in system (c) is only in one direction, the bi-directional switches in the RMC are still necessary, since both sides of the converter are AC.

Even if the elimination of the offshore platform results in lower investment cost and a compact solution, it has to be considered that series connection of wind turbines with direct HVDC transmission to shore presents some big challenges. If there is no redundancy of the cables that interconnect the turbines, the entire wind farm will be affected in case of a fault. However, although there was redundancy, it would be a problem if one of the turbines was out of operation since the total voltage for HVDC transmission would decrease. In [21] it is also mentioned the problem that the last wind turbine of the series coupling experiences a much higher voltage than it develops itself.

Since the future brings larger wind farms which are sited farther from shore, it is probable that more and more farms are equipped with a constant service team during the year. The offshore wind farms Bard Offshore 1 and Horns Rev 2 are two examples of the starting trend [22], [23]; in order to reduce the transport to and from the farm, the offshore platform is used as accommodation for the personnel in addition to house the electric equipment, such as transformer and converter. Thus, if the wind farm is built with platform irrespective of the transmission solution, the series connection with direct HVDC transmission to shore should be reconsidered among other more reliable solutions, such as cluster and parallel connection.

Chapter 3

Reduced matrix converter

The reduced matrix converter will be the topic of the further study. The RMC converts a 3-phase AC low frequency (around 50 Hz) sinusoidal signal in the generator side, later mentioned as input, into a 1-phase AC high frequency (kHz) square wave signal in the transformer side, later mentioned as output. This is performed by 6 bi-directional switches which consist of two RB-IGBTs in antiparellel. The switches make up three switch couples, where phase a, b and c in the 3-phase input is flowing through switch couple A, B and C respectively. The phase current flows at any time through only one switch of the switch couple, where the couple consists of what is mentioned later as the positive (P) and the negative (N) switch, see figure 3.1 (a).

As the name of the reduced matrix converter implies, it is a modified version of the conventional matrix converter (MC). However it has also features which is similar to what characterizes the conventional AC-DC three-phase converter of the back to back converter. The link to both the 3-phase converter and the MC brings both advantages and disadvantages to the operation of the RMC.

From the MC it inherits the feature of being a direct AC-AC converter [24]. On the one hand this is an advantage since the direct conversion stage makes the bulky DC-link capacitor redundant. On the other hand this is a disadvantage since the topology of the switches designed for direct AC-AC conversion result in the need of an additional protection scheme. This is further explained in chapter 6.

Due to the similarity between the AC-DC three-phase converter and the reduced matrix converter, other literature has referred to the RMC as a "bi-directional power-flow three-phase rectifier" [25]. This is because the output can be looked at as a DC. However, since the RMC in this study is operated as a voltage source converter and not as a current source converter like in [25], it is more convenient to compare it with the inverter. While the inverter has a constant DC output, the DC output of the RMC is changing between positive and negative polarity, thus forming a high frequency square wave. The result is that the voltage utilization in the RMC is the same as for the AC-DC inverter, i.e. 100 %. This is an advantage compared to the MC where the sinusoidal waveform in both converter sides cause the voltage utilization to be maximum 87 %, and with carrier based modulation it can be as low as 50 % [24]. As will be explained in chapter 5 the modulation technique

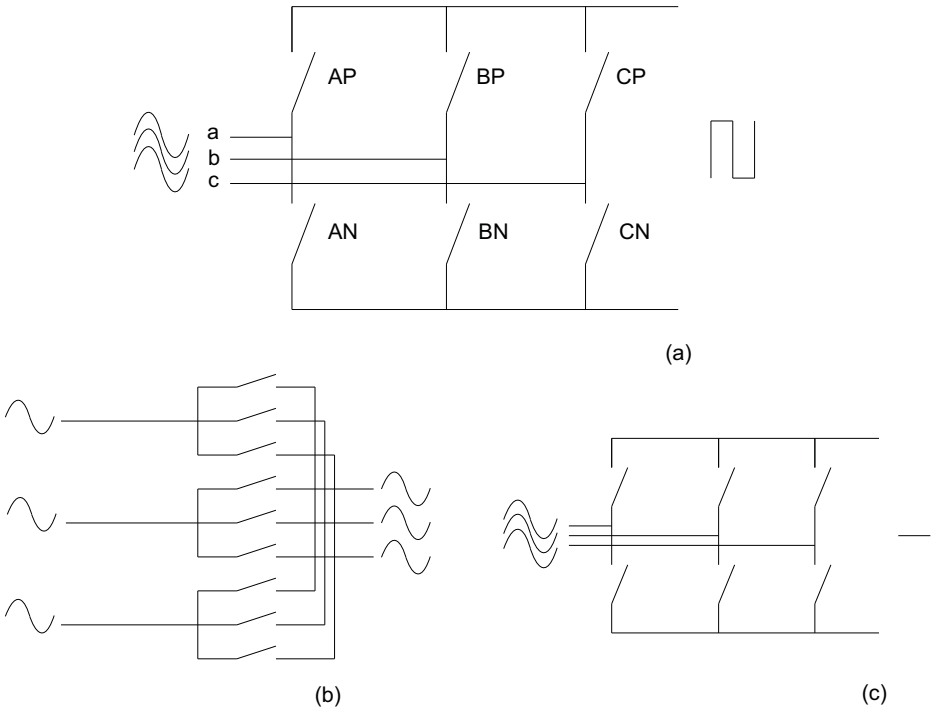

Figure 3.1: (a) Reduced matrix converter with bi-directional switches, (b) Matrix converter with bi-directional switches, (c) AC-DC 3-phase converter with unidirectional switches.

is similar to that of the inverter, but the changing polarity of the DC has to be considered.

Chapter 4

Bi-directional switches

Both the bi-directional and the uni-directional switch can assist power flow in both directions. This is required for operation where the current changes direction. In figure 4.1(a) one leg of the AC-DC voltage source converter (VSC) is depicted, implemented with uni-directional switches made of standard IGBT with freewheeling diode in antiparallel [26]. Only one of the three phase currents will flow through the leg, and dependent on the direction of this current either the diode will conduct, i.e. the current direction is positive, or the IGBT will conduct, i.e. the current direction is negative.

The need for an improved switch topology appears when the DC side of the voltage source converter is changed with AC square wave voltage, which is the case for the reduced matrix converter. The voltage of both sides of the converter will now be of alternating polarity and it is required a device which can withstand voltage of both polarities and allow current in both directions. The uni-directional switch cannot meet this demand. The reason is that if the IGBT is in off-state and the square wave voltage changes to the opposite polarity of what figure 4.1(a) shows, the diode in antiparallel will be forward biased and thus in on-state, while the IGBT will be reverse biased. As explained in Chapter

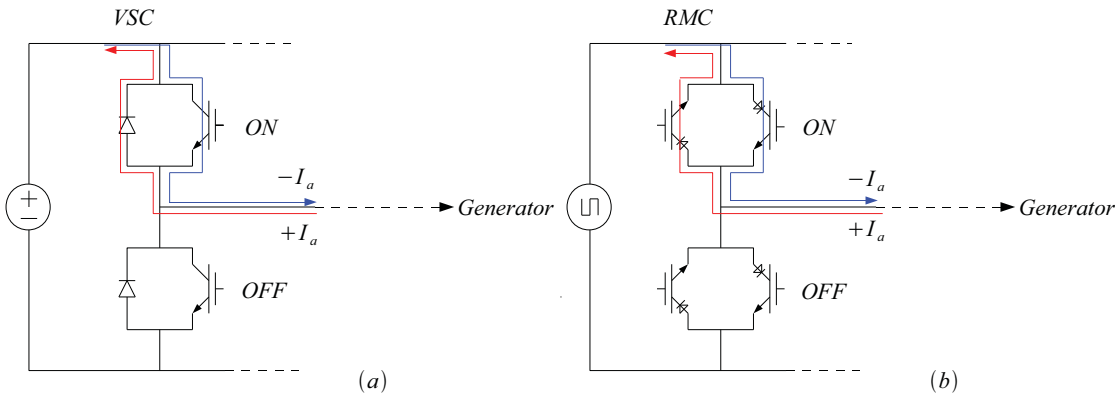

Figure 4.1: (a) One leg of AC-DC VSC with uni-directional switches, (b) one leg of AC-AC RMC with bi-directional switches.

4.1 the IGBT is not convenient built to withstand reverse voltages and will go in breakdown mode. However, if the diode was connected to the IGBT in such a way that both of the devices were reverse biased simultaneously, the diode could assist the IGBT in blocking the voltage since it has much better blocking capability in reverse bias, but then it could not provide bi-directional current flow.

On the other hand the bi-directional switch fulfills the characteristics needed, which is the reason to why the reduced matrix converter has bi-directional switches. The leg with bi-directional switches of the reduced matrix converter where phase current a flows is depicted in figure 4.1(b).

There are various topologies of the bi-directional switches available at the market. The most common is made of two uni-directional switches in series, consisting of two diodes in antiparallel with two IGBTs, see figure 4.2(a). The red and blue lines demonstrate the current path in conduction mode (on-state) for the two possible directions. Due to the diodes in series, either coupled anode to anode or cathode to cathode, it is possible to achieve the required blocking capability for both polarities of the voltage, but additionally the diodes increase the on-state losses. However, recently it is developed a more compact bi-directional switch with less components, see figure 4.2(b). This is made up of two reverse blocking IGBTs in antiparallel, and the result is a decreased number of semiconductor devices in the RMC, from 24 with the old version of bi-directional switch, to 12 with the new version where both the cost and the size is reduced [27]. In [2] it is shown how changing the design of the bi-directional switch from the conventional with two IGBTs with antiparalleled diodes to the one with two RB-IGBTs in antiparallel, can reduce the total losses.

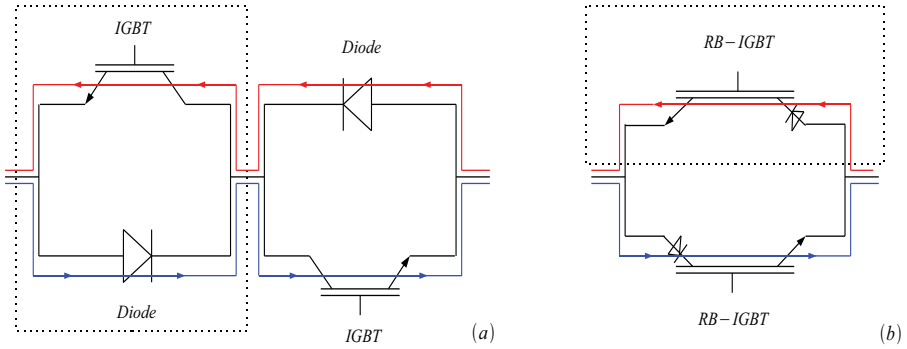

Figure 4.2: Bi-directional switch topology as (a) the conventional, or (b) the newly developed, where the current path is drawn for the two possible directions.

In figure 4.3 the behavior of the two different switch topologies in off-state is shown. When a voltage V_s is applied to the switch in (a) the collector-emitter terminals of the IGBT in the upper series connection is reverse biased, and will not be able to block the voltage. However, the diode in series connection with the IGBT is also reverse biased, and the diode characteristics makes it able to block high reverse voltages therefore the current

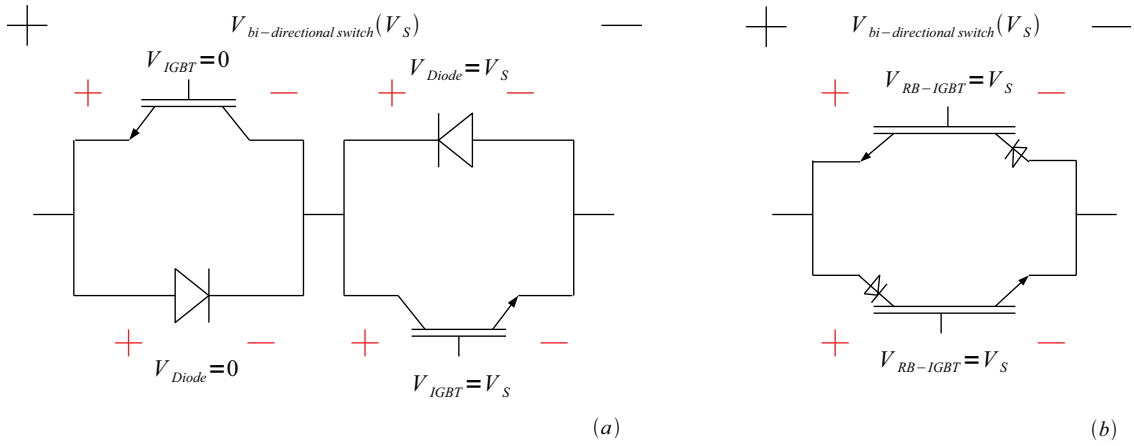

Figure 4.3: The two bi-directional switch topologies behavior in off-state.

cannot flow through the devices. In the lower series connection the diode is forward biased and would allow the current to flow if the IGBT was not coupled in series with it. The collector-emitter terminals of the IGBT in the series connection is forward biased and the IGBT is in off-state, its characteristics make it then able to withstand the forward voltage. In (b) the special bi-directional switch made of only two devices is depicted. Due to its special characteristics the upper RB-IGBT can block the reverse bias applied to it and the lower RB-IGBT can block the forward bias applied to it without the need of antiparallel diodes.

4.1 Reverse blocking IGBT (RB-IGBT)

The reverse blocking IGBT is a transistor similar to IGBT, and has therefore adapted most of its characteristics. However, where the IGBT is not convenient constructed to block reverse voltages in off-state, the RB-IGBT has a symmetrical behavior which means that it has equal forward and reverse breakdown voltage.

4.1.1 Device structure

Three different designs of the RB-IGBT are well known; Mesa type, double-sided type and diffusion isolation type [27]. In this study the isolation type is used, which is the only version open for commercial use [28].

The structure of the isolation type RB-IGBT is very similar to that of the conventional IGBT. It has three terminals, respectively gate, collector and emitter, and a $n^+pn^-p^+$ structure. The exception from the IGBT is the isolation region of the RB-IGBT which is made by extending the bottom p^+ region to include the vertical, dicing surface of the chip side. The p^+-isolation region together with the n^--drift region constitute what can best be characterized as an intrinsic diode of the device. In reverse bias this region is preventing

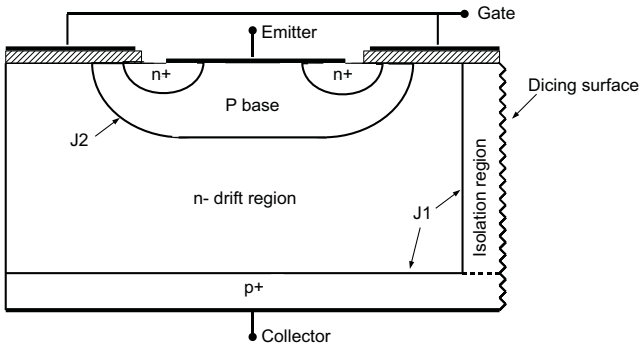

Figure 4.4: Vertical cross section of the structure of the RB-IGBT with isolation region.

the depletion region to reach the dicing surface where severe roughness remains after the mechanical dicing process [29]. The presence of the isolation region is the difference between the RB-IGBT and another version of the IGBT, the non-punch-through IGBT (NPT-IGBT). The NPT-IGBT is also capable of blocking reverse voltage, but in the reverse bias condition the depletion region extends to the dicing surface of the chip side and a high leakage current is generated [30].

4.1.2 Operation of the RB-IGBT

In an equivalent circuit of the RB-IGBT, the intrinsic diode can be extracted from the model. It will then appear in series connection with the IGBT portion of the transistor, and together with the diode drawn with a dashed line the intrinsic diode also constitutes the bipolar junction transistor (PNP BJT) portion of the device, see figure 4.5. Even if the intrinsic diode appears as an external part to the rest of the model, it is important to remember that it "does not exist physically in the switch module" [30].

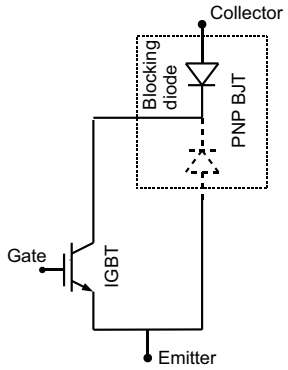

Figure 4.5: Circuit model of RB-IGBT with the intrinsic diode extracted.

The operation of the intrinsic diode of the RB-IGBT demonstrates that the diode does not operate as a conventional, external diode. When the conventional diode is reverse biased, it prevents the current to flow through it, and the diode is forced to be in off-state until the voltage change to positive polarity. In forward bias the diode can conduct, and pursuant to its characteristics, the voltage across it is zero [31]. On the other hand, the intrinsic diode in the RB-IGBT is not controlled by the polarity of the varying voltage applied to it, but rather by the on and off-state of the RB-IGBT. The RB-IGBT has zero voltage applied when it is in on-state and blocks a finite voltage when it is in off-state. In this case the finite voltage is constant with varying polarity following the square wave voltage output of the RMC. The result is that even if the intrinsic diode is forward biased it cannot conduct if the RB-IGBT is turned off, and when the intrinsic diode is reverse biased it does not have to be forward biased to start to conduct; it is enough that the RB-IGBT is switched on, so that the voltage across the element goes to zero. Thus, the intrinsic diode is indirectly controlled by the gate emitter voltage signal applied to turn on or off the RB-IGBT.

Two cases will be explained further and is depicted in figure 4.6. In the first case the RB-IGBT is forward biased, and in the second case the RB-IGBT is reverse biased. The device is in off-state in both cases.

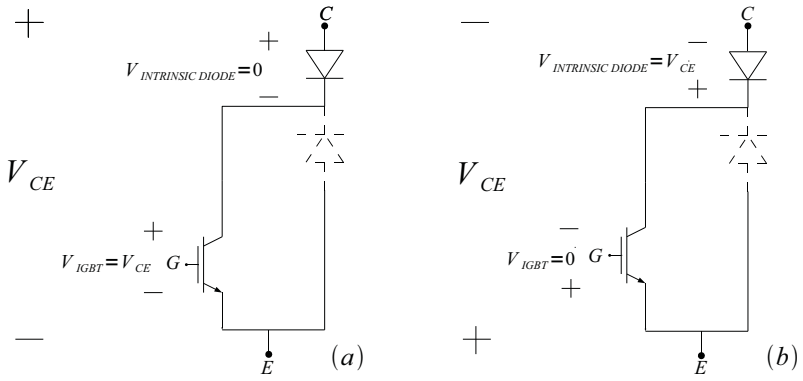

Figure 4.6: In (a) the RB-IGBT is forward biased, and in (b) it is reverse biased.

4.1.2.1 Forward bias of the RB-IGBT

When the RB-IGBT with the intrinsic diode is forward biased, the voltage is blocked by junction 2 (J2) consisting of p-base and n^--drift region, see figure 4.4. The device operates like a conventional IGBT, and all the collector emitter voltage, will be across the IGBT portion of the RB-IGBT, $V_{IGBT} = V_{ce}$. The intrinsic diode has no special function in this case, since a conventional IGBT can withstand high positive voltages, and the voltage across it is zero, $V_{Intrinsic\ diode} = 0$.

4.1.2.2 Reverse bias of the RB-IGBT

When the RB-IGBT is in reverse bias the intrinsic diode plays an important role of the operation. Since the conventional IGBT does not have a convenient structure to withstand high reverse voltage, and either goes in breakdown mode (Punch-through IGBT) or have high leakage current (NPT-IGBT), the intrinsic diode is implemented in the device to increase the reverse voltage level. Therefore, when a reverse voltage is applied to the transistor, the voltage is blocked by the collector-isolation p^+-region and the drift n^--region, constituting junction 1 (J1) in figure 4.4. These are also the regions constituting the intrinsic diode [32]. The result is zero voltage across the IGBT portion of the RB-IGBT, $V_{IGBT} = 0$ because the intrinsic diode withstands all the negative collector emitter voltage alone, $V_{Intrinsic\ diode} = V_{ce}$.

4.2 Losses in the bi-directional switches

The losses in the bi-directional switches are generated due to the operation of the RB-IGBTs, and can be divided into two categories: losses generated in conduction mode and losses generated by the switching action of the RB-IGBTs. There are two different types of switching losses: the losses concerning the IGBT part of the device; turn on and turn off losses, and the losses concerning the intrinsic diode portion of the device; reverse recovery losses. A simplified version of the current and voltage waveforms by turn off, turn on and in conduction mode is depicted in figure 4.7 and 4.8. In the figure E_{on} is the turn on losses and E_{off} the turn off losses generated in the IGBT portion when a hard switching occurs, E_{rr} is the losses generated in the intrinsic diode portion by turn on or turn off when a soft switching occurs and E_{cond} is the conduction losses.

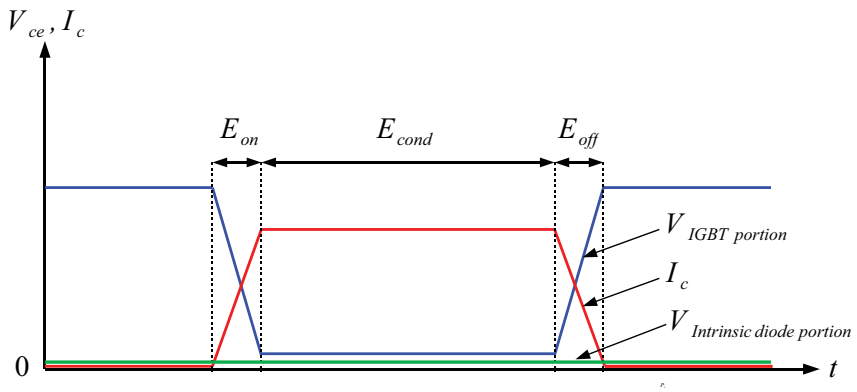

Figure 4.7: Current and voltage waveforms in forward bias.

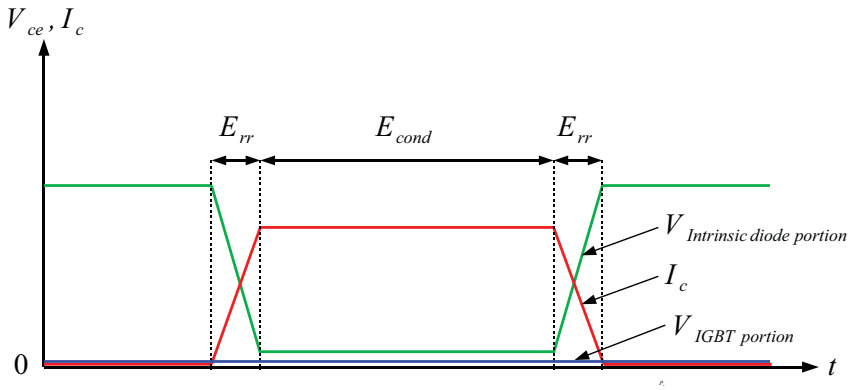

Figure 4.8: Current and voltage waveforms in reverse bias.

4.2.1 Conduction losses

An ideal semiconductor device would have zero voltage applied when it is in on-state, however, this is impossible. In the RB-IGBT it is mainly because of the voltage drop over the drift region of the device [31]. Thus, the power dissipation in conduction mode will be a function of the voltage between the terminals of emitter and collector in on state, and the current flowing through the device. The I-V characteristics of a RB-IGBT (600V/200A) can be seen in figure 4.9

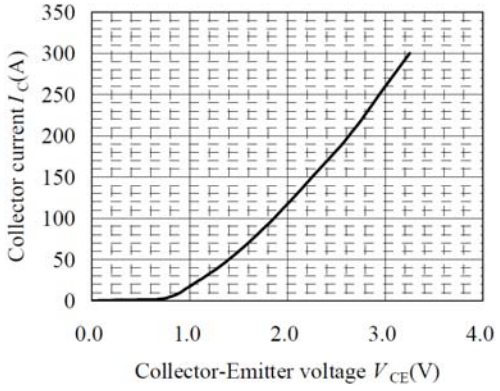

Figure 4.9: I-V characteristic in conduction mode [2].

4.2.2 Switching losses

While the switching losses in a conventional IGBT are generated due to the hard switching of the device, the RB-IGBT can either have a hard or soft switching transient of the voltage when turning it on or off. The hard switching of the device is associated with the case when the power dissipation is in the IGBT portion of the RB-GBT, respectively turn on

and turn off losses, and the soft switching is associated with the case when the energy dissipation is in the intrinsic diode portion of the RB-IGBT; the reverse recovery losses.

4.2.2.1 Losses generated in the IGBT portion of the RB-IGBT; turn on and turn off losses

The losses in the IGBT portion of the RB-IGBT are generated due to the hard switching of the device. The hard switching occurs when the RB-IGBT operates like a conventional IGBT, as explained in 4.1.2.1 with figure 4.6(a), i.e. when the device is forward biased either before turning it on, or after turning it off. In the situation where the device is turned on by applying a gate signal to the RB-IGBT, the emitter collector voltage across the IGBT portion will use some time to decrease and the collector current will use some time to increase, before approaching steady state. The dissipation of power will be in the IGBT portion of the RB-IGBT. The same principle is valid for turning off the RB-IGBT; power will be dissipated in the IGBT portion due to the time it takes for the forward voltage and current to stabilize at their respectively off state values.

4.2.2.2 Losses generated in the intrinsic diode portion of the RB-IGBT; reverse recovery losses

Energy is dissipated in the intrinsic diode portion of the RB-IGBT when all the collector emitter voltage is across this part either before turn on or after turn off of the device, the case is depicted in figure 4.6(b). When the RB-IGBT is turned on, the voltage across the intrinsic diode portion changes to zero in a finite time, and the current through the device increases to a fixed value. In the time period it takes to reach steady state, energy will be dissipated only in the intrinsic diode portion of the RB-IGBT; there will be generated reverse recovery losses. The same principle is valid for turn off of the RB-IGBT when the intrinsic diode portion is under the same conditions, but in this case the voltage is increasing to a finite negative value and the current is decreasing to zero.

The definition of reverse recovery losses for a conventional diode is associated to the turn off transient of the element. However, for the intrinsic diode reverse recovery losses are generated both by turn on and turn off. In [2] simulation methods to calculate losses for a RB-IGBT (600V/200A) have been suggested. In the loss characteristics reported, it has been measured that reverse recovery losses of the intrinsic diode are lower than turn on and turn off losses of the IGBT portion of the device, this will reduce the total energy dissipation in the RB-IGBT compared to a conventional IGBT.

When the switching of the RB-IGBT occurs and the losses are reverse recovery losses of the intrinsic diode, the loss generation in the IGBT portion will be zero since the voltage across this element is constant zero during the switching action. Then there will be a soft switching of the IGBT portion of the RB-IGBT which is a natural feature of the device.

Chapter 5

Modulation techniques

The modulation of the reduced matrix converter is performed with a modified version of the pulse width modulation (PWM) used for the three phase converter. There are two well-known techniques which have been investigated for this study; these are the carrier based modulation (CBM) and the space vector modulation (SVM). The carrier based modulation has already been presented in previous work from this author [1]. However it was first presented in [8]. Later there have been published papers were both CBM and SVM has been investigated more thoroughly, this work can be found in [33].

5.1 Special considerations

Due to two changes in the system, there are some special considerations that have to be taken into account when implementing the modulation. Thus the modulation techniques in the literature previously referred to have to be modified. The two changes are listed below.

- The full-bridge converter consists only of diodes.
- The reduced matrix converter semiconductors are not assumed to be ideal devices.

5.1.1 Full-bridge converter based on diodes

In [1] the full-bridge converter was designed with unidirectional switches; one diode in antiparallel with one IGBT. The IGBTs allowed for controllable operation of the F-B converter, where the frequency of the square wave was modulated through this. As it is written in section 2.2.2 the IGBTs are redundant in the proposed wind energy conversion system investigated in this thesis. The F-B converter consists thus only of diodes. As known diodes are non-controllable semiconductor devices. The consequence of this change will be that it is not longer possible to modulate the square wave frequency through the F-B converter. This is solved by letting the reduced matrix converter modulate not only the sinusoidal input signal, as before, but also the square wave output signal. How this is implemented is explained further in the section 5.2 and 5.3.

5.1.2 RB-IGBTs assumed as non-ideal semiconductor devices

The second change is regarding the reduced matrix converter semiconductor devices, which are no longer assumed to be ideal devices. This gives consequences for the switching characteristic of the RB-IGBTs; while an ideal semiconductor turns on and off instantaneously when triggered, the non-ideal semiconductor turns on and off during a finite time. The result is that the positive and the negative switch of one leg will not turn on and off perfectly synchronous. This means that during a short time period it is possible that both switches are either open or closed simultaneously. There are several methods to avoid the problems this could cause, and the solution depends on whether the output side is mainly inductive or capacitive. In the back to back converter, the output to the inverter is mainly capacitive due to the DC-link capacitor. Given below is the equation of the current through the capacitor.

$$i = C \cdot \frac{dv}{dt} \tag{5.1}$$

Where C is the capacitance and dv/dt is the rate of change of the voltage across the capacitor. It is apparent that a fast change in the voltage will cause a large spike in the current. A fast change in the voltage occurs when there is a short circuit of the capacitor, i.e. when both switches of one leg are in on-state simultaneously. This is an unwanted action which will most probably damage the capacitor. In order to avoid an accident, it is necessary with a controlled commutation process. In [31] deadtime of the switches is introduced as a solution. When the phase current flowing through the switch of one leg is commutating to the opposite switch, there is an instant between when both switches are turned off, i.e. they are both open.

In the proposed system the DC-link capacitor is replaced with a transformer, thus the output of the RMC is mainly inductive. The above solution is therefore not valid in this case. The equation (5.2) for the voltage across the transformer demonstrates why.

$$v = L \cdot \frac{di}{dt} \tag{5.2}$$

Where L is the inductance and di/dt is the rate of change of the current through the transformer. The equation shows that a fast change in the voltage is a safe operation when the output of the converter is mainly inductive. On the other hand, a fast change in the current causes high voltage. Therefore it should not be an interruption of the current through the transformer, since it could be dangerous for the operation. An interruption of the current in the transformer occurs when both switches are in off-state simultaneously, i.e. there is an open circuit of the transformer. Deadtime is therefore not a solution to this case. Instead it is decided to implement an overlapping in the modulation; for every time the phase current changes between the positive and the negative switch, the gate signal which turns off the outgoing switch is delayed some microseconds compared with the gate signal which turns on the incoming switch, so that both switches are closed and lead a current in a short time period. This will lead to a short circuit of the transformer, which is a harmless operation mode and the current will always have a path to flow.

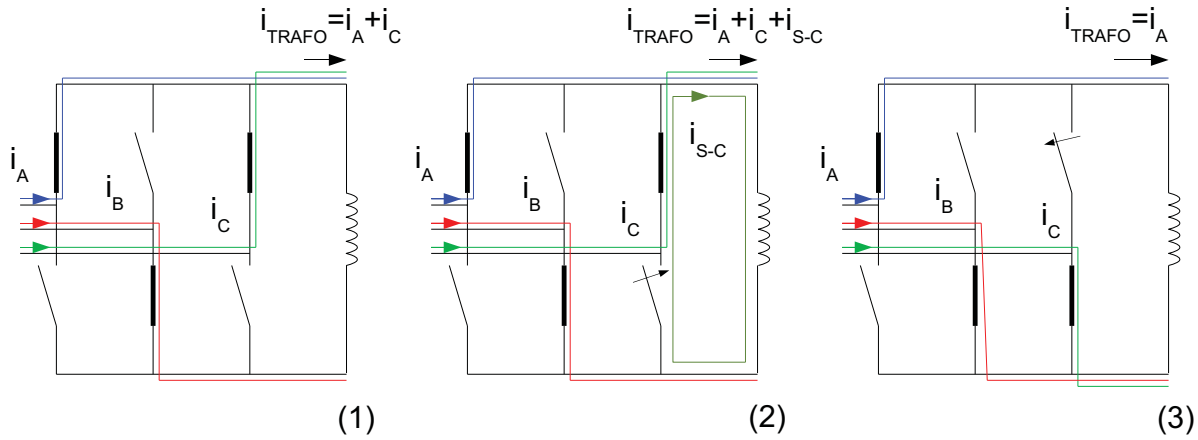

Figure 5.1: The overlapping process, inductor represents the primary winding of the transformer.

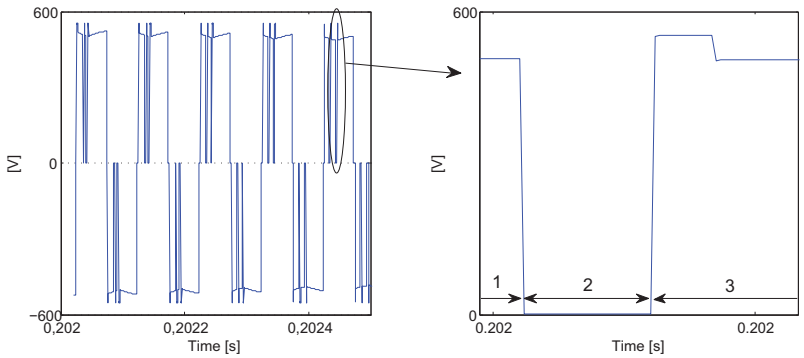

Figure 5.2: v_{trafo} during overlapping process.

Figure 5.1 shows how the commutation process is performed. The period phase current i_C is commutating from the positive to the negative switch, phase current i_A is flowing through switch AP, and phase current i_B is flowing through switch BN. Time 1 shows the initial positions of the switches before the commutation takes place. The current through the primary winding of the transformer i_{trafo} at that time is the sum of the phase currents i_A and i_C flowing through the positive (upper) leg. Since the phase currents are assumed to be balanced $i_A + i_B + i_C = 0$, i_{trafo} is also equal to $-i_B$. During time 2 the negative switch of leg C is turned on, this means that both switches of leg C are in on-state simultaneously. In addition to i_C which still flows through switch CP, a short circuit current i_{s-c} appears through leg C. This is added to the phase currents through the transformer. Due to the short circuit made by the two switches closed, the voltage across the transformer v_{trafo} is zero during the overlapping period. At time 3 the outgoing switch CP is turned off. Since switch CN already is closed there is no chance of making an open circuit of the transformer.

The period when switch CP is turned off, i_{trafo} changes fast and this provokes a spike in the voltage with a short duration as depicted in figure 5.2.

5.2 Carrier based modulation

The carrier based modulation for the reduced matrix converter is performed in a similar way as for the voltage source converter (VSC). As in [1] a sinusoidal voltage reference signal for each phase a, b and c is compared with a triangular carrier signal of the sinusoidal input voltage. This is performed in order to generate a sinusoidal wave with the desired amplitude and frequency.

The change in the polarity of the square wave is considered in the modulation of the RMC by multiplying each reference signal with a negative or positive unit value, depending on whether the square wave is of positive or negative polarity respectively. The frequency of the square wave output voltage is therefore determined by the frequency the unity signal is alternating. The unity signals can thus be looked at as a carrier for the square wave output; when a positive unit is multiplied with the reference signals, the carrier of the square wave is above the x-axis and when a negative unit is multiplied with the reference signals, the carrier of the square wave is below the x-axis.

Equation (5.3) gives the formula for the carrier $V_{carrier(input)}$ and the reference $V_{ref(input)}$

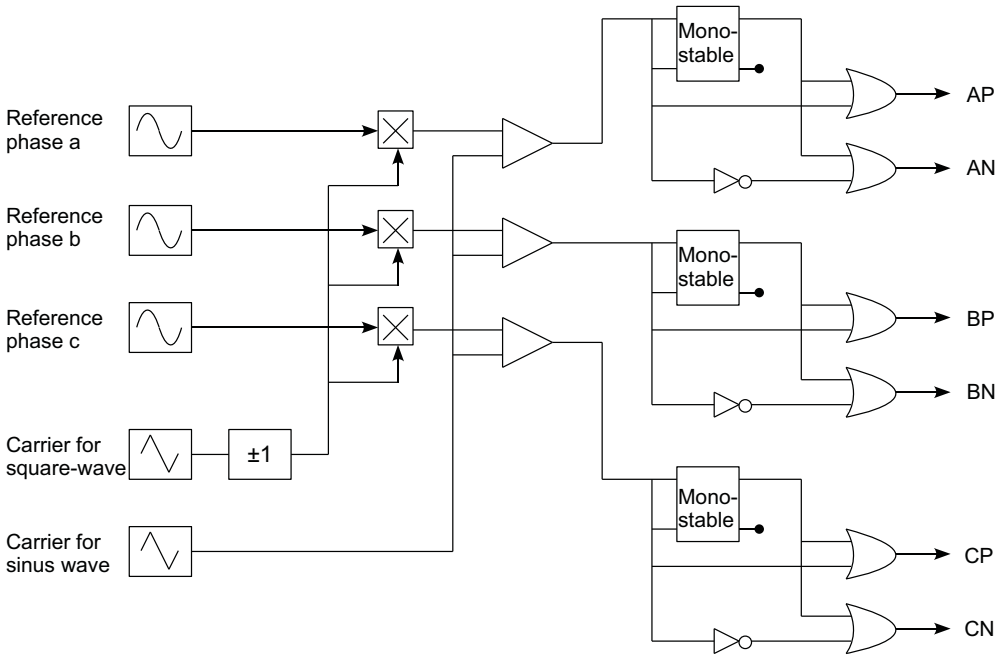

Figure 5.3: Carrier based modulation

of the sinusoidal input.

$$\begin{aligned} V_{carrier(input)}(t) &= 1 - \tfrac{2}{\pi} \cdot arccos\left(sin\left(\omega t\right)\right) \\ V_{ref(input)}(t) &= m_a \cdot cos\left(\omega t - \varphi\right) \end{aligned} \tag{5.3}$$

Where φ is 0 ° for phase a, 120 ° for phase b and -120 ° for phase c, m_a is the modulation amplitude.

Equation (5.4) gives the formula for the carrier $V_{carrier(output)}$ and the reference $V_{ref(output)}$ of the square wave output.

$$\begin{aligned} V_{carrier(output)}(t) &= 1 - \tfrac{2}{\pi} \cdot arccos\left(sin\left(\omega t - \theta\right)\right) \\ V_{ref(output)}(t) &= 0 \end{aligned} \tag{5.4}$$

Where θ is the phase displacement of the carrier of the square wave output with respect to the carrier of the sinusoidal input.

The reference signal of the sinusoidal input is modified in the following manner in order to obtain a square wave in the output of the converter.

$$\begin{aligned} V_{carrier(output)} > 0 \Rightarrow s = 1 \\ V_{carrier(output)} < 0 \Rightarrow s = -1 \\ V^*_{ref(input)} = V_{ref(input)} \cdot s \end{aligned} \tag{5.5}$$

Where $V^*_{ref(input)}$ is the modified reference signal.

Figure 5.3 shows how the process is working. The comparator generates a signal with value either 1 or 0, depending on whether the modified reference signal is above or below the carrier signal. Every instant the value out of the comparator is changing between 0 and 1, the monostable multivibrator generates a signal with value 1 which lasts some microseconds, and else it is 0. These microseconds lead to a short delay in the turn off signal sent to the outgoing switch, and provide the overlapping of the two switches of one leg. The turn on signal is the same as what is sent from the comparator. However it is inverted for the negative switches. Figure 5.4 demonstrates how the switching pattern of leg A is modulated when the carrier frequencies of the sinusoidal input and the square wave output is the same and the frequency of the reference signal of the sinusoidal input is much lower than the carrier frequencies. The carrier signal of the square wave output is displaced 90 degrees with respect to the carrier signal of the sinusoidal input.

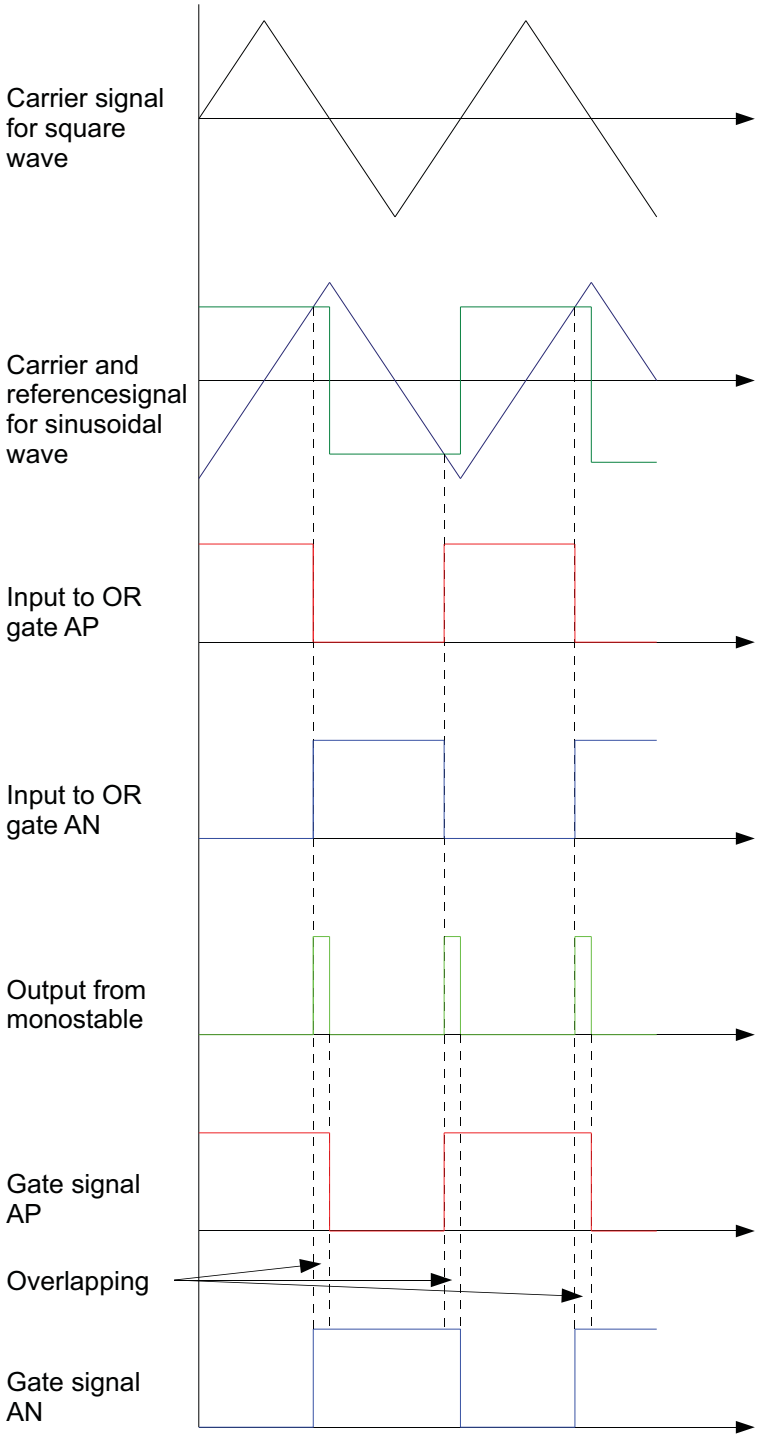

Figure 5.4: Carrier based modulation switching pattern leg A

5.3 Space vector modulation

The space vector modulation of the reduced matrix converter is built on the same principle as that of the voltage source converter. The three-phase voltages a, b and c, $v_a(t)$, $v_b(t)$, $v_c(t)$ respectively, compose an equivalent two-dimensional space vector V_s as in equation (5.6).

$$\vec{V_s} = v_a(t) + v_b(t) \cdot e^{j2\pi/3} + v_c(t) \cdot e^{-j2\pi/3} \tag{5.6}$$

The space vector V_s is rotating with constant speed in the counter clock wise direction forming a circle as the stippled one in figure 5.5, with radius equal to its amplitude. The space vector moves stepwise around the circle, where the total number of steps during one revolution is set by the switching frequency f_s. During one revolution it passes through 6 different sectors divided by 6 vectors that represent the active states of the converter. The tips of these vectors form a hexagon. The active states modulate a non-zero voltage in the input, and can be found in figure 5.6 as the six states from (a) to (f). The figure depicts in total 14 switching states, where the 8 remaining states are zero states and modulate a zero voltage input, (g)-(h), or zero input and output, (i)-(n). They are positioned in the centre of the hexagon. Only two of the zero vectors can be found in the SVM of the VSC, those are (g) and (h). The reason to why the RMC has 6 extra zero states, depicted from (i) to (n), is because the transformer in the output side allows both sides of the RMC to be the short-circuited. On the other hand the VSC only allows for short-circuiting of the

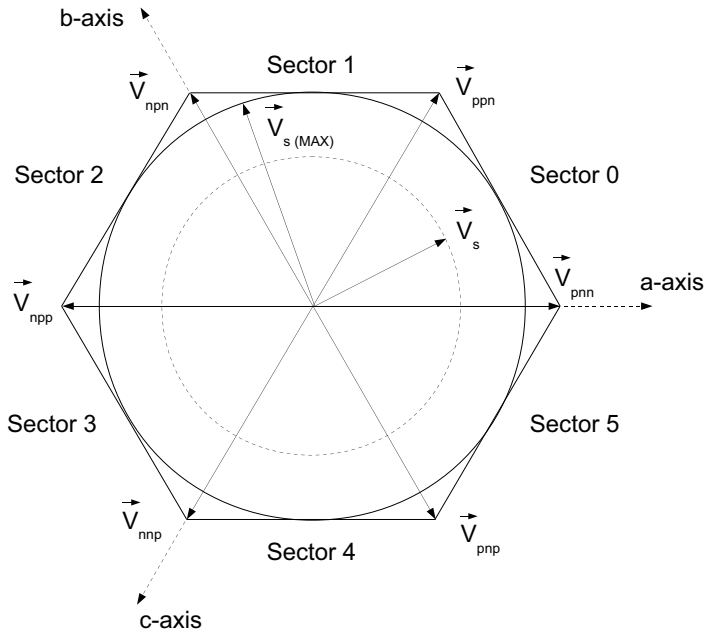

Figure 5.5: Space vector modulation.

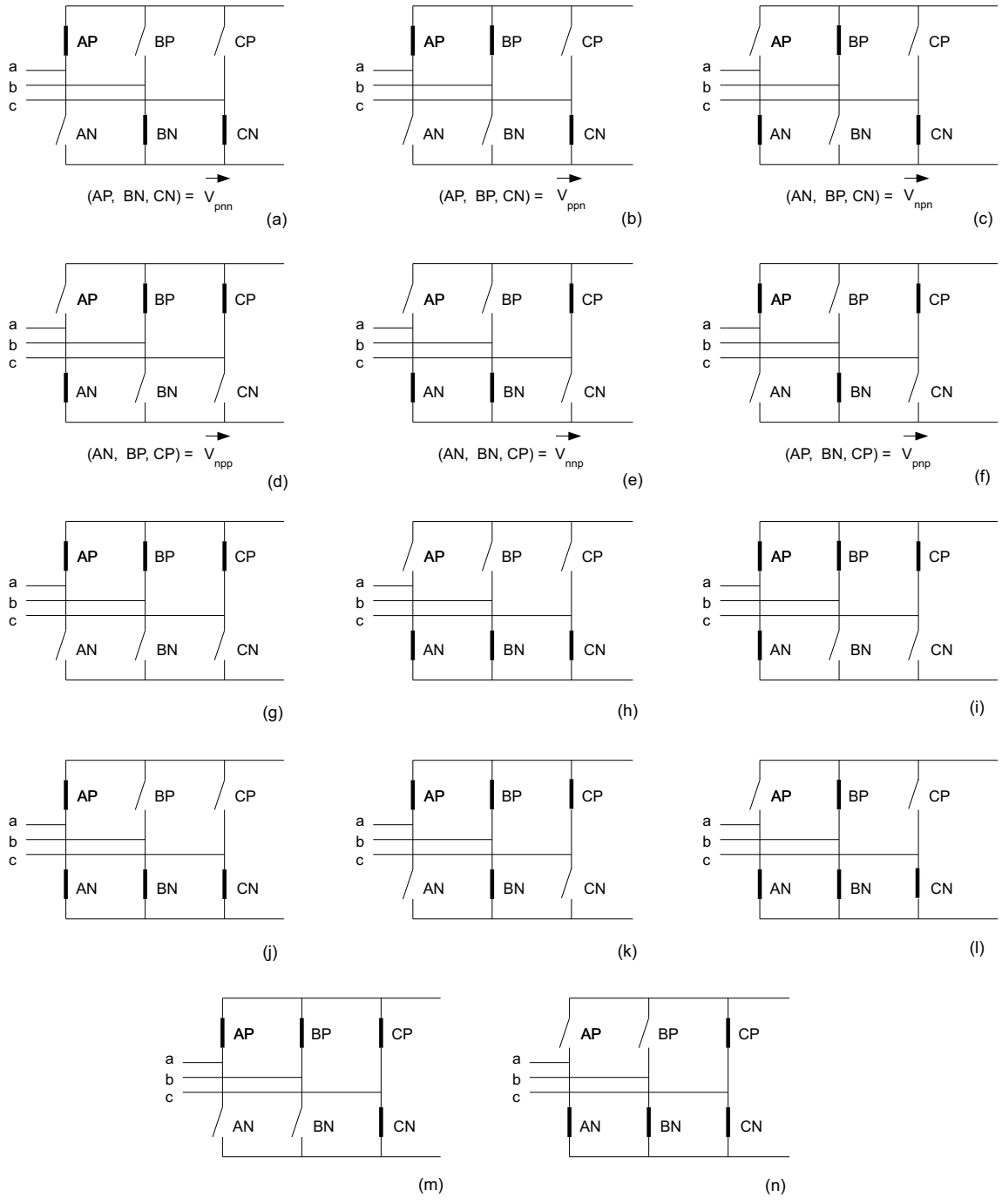

Figure 5.6: Switching states in SVM.

generator side due to the DC-link capacitor in the DC side.

Since the three-phase voltages are assumed have constant amplitudes, the circle the space vector makes during one revolution has to be with constant radius in a balanced sinusoidal steady state. This means that the space vector with maximum length cannot follow the sides of the hexagon, but is restricted to follow the largest circle possible within the sides of the hexagon. This circle is depicted in figure 5.5 with a continuous line. If the length of the space vector exceeds the radius of the circle, the RMC will operate in overmodulation and the harmonic content of the currents will increase [34].

5.3.1 Consideration of the square wave output

In the RMC it has to be taken into account the changing polarity of the square wave side, and that the modulation of this output signal has to be implemented in the converter in addition to the modulation of the sinusoidal voltage input. Figure 5.7 shows how this is working. When the positive part of the square wave is generated, the space vector is positioned in the same sector as it would be for a VSC. On the other hand, when the negative part of the square wave is generated the space vector has to change position to the sector at the opposite side of the circle.

A more thorough explanation is given by looking at the case where the phase voltages are in the positions marked with colored dots in figure 5.7. This desired sinusoidal input requires a space vector positioned in sector 1 during the positive part of the square wave, and in sector 4 during the negative part of the square wave as depicted in figure 5.8. When V_s is positioned in sector 1, the vectors adjacent to this sector are the most appropriate to use. Thus by applying in turn V_{ppn} and V_{npn} in addition to zero vectors during the sampling period T_s, the desired input of the phase voltages are generated.

The next step is to generate the negative part of the square wave. As figure 5.7 depicts, sector 4 can generate exactly the same phase voltages as in sector 1, but with opposite

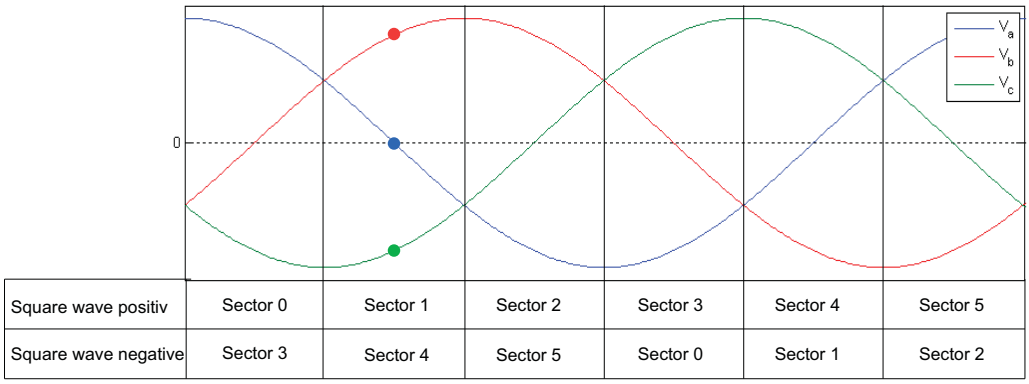

Figure 5.7: Position of the space vector according to the desired sinusoidal input and square wave output.

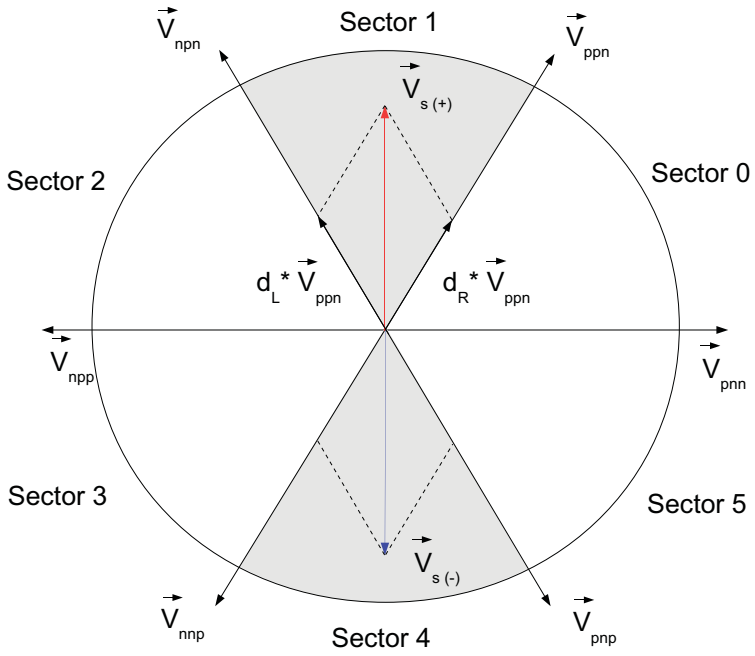

Figure 5.8: Synthesizing the voltage space vector during positive (+) and negative (-) part of the square wave.

polarities. *However, due to the negative square wave, the actual phase voltages modulated in the input will be the same as for the positive part of the square wave.*

The two active vectors adjacent to sector 4 are V_{nnp} and V_{pnp}. These vectors together with zero vectors are used to form the negative part of the square wave during the time period T_s. Since T_s denotes the required time to shape either the negative or the positive part of the square wave, the total time it takes to shape one period of the square wave is $2 \cdot T_s$. Thus the frequency of the square wave is half of the switching frequency f_s.

It should be noticed that the two active vectors of sector 1 generate states that turn on the opposite switches of what is turned on in sector 4; while the active states turned on in sector 1 are AP, BP and CN and AN, BP and CN, the active states turned on in sector 4 are AN, BN and CP and AP, BN and CP respectively. Figure 5.9 shows the states and how the alternating direction of the phase currents determines the polarity of the square wave output. In the first figure of (a), the positive switches of leg A and B in on-state result in downward direction of i_a and i_b through the primary winding of the transformer. On the other hand, the first figure of (b) shows that when the opposite directed active vector is applied, the negative switches of leg A and B in on-state result in the same phase currents through the transformer, but now in the opposite direction. The same process occurs when the second states of figure (a) and (b) are applied. Since current and voltage are assumed to be in phase, the square wave voltage changes polarity depending on the

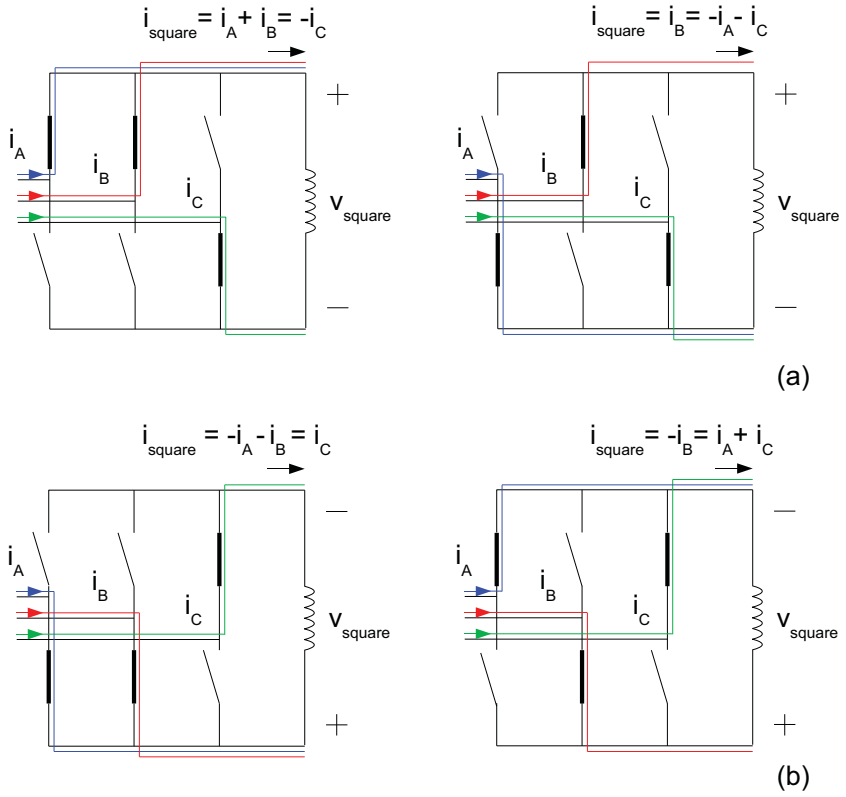

Figure 5.9: Phase current direction during the synthesizing of voltage space vector.

alternating direction of the phase currents.

5.3.2 Synthesizing the voltage space vector

In order to obtain a V_s with the desired length and angle with respect to the $a-axis$, the active and zero vectors have to be applied for specified time intervals during the total sampling time T_s. In which order the vectors are applied is not important for the synthesizing of V_s, but will rather impact on the switching losses.

As it was mentioned previously, each active state generates a non-zero sinusoidal input. The length of the vector is equal to the alternating DC voltage of the square wave. When V_s is synthesized the adjacent active vector to the right of the sector is applied over a time interval $d_R T_s$, the adjacent vector to the left is applied over a time interval $d_L T_s$ and the zero vectors are applied the remaining time $d_Z T_s$. Thus the total sampling time T_s can be expressed as in equation (5.7).

$$T_s = d_R T_s + d_L T_s + d_Z T_s \tag{5.7}$$

When dividing both sides with T_s, the expression will be as follows.

$$d_R + d_L + d_Z = 1 \tag{5.8}$$

The case of figure 5.8 is used as an example on how to calculate V_s for the positive part of the square wave output. The voltage space vector can be expressed as in equation (5.9).

$$\vec{V_s} = \frac{1}{T_s}\left(d_R T_s \cdot \vec{V}_{ppn} + d_L T_s \cdot \vec{V}_{npn} + d_Z T_s \cdot 0\right) \tag{5.9}$$

Thus

$$\vec{V_s} = d_R \cdot \vec{V}_{ppn} + d_L \cdot \vec{V}_{npn} \tag{5.10}$$

The figure depicts the projection of the two vectors in equation (5.10) which forms $\vec{V_s}$.

Since V_s has the same amplitude and angle (but negative) during the negative part of the square wave, the same duty cycles can be utilized in sector 4.

5.3.3 Switching pattern

Figure 5.10 depicts a proposed switching pattern when $\vec{V_s}$ is positioned in sector 1 during the positive part of the square wave and in sector 4 during the negative part of the square wave. The small areas between the stippled grey lines indicate the overlapping period. The overlapping is performed by introducing a delay with some few microseconds to the gate signal for turning off a switch. The letters in the top of the figure indicate which switching state from figure 5.6 which is utilized.

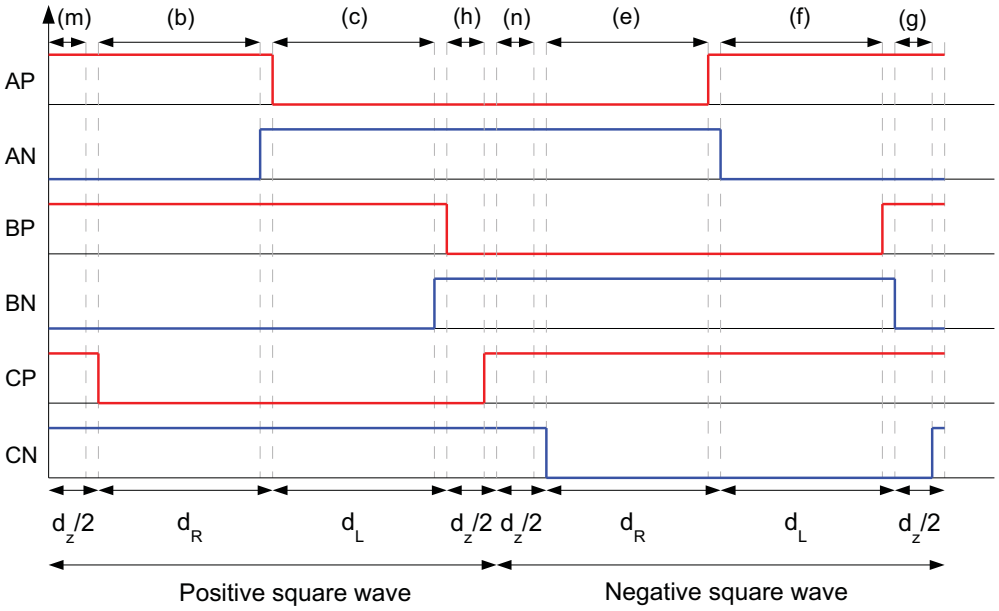

Figure 5.10: Switching pattern for SVM.

Chapter 6

Protection scheme

Unlike the voltage source converter (VSC) the reduced matrix converter is always implemented with some special protection scheme to secure safe operation of the switches during abnormal operation of the converter, i.e. when a fault occurs in the system. The reason is that the topology of the RMC has some salient differences compared to the VSC. These are given below:

- The RMC is a direct AC-AC converter.
- The RMC consists of bi-directional switches.

If a fault occurs and there is an overcurrent in the system, the strategy to protect the converter is to turn off all the switches. In order to avoid a sudden interruption in the inductive currents of the generator which can cause dangerous overvoltages, a freewheeling path is required. In that way the stored magnetic energy of the generator can be transported out to the DC link energy storage. In a VSC the diodes of the switch package allow the generator phase currents to continue flowing when the IGBTs are turned off and the DC-link capacitor provides the energy storage. However, the case of the RMC is different since its switches consist of RB-IGBTs, thus the current will have no natural path to freewheel through and an alternative solution is necessary.

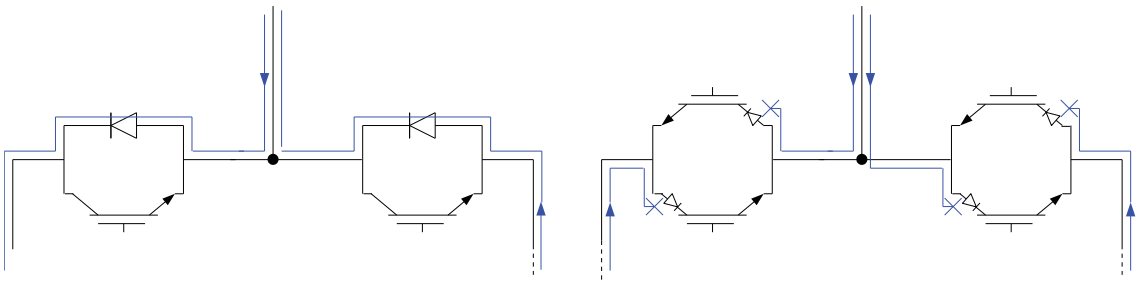

Figure 6.1: Current path in (a) VSC, and in (b) RMC when the transistors are turned off in emergency shutdown.

Since the features of the RMC are the same as what characterize the conventional matrix converter, a similar strategy of protection can be used for both converters. In 1996 P. Nielsen wrote in his PhD-thesis that the protection of the matrix converter was a field that had not yet been given a lot of attention [35]. One reason for that was most probably that the matrix converter was introduced as a "pure silicon converter", while its protection scheme normally requires reactive elements. However during the last years different protection schemes have been investigated and some of them will be presented here.

Figure 6.2 depicts three different protection schemes ((d) is only a modification of (c)). The protection scheme in (a) is presented in [36]. This is a compact and cheap solution because it requires few additional devices and it avoids the implementation of reactive storage components. However, it is still only available for low power solutions. The first part in (a) consists of 4 varistors. Three of the varistors are star-connected in the input of the converter, and one varistor is connected between the positive and the negative leg of the output. The varistors in the input provide the freewheeling path for the generator currents when the switches are turned off in an emergency shutdown of the converter. This allows the stored energy in the generator leakage inductances to be dissipated in the protection circuit. The varistor in the output protects the converter against abnormalities that occurs in the grid side. The critical moment of the varistor protection appears if all the switches has to be turned off at the same time, but one of the switches are delayed compared with the others. The result is that the switches which are already turned off will take the overvoltage and be destroyed. This is why the second scheme of (a) is introduced. It is a gate driver with suppressor diode protection, which protects the RB-IGBTs against overvoltages. This is connected to each semiconductor device and has to be implemented in addition to the varistors in input and output. The operation of the suppressor diode causes high losses in the RB-IGBT, but lasts only until all the devices are turned off. Since the devices used in this protection scheme are still not developed for high power solutions, the varistor with suppressor diode is not a feasible solution for the proposed system. Additionally the varistors have a limited lifetime due to ageing problems.

The solution in (b) is presented in [37]. It provides protection with the use of zener diodes connected between the input and the output of the RMC. It has the advantage of avoiding the use of reactive elements; the converter will thus maintain its compact topology. However, if the zener-diodes are activated in a repetitive manner, the diode will be over-heated and its clamping capability will be worsened. Since this is a relatively new protection scheme, it is still not available for high power systems.

The last protection scheme depicted in (c) and (d) is the clamp circuit. The clamp circuit has the most robust design, and will in this study be implemented in the system to protect the reduced matrix converter. A further study follows.

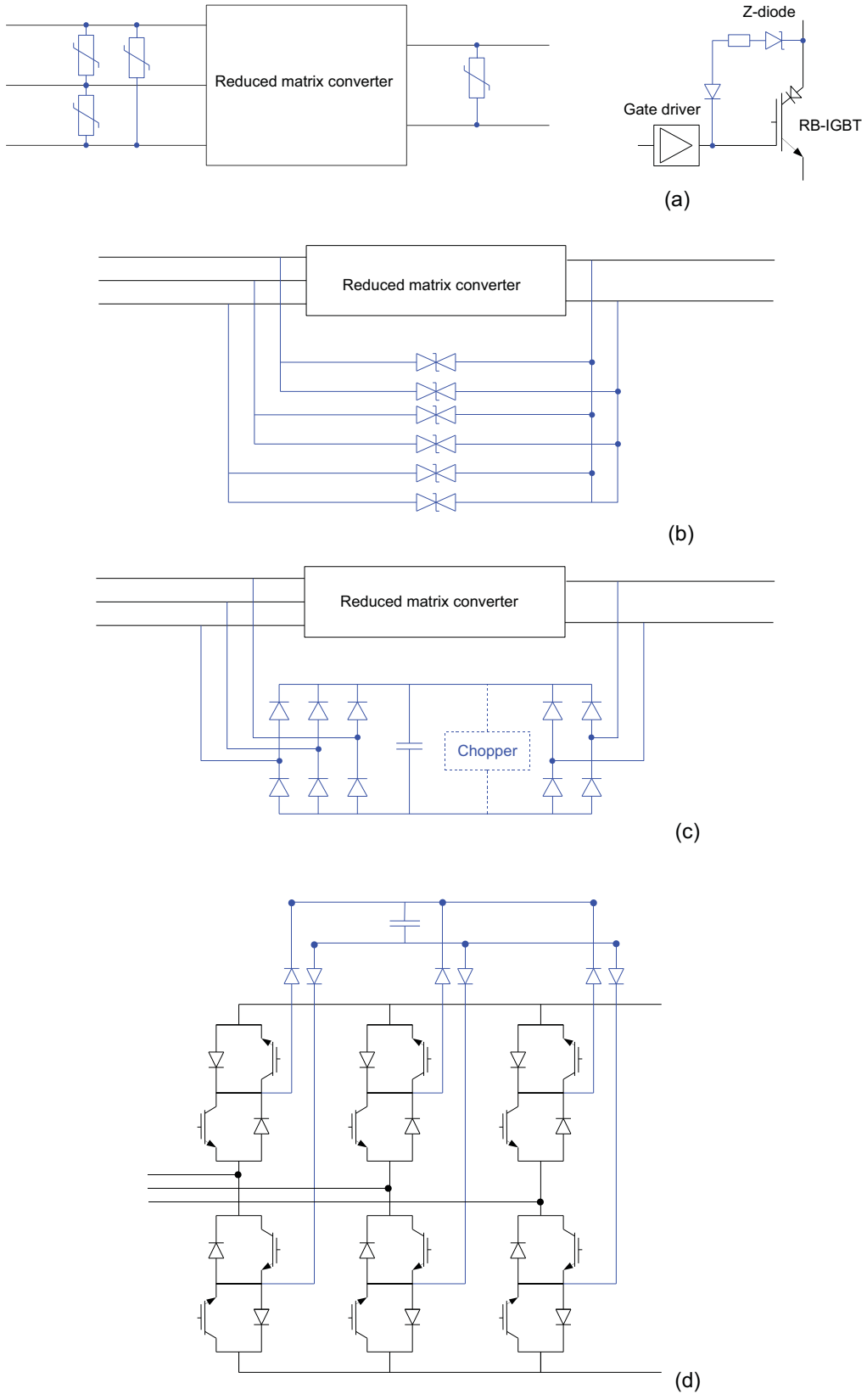

Figure 6.2: Different protection schemes for the RMC

6.1 Clamp circuit

The clamp circuit is presented in several papers as the most convenient protection scheme for the matrix converter [33], [38]. It provides the freewheeling path in emergency shutdown of the RMC and eliminates the need of snubber circuits which are normally implemented in the VSC to reduce the switching stresses during commutation. The elimination of the snubbers is an advantage since the RB-IGBTs are still only available as low rated devices, and need to be connected in series and parallel to fulfill the high power requirements of the wind energy conversion system. A snubber circuit for each RB-IGBT would therefore result in substantial energy losses [39], [35]. The clamp circuit also contributes to increase the total losses of the system and has a certain amount of reactive elements. However it is preferred due to its compactness and reliable operation.

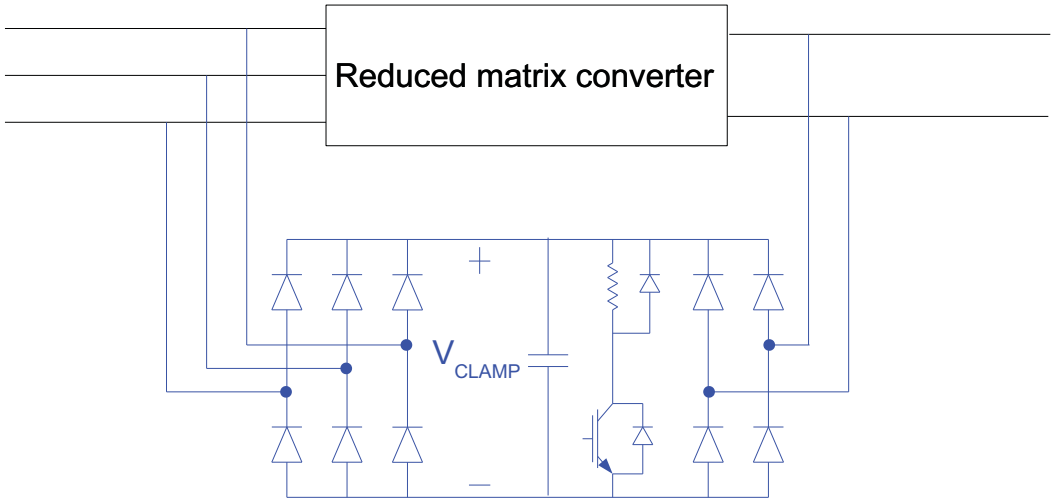

Figure 6.3: Clamp circuit with chopper

6.1.1 The topology

The clamp is connected to the input and output lines of the converter by two rectifier bridges which in total consist of 10 diodes. This is two diodes less than in the clamp of the 9-switch MC due to the 1-phase side of the RMC. In [40] it is proposed an alternative topology of the clamp where the diodes of one rectifier bridge are replaced by the series diodes of the bi-directional switches, see figure 6.2(c). However, since the switches are assumed to be of conventional type (with two diodes in antiparallell with two IGBTs), it is an inconvenient solution for the proposed system, where the bi-directional switches consist of RB-IGBTs. The current ratings of the diodes can be the same as that of the converter semiconductors since faults that cause overcurrent are not occurring at a repetitive basis.

This is possible because diodes are designed to withstand a non-repetitive current as high as 10-15 times the rated value without being destructed [41].

As figure 6.3 depicts, in addition to the two diode bridges, the clamp consists of a capacitor in parallel with a chopper circuit. In order to provide safe operation of the RMC, the voltage across the clamp capacitor has to be kept at a value which is lower than the rated voltage of the semiconductor devices. With that requirement fulfilled, the RB-IGBTs will not be damaged. Because if the voltage in one of the converter sides exceeds the clamp voltage, the diode bridge connected to the exposed side will be forward biased, and thus allow the voltage spike to be absorbed in the clamp capacitor.

The chopper circuit is implemented in the clamp circuit in order to minimize the size of the capacitor. This task is performed by turning on the IGBT when the voltage across the clamp exceeds a fixed level. The resistor is then able to discharge the capacitor, and the electric energy stored in the capacitor will be converted to thermal energy in the resistor. Since the resistor is only dissipating energy during short time periods, the use of heat sink, to maintain the temperature low, is avoided. According to [18], with the implementation of the chopper circuit it is possible to have a clamp which is 10-100 times more compact.

In the majority of the systems where the matrix converter is present, the clamp circuit is only activated during faulty situations. On the contrary, in the proposed system, the clamp circuit is of great importance not only during faults, but also in steady state operation.

6.1.2 Operation during steady state

The non-ideal high frequency transformer in the square wave side of the RMC is the reason to why the clamp circuit is needed in steady state. In a non-ideal transformer there is leakage inductance in the winding, in addition to the mutual inductance that links the primary and secondary winding. With the square wave current I_{trafo} flowing through the transformer, magnetic energy E is stored in the leakage inductance $L_{leakage}$ as in the following equation:

$$E = \frac{L_{leakage} \cdot I_{trafo}^2}{2} \tag{6.1}$$

In the instant a switch is turned off and the phase current is commutating to the complementary switch of the leg, the current through the outgoing switch falls rapidly at a rate di/dt and thus influences on the waveform of the square wave current. The fast change in the current through the transformer generates a voltage spike caused by the stored leakage energy [42]. The magnitude of the voltage spike $v_{leakage}$ is determined by equation (6.2).

$$v_{leakage} = L_{leakage} \cdot \frac{di_{trafo}}{dt} \tag{6.2}$$

The equation demonstrates that the magnitude of the voltage spike is not only dependent on the rate of change of the current, but also on the leakage inductance. It is therefore

important to design the transformer with as low leakage inductance as possible, to avoid unnecessarily overrated semiconductor devices.

6.1.3 Operation during faulty situations

Previously it has been mentioned that overcurrent causes the switches to turn off immediately in an emergency situation. However, the reasons to why the overcurrent appears have not yet been presented. An overcurrent in the system could most probably occur because of grid faults, commutation faults, abnormal operation of the generator, high inrush currents or circulating currents along the switches [43]. The clamp circuit provides the protection of the converter during the fault condition which is of great importance due to the energy stored in the leakage inductances of the generator.

6.1.4 Losses in the clamp circuit

It is necessary to include the losses in the clamp circuit in the study of the RMC. During operation there are generated losses in the resistance of the chopper circuit and in the diodes.

6.1.4.1 Chopper circuit

When the chopper circuit is activated, the resistance will draw current from the capacitor and discharge it. The electrical energy is converter to thermal energy, and losses are generated. The losses are function of the average current through the chopper circuit and the value of the resistance as equation (6.3) expresses.

$$P_{resistance} = avg\left(i_R\right)^2 \cdot R \tag{6.3}$$

6.1.4.2 Diodes

The diodes of the two rectifier bridges experience three different type of losses; conduction losses, turn on losses and turn off losses. Since the turn on losses normally are neglected, they will not be considered in this study [44]. The turn off losses are generated due to the finite time it takes to switch the diode from on state to blocking state. While the voltage is changing from its forward value (around 0V) to a negative voltage, the current has a reverse recovery waveform. The conduction losses are generated due to the small voltage drop across the diodes in conduction mode.

Chapter 7

Simulation model and results

7.1 Simulation model

The entire model of the proposed wind energy conversion system, from the generator to the DC output of the wind turbine is simulated in PSIM. The model is built in order to study the operation of the clamp circuit in normal operation and to simulate the losses in the clamp circuit and the bi-directional switches of the reduced matrix converter. In order to have a more realistic approach than in [1], the transformer and the semiconductor devices are implemented as non-ideal elements. The system represents the WECS in steady state for a constant wind speed. The parameters are based on a generator frequency of 50 Hz with a high frequency square wave output of the RMC.

Where nothing else is specified, the simulation is performed with modulation amplitude of 0.95 for both the CBM and SVM. The CBM is implemented with a carrier frequency of 10 kHz for both the sinusoidal input and the square wave output, while the switching frequency of the SVM is 10 kHz. The parameters of the devices in the circuit is given in appendix A. When the simulation time step was set to 10^{-6}, the voltage spikes in the square wave output did not appear. Thus in order to extract the desired information from the model, the simulation time step is set to 10^{-7}. The simulations are performed from the point in time 0.2 to 0.3 seconds.

7.1.1 Permanent magnet generator

The permanent magnet generator is modeled as a constant three-phase sinusoidal voltage source connected in series with a resistor and an inductor that are representing the internal values of the generator. The generator values are given in appendix A. It produces a line to line voltage of 290.87V. The low voltage is set due to the ratings of the bi-directional switches.

7.1.2 Reduced matrix converter

For the converter it is used medium power ratings. The reason is that the method which is used to calculate the losses of the bi-directional switches, given in [2], is validated through an experiment of reverse blocking IGBTs with ratings 600V/200A. The model is therefore very accurate. It is implemented in PSIM as a DLL-file, written in C++. During simulations voltage and current sensors connected to each switch send data to the DLL-file. An explanation of the loss method can be found in appendix B.

The bi-directional switches in the RMC is modulated with either carrier based modulation or space vector modulation after the methods explained in chapter 5. Although both modulation techniques are implemented as if the bi-directional switches were non-ideal semiconductors (switching on and off during a finite time), the switches used in the simulation model are ideal. This is because there are no semiconductor data which represents the RB-IGBT with the desired characteristic in PSIM yet.

7.1.3 Clamp circuit

The diodes of the clamp circuit are of type Fairchild Semiconductor ISL9R3060G2. They have a non-ideal characteristic with rating 600V/30A. The conduction losses and switching losses they produce are calculated by PSIM with values stored in its database. The IGBT in the chopper circuit is triggered by signals sent from a comparator. The comparator compares the capacitor voltage, measured with a voltage sensor, with a fixed value. The fixed value has to be lower than the voltage ratings of the RB-IGBTs. In this case the clamp circuit provides safe operation of the switches when the value is set to 550 V. The IGBT is turned on when the capacitor voltage is higher than 550V, and turned off when the capacitor voltage is lower than 550V. The values of the resistance and the capacitor is given i appendix A.

7.1.4 High frequency transformer

The transformer is a one-phase, two winding transformer with a 1:1 winding. It is implemented as a non-ideal component; with leakage inductance, magnetizing inductance and resistance. The parameters are given in appendix A. The following simulation results will always depict the behavior of the primary side of the transformer. That is the side which is directly connected to the RMC output.

7.1.5 Full-bridge converter

The full-bridge converter consists of four diodes. The diodes are found in the library of PSIM and are of type Powerex CS240650. They have a non-ideal characteristic with rating 600V/50A.

7.1.6 DC output

The output to the DC grid is modeled as a DC voltage source. The DC voltage has a value of 500V. This voltage is the same as the alternating voltage of the square wave, and will therefore be applied to the bi-directional switches of the RMC, either as negative or positive polarity. 500 V is thus a safe approach to avoid operation above the voltage rating of the RB-IGBTs. The DC output from the full-bridge is filtered by a capacitor and an inductor.

7.2 Clamp circuit

The next sections will show the importance of selected components of the clamp circuit and why they have to be given the correct parameters to provide safe operation of the RMC. Also the operation with and without clamp circuit will be studied in addition to a comparison between clamp operation when the RMC is modulated with CBM and SVM. Simulation figures are included to make the theory from section 6.1 more comprehensible.

Figure 7.1 depicts the results of the simulation for the clamp circuit in steady state. The RMC is modulated with CBM. In order to understand the operation of the clamp circuit as it was explained in section 6.1.2, the process can be followed step by step in the figure. When a switch turns off, the current through the transformer I_{TRAFO} experiences a transient. The current transient causes a voltage spike to appear in the transformer voltage V_{TRAFO}. As V_{TRAFO} exceeds the clamp voltage across the capacitor $V_{CAPACITOR}$, the clamp diodes get forward biased and allow the excess energy in the square wave output to be dissipated in the capacitor. The result is that the capacitor voltage increases. If it exceeds the fixed value in the comparator, the IGBT of the chopper circuit turns on and allows the resistance to discharge the capacitor until it decrease to 550V again. Hence the current $I_{RESISTANCE}$ through the resistance consists of short spikes.

7.2.1 Comparison of operation with carrier based modulation and space vector modulation

There are few differences in the operation of the RMC modulated with CBM and modulated with SVM. It is observed that the voltage across the capacitor is higher with SVM than what is with CBM. With SVM the maximum capacitor voltage reaches 551.7V while with CBM it reaches 550.03V. Another observation is that the total losses with SVM are lower than with CBM, it is 14.6W with SVM and 25.5W with CBM.

7.2.2 The importance of the chopper circuit

Due to the repetitive voltage spikes in the square wave output in steady state operation, it is important to have an appropriate design of the clamp circuit. In the section 6.1.1, it was mentioned that the implementation of the chopper circuit reduces the size of the capacitor.

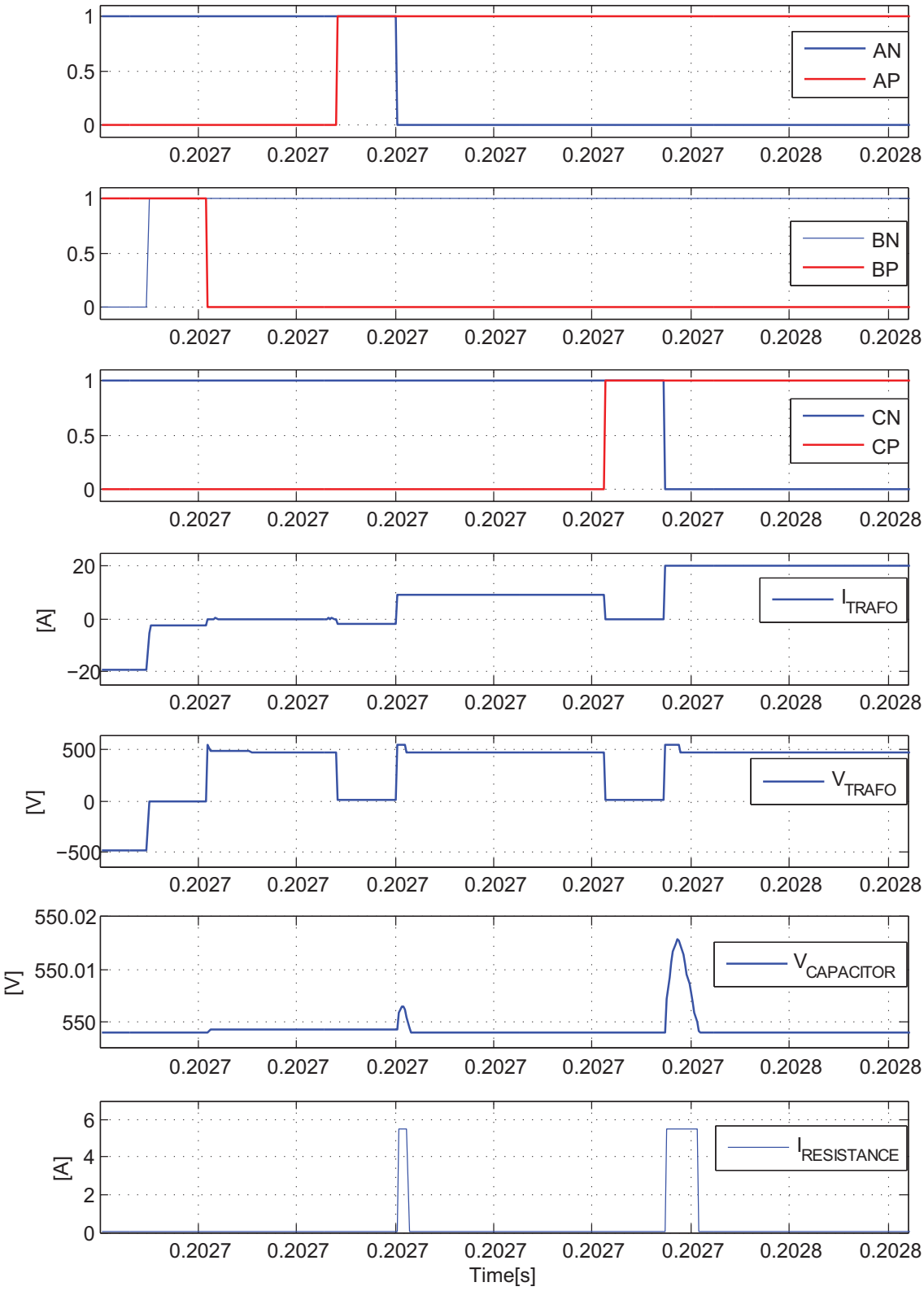

Figure 7.1: Clamp circuit operation in steady state.

The importance it has in the system is indicated in figure 7.2 and 7.3, where respectively the clamp voltage without and with the chopper is showed. Without the chopper circuit, the capacitor voltage increases gradually. This will continue until it exceeds its maximum voltage capability, and thus get damaged. As it can be seen from the figure, the voltage is already 700V after 0.2 seconds. Since this is higher than the ratings of the RB-IGBTs (600V), they are not protected by the clamp anymore. On the other hand, the graph where the chopper is implemented in the clamp circuit shows that the variation of the capacitor voltage is limited due to the operation of the resistor. The voltage is kept around 550V, thus if the transformer voltage exceeds 550V, the diodes connected to the output side of the RMC will be forward biased and the capacitor will be able to dissipate the leakage energy. The voltage in the transformer does not exceed the rating of the RB-IGBTs, and the clamp provides a reliable operation of the semiconductor devices.

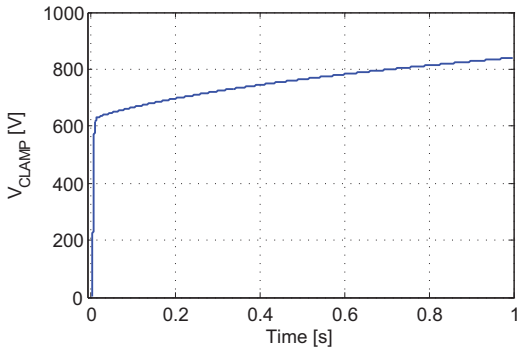

Figure 7.2: V_{clamp} without chopper present in clamp circuit.

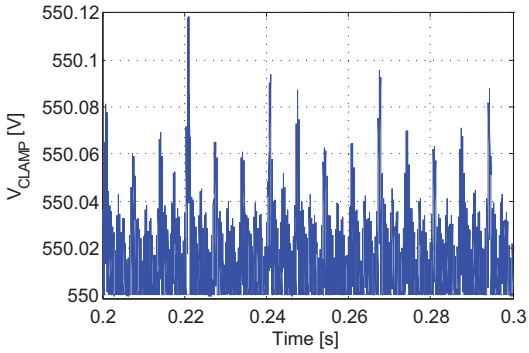

Figure 7.3: V_{clamp} with chopper present in clamp circuit.

7.2.3 Clamp parameters impacts on the operation

7.2.3.1 The chopper circuit resistance

The losses in the clamp circuit are strongly dependent on the resistance in the chopper circuit. It is thus important to keep its value as low as possible without reducing the overall performance of the reduced matrix converter. Simulations were performed with different values of the resistance both for CBM and SVM, and the results are given in table 7.1. The table shows the average current I_R through the resistance, which is used to calculate the losses in the resistance. The conduction losses and switching losses of the diodes of the clamp is also included.

According to the table, the average current I_R is not varying a lot for different values of the resistance. However when the waveform of I_R was studied more carefully, it was observed that by increasing the value of the resistance, the current spikes which appeared through it every time the IGBT turned on was decreasing in height but increasing in length. The current that was observed for 10Ω, 100Ω and 1000Ω in CBM was 55A, 5A

and 0.55A respectively, and the average length of the spikes was $0.3\mu s$, $2.3\mu s$ and $7.0\mu s$ respectively. This phenomenon can be explained with the fact that the circuit with the resistance and capacitor is equivalent to a RC circuit. Hence by increasing the resistance, the time constant increases and cause the voltage applied to the capacitor to decrease in a slower rate. The result is that the chopper circuit is connected during longer time periods because the same amount of energy in the capacitor has to be dissipated in the resistance independent of its size. It was also observed that the size of the resistance influences on the maximum voltage which appears across the capacitor. When the size of the resistance is reduced the maximum voltage is also reduced.

It is the average current in the resistance which is of interest when the losses are calculated. The table indicates that a resistance with value 100Ω gives the optimal result both for CBM and SVM. It produces the lowest amount of losses in the clamp and the operation of the RMC does not present any abnormalities.

Although the test results from 2000Ω does not appear in the table, it is interesting to mention that simulations with this value gives a clamp voltage which is always higher than 550V. Since the clamp voltage is compared with 550V in the comparator, which in turns trigger the IGBT in the chopper circuit, the IGBT is maintained in on state during the entire simulation. The result is that the resistor is continuously discharging the capacitor which is not good if the use of heatsink in the chopper circuit should be avoided.

			Losses [W]			
Modulation	R[Ω]	$I_R(avg)[A]$	$P_{resistance}$	$P_{conduction}$	$P_{switching}$	P_{total}
CBM	1000	0.35	122.5	1.17	7.26	130.93
	100	0.35	12.25	1.3	11.9	**25.45**
	10	0.41	16.81	1.79	153.9	172.5
SVM	1000	0.27	72.9	0.95	2.86	76.71
	l00	0.27	7.29	1.13	6.15	**14.57**
	l0	0.31	9.61	1.57	118.1	129.28

Table 7.1: Losses in the clamp circuit changing with the resistance, for CBM and SVM.

Observation:

During the simulations where the impacts of changing the resistance in the chopper circuit was studied, it was observed that in some cases the voltage spikes in the square wave output did not only result in a current flow through the clamp diodes connected to the square wave side, but also through the clamp diodes connected to the generator side. Table 7.2 shows the observations. In other literature there is always depicted the case where only one diode side of the clamp is conducting and that is the side which is connected to place where the overvoltage appears [18]. Although that literature only discusses overvoltages in the generator side with the MC implemented in a motor drive, the same principle should be valid here. Thus according to the referred literature and what was explained in section 6.1.1 it is not logic behavior of the clamp circuit.

Modulation	R[Ω]	Clamp diodes activated in
CBM	1000	Transformer side
	100	Transformer and generator side
	10	Transformer side
SVM	1000	Transformer and generator side
	100	Generator side
	10	Transformer side

Table 7.2: Activated clamp side during voltage spike in square wave output.

7.2.3.2 The fixed value in the comparator

The fixed value in the comparator determines when the IGBT of the chopper circuit is turned on in order to allow the resistance to discharge the capacitor. The capacitor voltage will then be able to return to the same level as the fixed value in the comparator. Three fixed values were tested in the simulation; 500, 550 and 600 respectively. When the fixed value is set to 500, the IGBT is in continuous on-state because the capacitor voltage is not able to decrease to 500V. Thus the resistance is always discharging the capacitor and the average current is high, ca. 5A. The square wave output waveform is distorted. When the clamp circuited is operated with a fixed value of 550 in the comparator, the capacitor voltage is discharged between each voltage spike that appears in the square wave output. Hence the resistance will be connected less frequent and the average current is decreased to 0.35A due to the intervals of zero current. The square wave output waveform is satisfactory, where the voltage spikes are limited to 550V. At a fixed value of 600, the simulations show that the voltage spikes is always a little higher than 600V. A capacitor voltage of 600V is easily obtained, thus the average current through the resistance is only 0.17A.

As the rated voltage of the RB-IGBTs is 600V it is necessary to avoid voltage spikes which increases above that level. The case where the fixed value is set to 600 gives the lowest average current in the resistance, thus the lowest losses in the chopper circuit. On the other hand it does not provide a safe operation of the RB-IGBTs. The reason is that the voltage spikes are too close the rated value of the RB-IGBTs. Therefore it is decided to implement the comparator with fixed value of 550V. This is both because it allows for safe operation of the semiconductor devices and also because the clamp losses are maintained at a satisfactory level.

7.2.4 The impact of current transients in the transformer

In chapter 6.1 it is mentioned that every time a switch is turned off and cause a transient in the current through the transformer, a spike is generated in the transformer voltage. The size of the spike is according to equation (6.2) dependent of the size of the transient, i.e. how large the difference is between the current before and after the turn off. In figure 7.1 three cases where a voltage spike appears confirm the theory. The first case depicts a small voltage spike. The spike is provoked by the turn off of switch BP. The time period

before switch BP is turned off, both switches of leg B is in on-state simultaneously in order to have the required time with overlapping. This result in a short circuit current in leg B which is added to the phase currents through the transformer. This contributes to increase the current in the instant before switch BP is turned off. The instant after switch BP is turned off, only the negative switches of each leg is in on-state. Thus a short circuit of the generator is produced and the current through the transformer goes to zero. The result is that the current is only changing slightly during the transient, from -2.9A to 0A, a difference of 2.9A. The small voltage spike which is provoked is easily dissipated by the clamp. The second case produces a larger spike. This time the spike is provoked by the turn off of switch AN. The current through the transformer changes fast from -2.0A to 9.2A during a short time period. The difference in the current is 11.2A. Hence the spike is larger than before, and the clamp circuit has to dissipate more energy. In the third case the largest spike appears in the voltage. When switch CN is turned off, the current changes from -0.6A to 19.9A, a difference of 20.5A. The clamp circuit dissipates the largest amount of energy.

Observation: By observation of the transformer current I_{TRAFO} in figure 7.1, it is obvious that transients in the current also occur when a switch turns on. The transient is even larger than what is when turning off a switch. Nevertheless, there are not generated voltage spikes during turn on of the switches. The solution can be that every turn on is followed by an overlapping of the switches of the leg. This cause a short circuit of the transformer, and the voltage across it goes immediately to zero. Thus a spike cannot appear in a short circuited transformer.

7.2.5 Operation without clamp circuit

It is not straightforward to perform simulations where the clamp circuit is removed from the model. Without the clamp circuit present, the square wave voltage is highly distorted and follows a sinusoidal waveform and the spikes do not appear anymore. Since the results in [1] depicted a prefect performance of the square wave voltage when the clamp circuit was not present in the circuit, it has to be the modifications which has been implemented in the proposed model which cause the distortion. Thus, either the implementation of a non-ideal transformer or the change from a controllable to a non-controllable full-bridge converter. Probably these modifications prevent the system to go in steady state when the PM generator is started. Instead, to simulate the system without the clamp, the fixed value in the comparator of the clamp circuit has to be set to a very high value. The capacitor will then increase rapidly to a high value because the IGBT in the chopper circuit is not turned on in order to allow the resistance to discharge the capacitor. The result is that the square wave voltage does not exceed the capacitor voltage, thus the clamp diodes will not be forward biased and the clamp circuit is not activated. The simulation of the system under these conditions is similar to the operation without clamp circuit. The result is showed in figure 7.4. Since the voltage spikes are not limited by the clamp circuit, they reach 700V. In comparison are the voltage spikes limited to around 550V when the clamp circuit is implemented in the model.

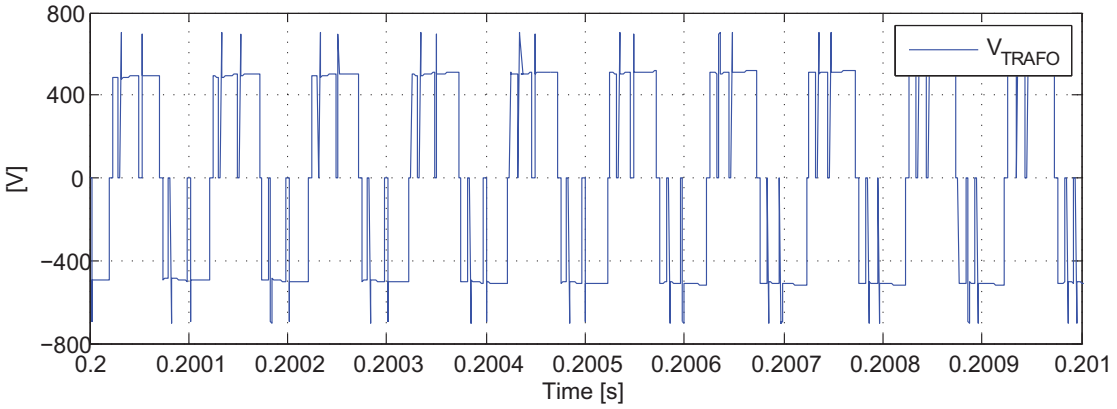

Figure 7.4: Voltage spikes in square wave output during normal operation of the RMC without clamp circuit protecting the switches.

7.3 The impacts of modulation technique on the losses

In this section the simulation results of the losses generated in the bi-directional switches and in the clamp circuit is studied. Both losses are related to the reduced matrix converter and should be kept at a minimum. The loss study explores thoroughly the switching conditions of carrier based modulation and it also includes a study of the more complicated modulation technique, space vector modulation. The aim is to find the optimal case where losses are maintained at a minimum meanwhile a decrease in the quality of the voltage and current waveform is avoided. The study is performed by changing the modulation technique parameters. The loss model of [2] is used to calculate the switching losses in PSIM.

7.3.1 Carrier based modulation

7.3.1.1 Switching losses

For the carrier based modulation there are two parameters which are varied. The first one is the carrier frequency of the square wave, where there is decided to look at four different cases, respectively with frequency 10kHz, 5kHz, 2.5kHz and 1kHz. For all four cases the carrier frequency of the sinusoidal wave is kept at 10 kHz. The second parameter to be varied is the displacement angle between the carrier of the square wave and the carrier of the sinusoidal wave. It is important to notice that for each case the carrier of the square wave is displaced with an angle increasing from 0 to 180 degrees with respect to the carrier of the sinusoidal wave. As explained in part 5.2 the waveform of reference signal of the sinusoidal wave is dependent of the carrier of the square wave in such a way that it is inverted for every time the carrier of the square wave is lower than zero. Thus by a displacement of the carrier of the square wave or a change in its frequency, the reference signal will be modified accordingly. The results of the total losses are depicted in figure

7.5-7.8.

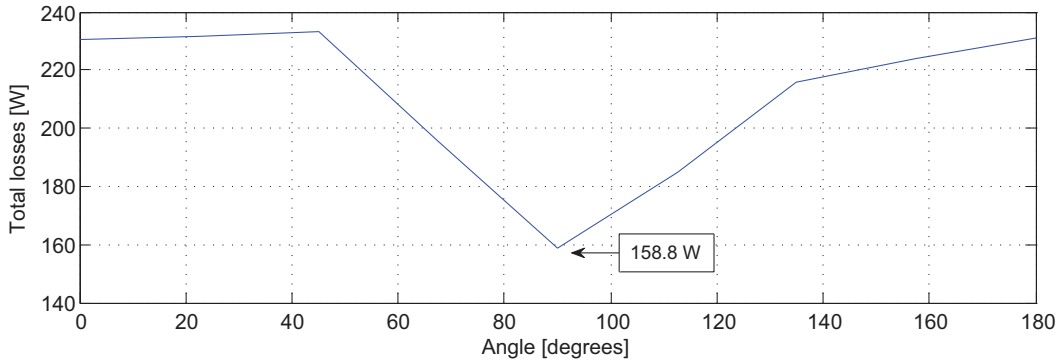

Figure 7.5: CBM: Total losses as a function of phase displacement, frequency 10kHz.

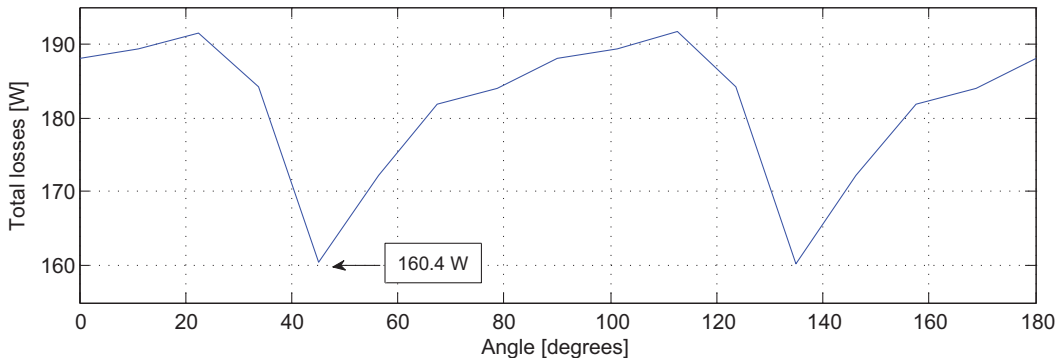

Figure 7.6: CBM: Total losses as a function of phase displacement, frequency 5kHz.

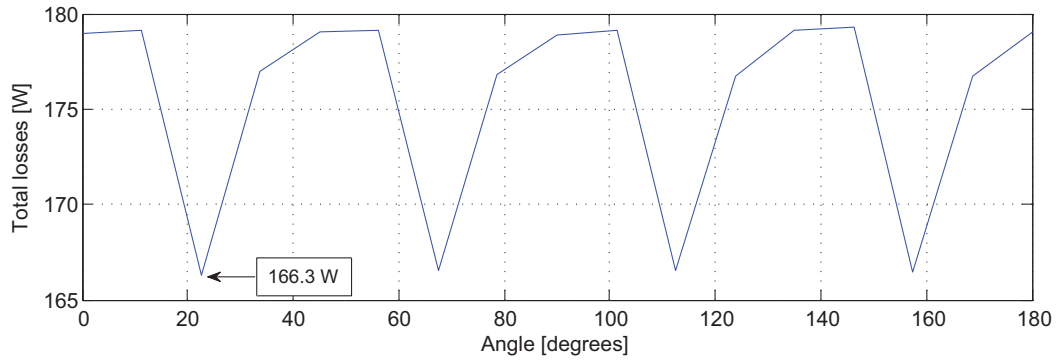

Figure 7.7: CBM: Total losses as a function of phase displacement, frequency 2.5kHz.

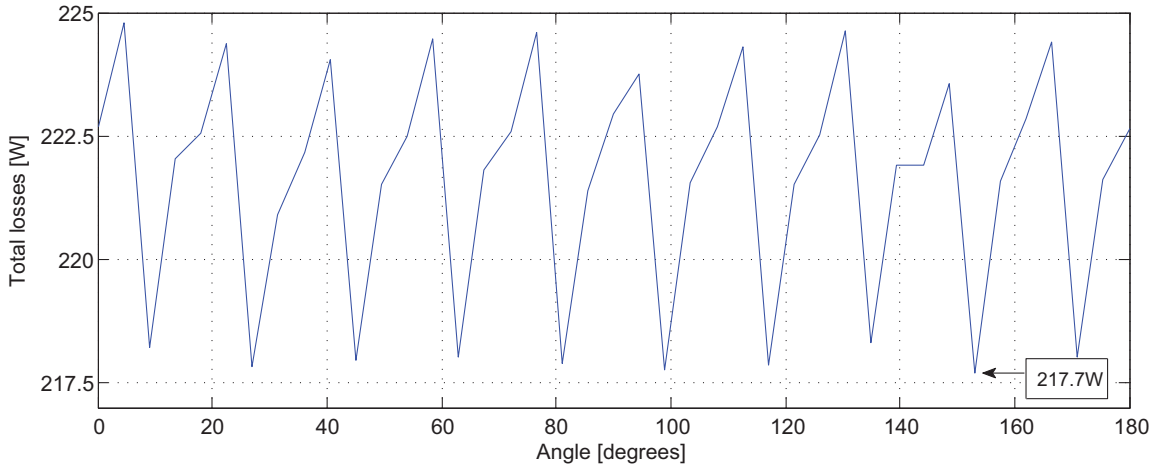

Figure 7.8: CBM: Total losses as a function of phase displacement, frequency 1kHz.

As there can be seen from the figures there is a relation between the ratio of the two carrier frequencies and the number of times the curve is repeated along the x-axis. The case where the carrier frequency of the square wave is 5kHz is chosen as an example. 10kHz divided by 5kHz is 2, which is also the number of times the curve is repeated along the x-axis. The same relation yields for the three other cases, where the ratio is 1 for frequency 10kHz, 4 for frequency 2.5kHz and 10 for frequency 1kHz, and the curve is repeated accordingly. This pattern can be explained by returning to the case where the carrier frequency of the square wave is 5 kHz which gives a ratio of 2. Figure 7.9 depicts the displacement of the reference signal in two situations which according to figure 7.7 gives the lowest losses for this case. In order to distinguish the situations from each other, the reference drawn in blue has two different amplitudes, where the curve with the large amplitude represents the reference when the displacement angle is 45 degrees, and the curve with small amplitude represents the reference with displacement angle of 135 degrees. The red curve is the carrier signal of the sinusoidal wave. The figure shows that the positive periods of the reference signal with displacement angle of 45 degrees cross the carrier signal in the same points as the negative periods of the reference signal with displacement angle of 135 degrees, and the negative periods of the reference signal with displacement angle of 45 degrees cross the carrier signal in the same points as the positive periods of the reference signal with displacement angle of 135 degrees. The two situations has therefore exactly the same amount of switching losses which indicates that for every 90 degrees of an arbitrary displacement angle, the losses will be similar, and thus the curve is repeated. The similar occurs in the other cases, with 10kHz the losses is the similar every 180 degrees, with 2.5kHz the losses are the similar every 45 degrees and with 1kHz the losses are similar every 18 degrees.

The optimal condition which produces fewer losses is the case where both carrier frequencies are the same, i.e. 10kHz, and the displacement angle is 90 degrees. The losses

are then 158.8W.

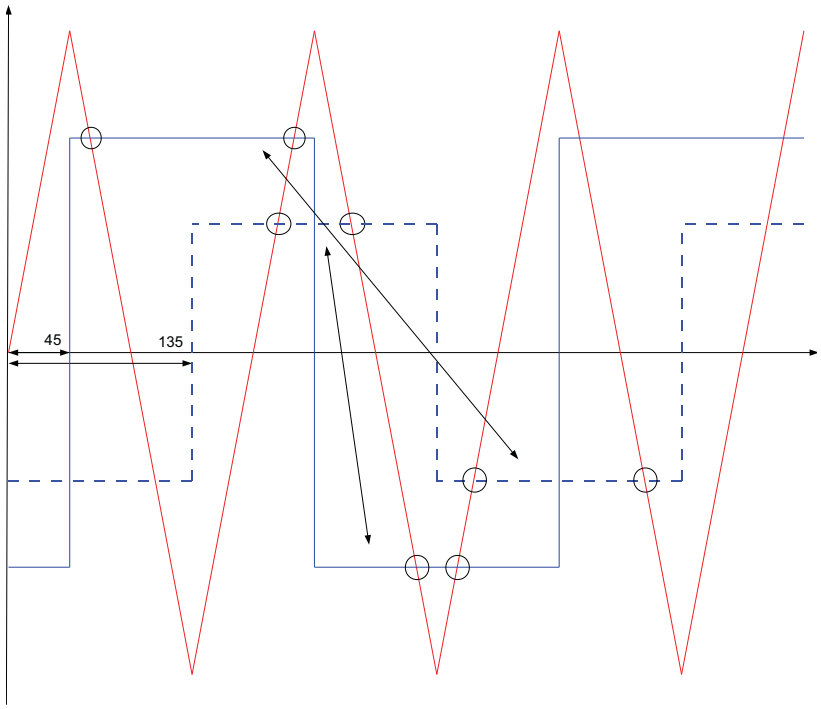

Figure 7.9: Reference displaced with angles of 45 and 135 degrees.

7.3.1.2 Clamp circuit losses

The losses in the clamp circuit is calculated for each case with frequency 10kHz, 5kHz, 2.5kHz and 1kHz, but only with the switching conditions which in the previous section generated the lowest switching losses. Hence four simulations are performed and the result is given in table 7.3. Similar to the switching losses, 10kHz is the case which generates fewer losses in the clamp circuit.

Carrier frequency [kHz]	$P_{resistance}[W]$	$P_{conduction}[W]$	$P_{switching}[W]$	$P_{total}[W]$
10	12.3	1.3	11.9	**25.5**
5	14.4	1.4	13.8	29.7
2.5	13.7	1.6	14.6	29.9
1	39.7	1.4	2.4	43.5

Table 7.3: Clamp losses in operation with CBM

7.3.2 Space vector modulation

7.3.2.1 Switching losses

The SVM has limitations regarding the operational parameters which make it difficult to perform a similar study of the impacts from the frequency and phase displacement as CBM provides. With the modulation method explained in 5.3 the square wave frequency will always be half of the switching frequency of the sinusoidal wave. Simulations are performed to find the relation between the switching frequency and the total losses, the result is showed in figure. As depicted, the total losses decrease approximately linearly from 10 kHz and until the switching frequency reaches 2 kHz, then the losses suddenly increase again. The reason is that the phase currents are highly distorted, and this is reflected in the rms value of the current; the rms value increase from 15A for switching frequency 10kHz to 33A for frequency of 1kHz. The effect of this is higher conduction losses. Actually the conduction losses increase gradually from 10kHz to 2kHz, however since the switching losses decrease with a higher rate, the total losses decrease.

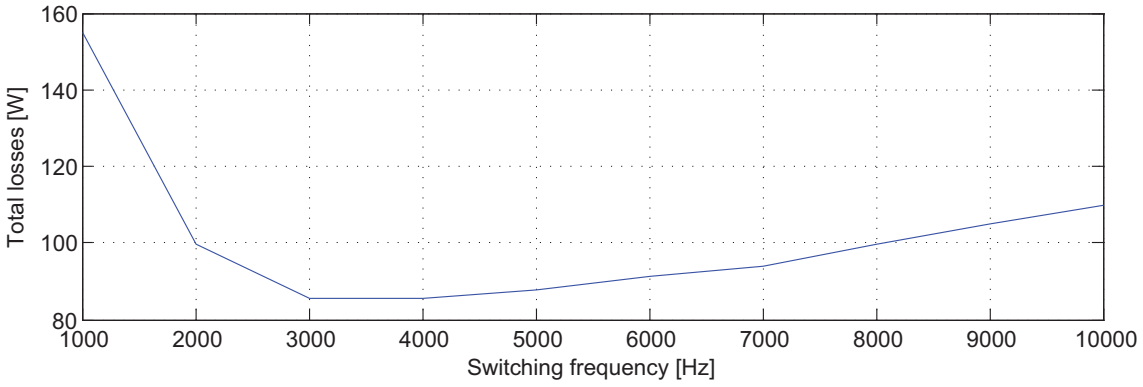

Figure 7.10: SVM: Total losses as a function of switching frequency.

Even if the case where the switching frequency is 10kHz generates higher losses than other frequencies, it is decided to use this for further comparison with the optimal case from carrier based modulation since high switching frequencies lead to fewer harmonics.

7.3.2.2 Clamp losses

Since the case where the switching frequency is 10kHz is the optimal case for SVM, only the result of the clamp losses from this case will be presented. Table 7.4 shows the results.

Switching frequency [kHz]	$P_{resistance}[W]$	$P_{conduction}[W]$	$P_{switching}[W]$	$P_{total}[W]$
10	7.3	1.1	6.2	14.6

Table 7.4: Clamp losses in operation with SVM

7.4 Comparison of carrier based and space vector modulation

7.4.1 Operation

Figure 7.11 and 7.12 depicts the square wave voltage output, the three-phase sinusoidal current input and the line to line voltage harmonics when the RMC is modulated with CBM and SVM respectively. Here it is possible to see that the square wave voltage for SVM has a frequency which is half of the frequency of the square wave signal with CBM. Nevertheless is the switching frequency of the sinusoidal input for both modulation techniques 10kHz. Another observation is regarding the voltage spikes in the square wave voltage. If the voltages for CBM and SVM are compared during the same time period, it can be seen that the voltage for CBM experiences more spikes than for SVM. The reason is that for SVM some of the switches turn on and off when the zero vector which short circuit both the input and the output are applied, thus while the transformer is short circuited. As it was discovered in the observation-part in section 7.2.4 the voltage spikes are then avoided.

In the line to line voltage harmonic spectrum for CBM the fundamental component appears in the frequency which is set as input frequency for the sinusoidal signal, i.e. 50Hz. The same occurs also for SVM. As the switching frequency is set to 10kHz there should also appear harmonics around that frequency [31]. On the other hand, this occurs only for SVM. For CBM there are no harmonics around the switching frequency, but rather around the double of the switching frequency. This should be investigated further. The harmonic spectrum of the square wave voltage is not depicted here, but for both CBM and SVM it appears harmonics around the frequencies determined in the modulation, 10kHz and 5kHz respectively.

Figure 7.13 depicts the modulation characteristic when the RMC is modulated with CBM and SVM.

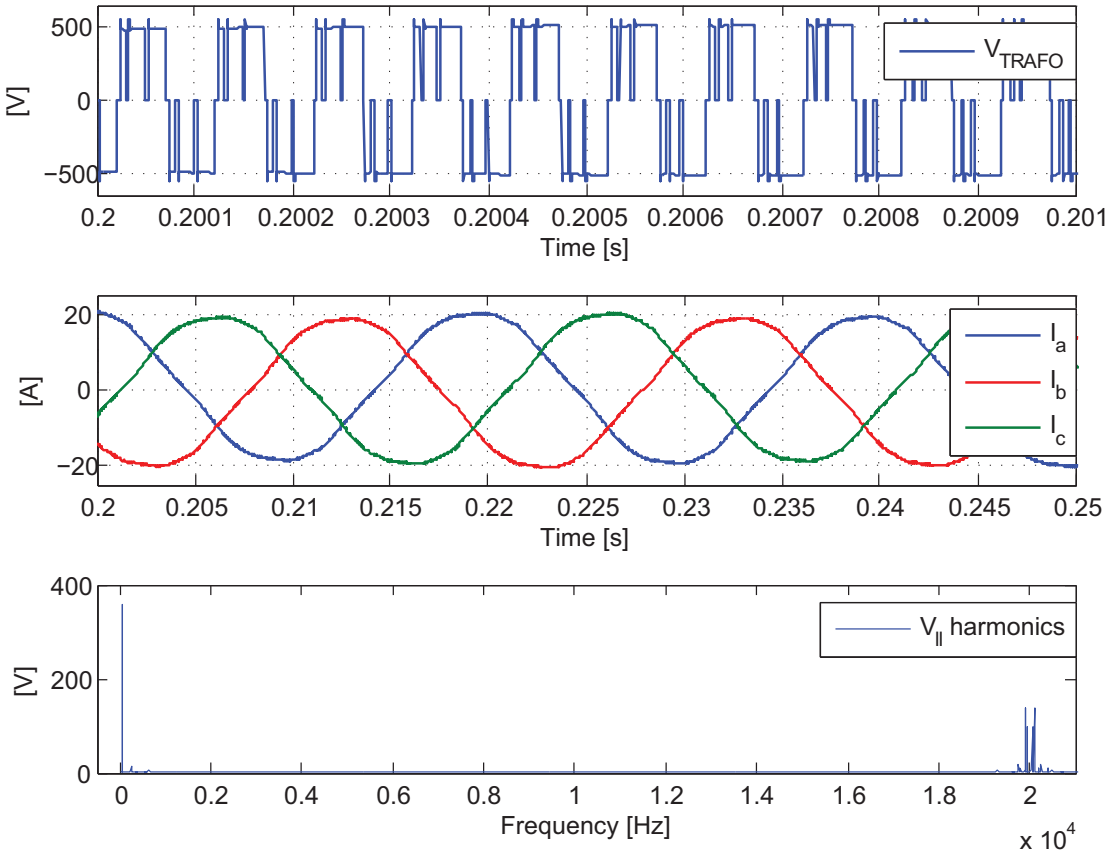

Figure 7.11: CBM: voltage output, current input and voltage input harmonics of the RMC.

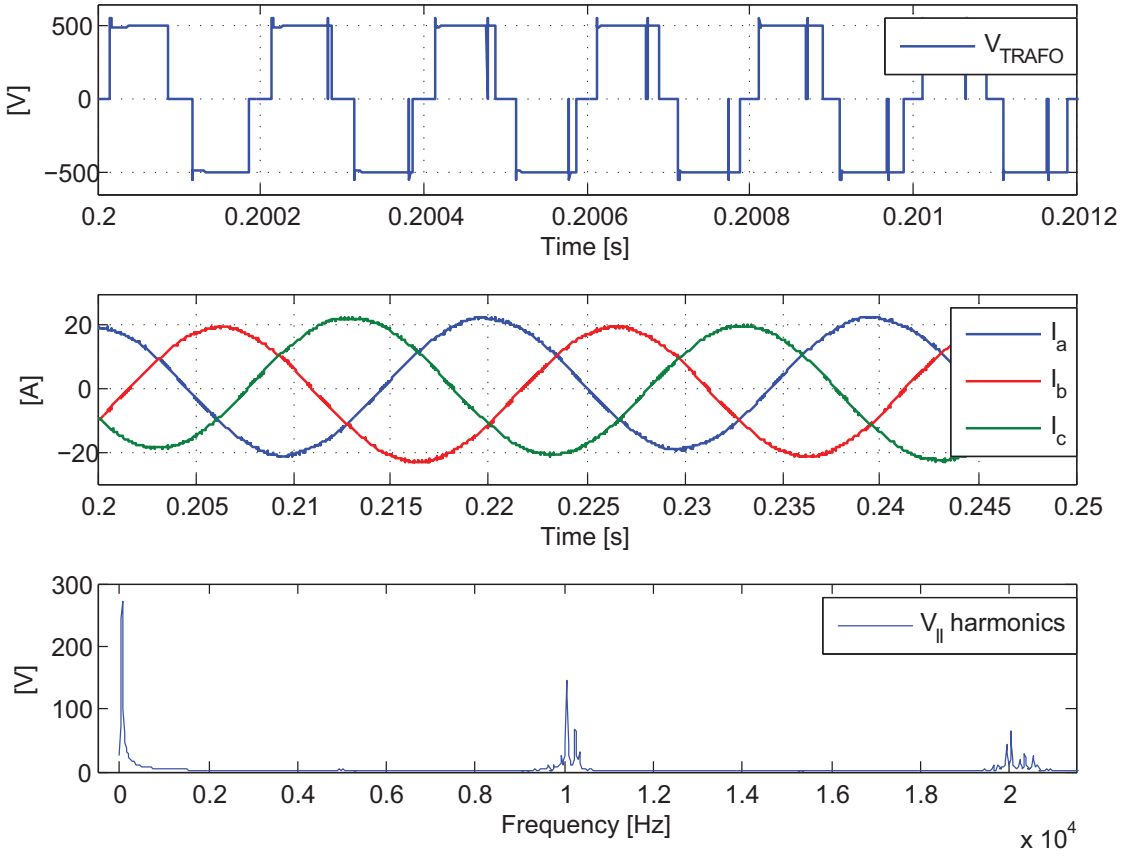

Figure 7.12: SVM: voltage output, current input and voltage input harmonics of the RMC.

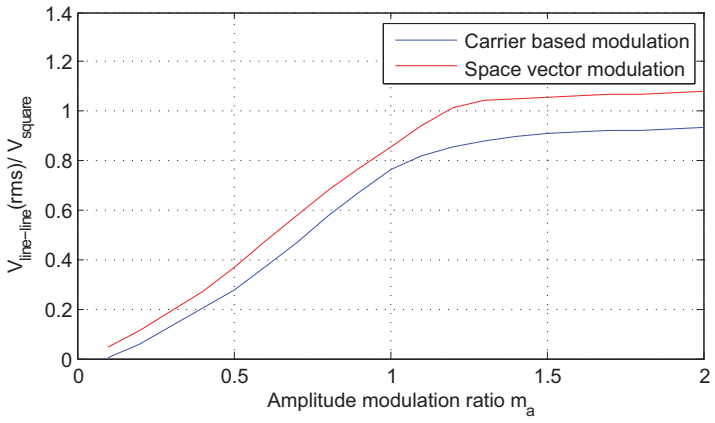

Figure 7.13: Modulation characteristic for RMC modulated with CBM and SVM

7.4.2 Losses

The bars of figure 7.14 show the distribution of losses in carrier based modulation and space vector modulation with switching frequencies 10 kHz. Both modulation techniques give almost the same amount of conduction losses; however the switching losses appear to be quite different. The turn on and turn off losses of CBM are nearly doubled compared to SVM, while the reverse recovery losses in both situations are close to zero. The low switching losses of SVM can be explained with the fact that the transition between the switching states is more efficient and require less switching actions than CBM, both because there are more zero vectors available and also because it is easier to control which zero vector will be utilized. The clamp losses are less when the RMC is modulated with SVM. As the square wave voltage for SVM generates fewer spikes than for CBM this contributes to decrease the clamp losses.

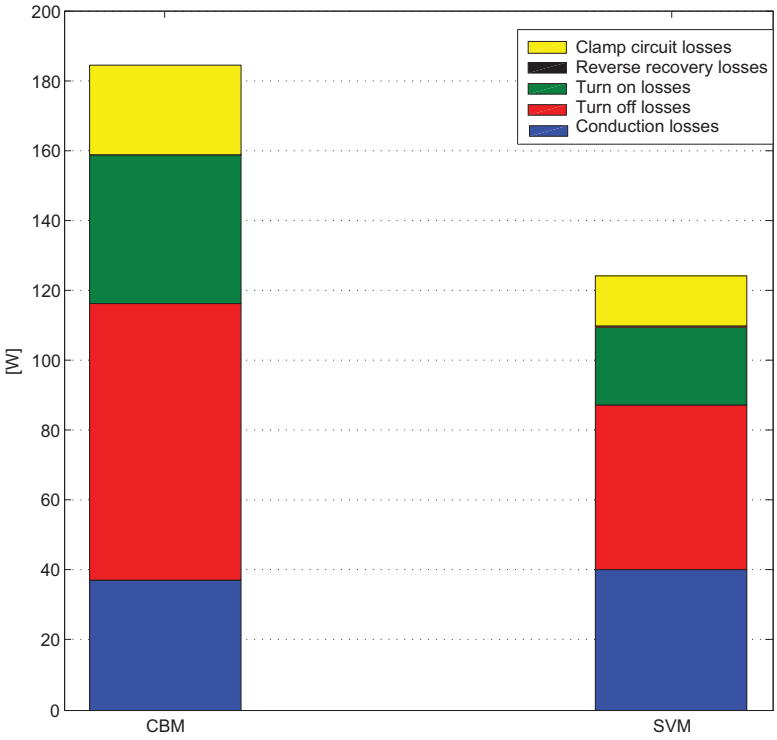

Figure 7.14: Loss distribution for CBM and SVM

Since the operation of the reduced matrix converter does not show any abnormalities and is reliable for both modulation techniques CBM and SVM, it is the switching and clamp losses which is the decisive factor. As the losses generated for SVM are 43 % less than when the RMC is modulated with CBM, the results indicate that operation of the RMC with SVM is the best solution .

7.5 The impacts of overlapping on the switching losses

A remarkable point with the distribution of the switching losses is that compared to the results obtained with CBM in [1] the reverse recovery losses are close to absent, while the turn off losses have increased drastically. The reasons for this are 1) due to the modifications in the modulation where overlapping of the switches is introduced as a method to avoid open-circuit of the transformer, and 2) due to the $L_{leakage}\frac{di}{dt}$ of the transformer which appears every time a switch is turned off. Figure 7.15 depicts the voltage and current waveform when CBM is used to modulate the switches.

When the positive switch turns on, the voltage across it decreases to zero. The current through the switch is at the same time only increasing slightly to contribute to the short circuit current in the leg due to the overlapping of the switches, and will thus not immediately start to lead the phase current. Therefore, instead of calculating the switching loss with the negative directed phase current through the switch, it will be calculated with the short circuit current which is both smaller and in the opposite direction of the phase current. This is the reason why there is a turn on loss instead of a reverse recovery loss, since a switch which has a positive applied voltage in the instant before it is turned on and starts to lead a positive directed current generates turn on losses. However, without the overlapping the switch would have started to lead a negative directed current, and that would have generated reverse recovery losses. Due to the short circuit current the reverse recovery losses are decreased to almost zero compared with the result in [1], and the turn on losses are lower than they normally would be since the short circuit current is much lower than the phase current.

The instant before the negative switch turns off, the switch leads both the positive directed phase current and the short-circuit current. This, in addition to the overvoltage which appears due to the turn off of the switch result in an increase in the turn off losses compared to an ideal situation where both overlapping of the switches and leakage inductance in the transformer could be omitted.

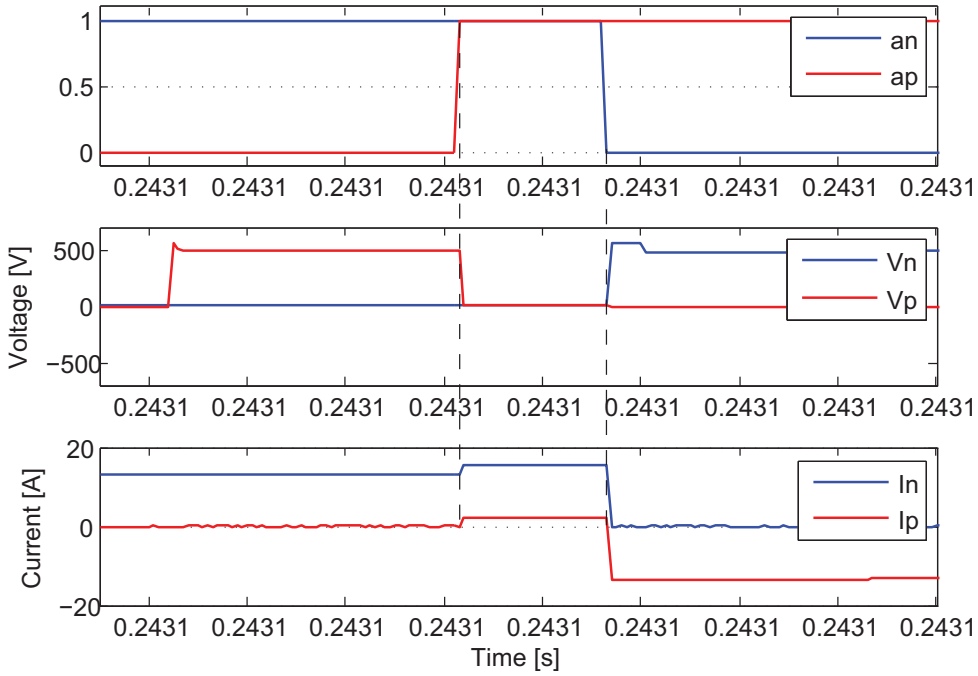

Figure 7.15: Voltage and current waveform in switching

Chapter 8

Conclusion and further work

In this thesis the reduced matrix converter and its operational features have been in focus. It is implemented in a wind energy conversion system for an offshore wind turbine. The WECS follows the direct-drive concept and consists of a permanent magnet generator, the reduced matrix converter, a high frequency transformer and a full-bridge converter. The proposed WECS is more reliable, compact and energy efficient than the WECS of the state of the art for research with indirect-drive, back to back converter and low frequency transformer. First, because the direct-drive concept does not require gearbox with low reliability. Second, the conversion from AC to AC is performed direct by the reduced matrix converter, thus the bulky capacitor which has the highest failure rate of the power electronics equipment can be omitted. Third, because of the high frequency output side of the reduced matrix converter a HF transformer can be implemented instead of the heavier low frequency transformer.

Series connection of the wind turbines in a DC interconnection grid with direct HVDC transmission to shore gives the advantage of making the expensive offshore platform redundant. However, the challenge it presents regarding the reliability has to be considered.

The reduced matrix converter is composed of six switches and is a direct AC-AC converter. It is demonstrated that bi-directional switches are required for this converter. In contrast to the unidirectional switch, the bi-directional switch can withstand voltage of both polarities and allow current in both directions. The bi-directional switch can have different architectures. However, it is the switch topology consisting of two newly developed reverse blocking IGBTs in antiparallel which present the best characteristics. This switch is more compact than the conventional which consists of two diodes and two IGBTs. In addition, the reduced number of semiconductor devices in the switch result in a decrease in the conduction losses.

The structure of the RB-IGBT is different from the conventional IGBT due to the intrinsic diode. It is the intrinsic diode which blocks the voltage when the RB-IGBT is reverse biased. When intrinsic diode portion blocks a reverse biased voltage before or after the RB-IGBT conducts a current, the losses generated in the intrinsic diode portion are reverse recovery losses. When the IGBT portion blocks the forward biased voltage before or after the RB-IGBT conducts a current, the losses generated in the IGBT portion are

turn on or turn off losses.

Since the reduced matrix converter has operational features which is similar to the conventional matrix converter, a special protection scheme is required to assure safe operation of the switches. Normally this protection scheme is only activated during faults. However, due to the non-ideal transformer in the square wave output of the RMC, the protection scheme is also activated during steady state. The protection is implemented by means of a clamp circuit connected to the input and the output of the RMC with two diode bridges.

The clamp circuit consists always of a capacitor. In order to maintain a compact design of the converter, a resistance is implemented in parallel with the capacitor to discharge it. As the resistance produces losses, it is important to find its optimal size. 100Ω is the value which gives the lowest losses in the clamp. The resistance is not continuously discharging the capacitor, but is only connected to the clamp circuit when the capacitor voltage exceeds 550V. The clamp voltage is then maintained around 550V. If the voltage in one of the converter sides increases over 550V, the clamp circuit is immediately activated and absorbs the excess energy. The RB-IGBTs with rating 600V/200A are therefore protected.

The losses in the reduced matrix converter are generated in the bi-directional switches and in the clamp circuit. These losses are important to maintain as low as possible in order to provide an energy efficient converter solution for the WECS. Due to the loss calculation model in [2] an accurate analysis of the switching losses is performed in PSIM, both for the operation when the RMC is modulated with carrier based modulation and space vector modulation. The switching losses in CBM operation were calculated for different frequencies and displacement angles of the carrier of the square wave output. The lowest losses were generated when the frequency of the carrier of the square wave output and the carrier of the sinusoidal input were the same (10kHz) and the carrier of the square wave was displaced 90 degrees with respect to the carrier of the sinusoidal wave. A similar study was performed for SVM operation, although this study was constrained in such a way that the switching frequency of the square wave always was half of the switching frequency of the sinusoidal wave. The optimal result with SVM was when the switching frequency of the sinusoidal signal was 10kHz.

The switching losses and clamp circuit losses were less when the reduced matrix converter was modulated with space vector modulation. Compared to carrier based modulation, the losses were reduced with 43%. The operation of the RMC was similar for both modulation techniques. This indicates that operation of the reduced matrix converter modulated with space vector modulation is the most energy efficient solution.

8.1 Further work

- Verification of the results obtained from the operation of the clamp circuit in steady state through a prototype would confirm the results presented in the thesis and demonstrate the actual behavior of such protection circuit.

- Study of the operation of the clamp circuit during overcurrent and overvoltage faults

in generator and grid side should be performed in the simulation program PSIM.

- Overall study of the system losses.
- Operation and loss study for different wind speeds, and an overall study of the system losses.
- A study of the high frequency transformer.
- Implementation of a control system for the proposed WECS.

Bibliography

[1] M. R. Hanssen. Operation features of a reduced matrix converter for offshore wind power. Technical report, Norwegain University of Science and Technology, 2009.

[2] A. Odaka, J. Itoh, I. Sato, H. Ohguchi, H. Kodachi, N. Eguchi, and H. Umida. Analysis of loss and junction temperature in power semiconductors of the matrix converter using simple simulation methods. In *Industry Applications Conference, 2004. 39th IAS Annual Meeting. Conference Record of the 2004 IEEE*, volume 2, pages 850–855 vol.2, Oct. 2004.

[3] J. Twidell and G. Gaudiosi. *Offshore Wind Power*. Multi-Science Publishing Co. Ltd, 2009.

[4] European Wind Energy Association. Oceans of opportunity. Technical report, 2009.

[5] M.R. Patel. *Wind and solar power systems; design, analysis and operation*. Taylor & Francis, second edition, 2006.

[6] N. Negra, J. Todorovic, and T. Ackermann. Loss evaluation of hvac and hvdc transmission for large offshore wind farms. In *Science Direct*, number 76, pages 916–927, 2005.

[7] BARD Engineering GmbH. Bard offshore 1. `http://www.bard-offshore.de/proj_bard_offshore_1-en.php`, 2009.

[8] A. B. Mogstad. New switching pattern for ac/ac converters with rb-igbts for offshore wind parks. Master's thesis, Norwegain University of Science and Technology, 2008.

[9] F. Besnard, M. Patriksson, A.-B. Stromberg, A. Wojciechowskit, and L. Bertling. An optimization framework for opportunistic maintenance of offshore wind power system. In *PowerTech, 2009 IEEE Bucharest*, pages 1 –7, july 2009.

[10] S. Vestgaard. Offshore technology/operation maintenance - accessibility. In *Proc. Copenhagen Offshore Wind 05*, 2005.

[11] G.J.W van Bussel and W.A.A.M Bierbooms. The dowec offshore reference windfarm: analysis of transportation for operation and maintenance. In *Wind Engineering*, 2003.

[12] Z. Chen, J.M. Guerrero, and F. Blaabjerg. A review of the state of the art of power electronics for wind turbines. *Power Electronics, IEEE Transactions on*, 24(8):1859 –1875, aug. 2009.

[13] Siemens. New siemens direct drive wind turbine ready for sale. `http://www.siemens.com/press/en/pressrelease/?press=/en/pressrelease/2010/renewable_energy/ere201004062.htm`, April 2010.

[14] T Ashuri and M.B Zaaijer. Reviews of design concept, methods and considerations of offshore wind turbines. *Presentation of the European Offshore Wind Conference*, 2007.

[15] M.Y. Lee, P. Wheeler, and C. Klumpner. A new modulation method for the three-level-output-stage matrix converter. In *Power Conversion Conference - Nagoya, 2007. PCC '07*, pages 776 –783, april 2007.

[16] S. Yang, A. Bryant, P. Mawby, D. Xiang, L. Ran, and P. Tavner. An industry-based survey of reliability in power electronic converters. In *Energy Conversion Congress and Exposition, 2009. ECCE 2009. IEEE*, pages 3151 –3157, sept. 2009.

[17] IXYS. Igbt with reverse blocking capability. `http://ixdev.ixys.com/DataSheet/L601.pdf`.

[18] C. Klumpner and F. Blaabjerg. Short term braking capability during power interruptions for integrated matrix converter-motor drives. *Power Electronics, IEEE Transactions on*, 19(2):303 – 311, march 2004.

[19] A. Garce? ands and M. Molinas. Impact of operation principle on the losses of a reduced matrix converter for offshore wind parks. In *Industrial Electronics (ISIE), 2010 IEEE International Symposium on*, pages 2412 –2419, 2010.

[20] W.-J. Gu and R. Liu. A study of volume and weight vs. frequency for high-frequency transformers. In *Power Electronics Specialists Conference, 1993. PESC '93 Record., 24th Annual IEEE*, pages 1123 –1129, June 1993.

[21] E. Veilleux. Interconnection of direct-drive wind turbines using a series connected dc grid. Master's thesis, University of Toronto, 2009.

[22] BARD Engineering GmbH. Trafo platform. `http://www.bard-offshore.de/en/concept/operation/transformer-platform`.

[23] DONG Energy. Horns rev 2 taking offshore wind energy to the next level. `http://www.dongenergy.com/en/business\%20activities/generation/electricity\%20generation/wind/pages/horns_rev_2.aspx`.

[24] P.W. Wheeler, J. Rodriguez, J.C. Clare, L. Empringham, and A. Weinstein. Matrix converters: a technology review. *Industrial Electronics, IEEE Transactions on*, 49(2):276 –288, april 2002.

[25] R. Garcia-Gil, J.M. Espi, E.J. Dede, and E. Sanchis-Kilders. A bidirectional and isolated three-phase rectifier with soft-switching operation. *Industrial Electronics, IEEE Transactions on*, 52(3):765 – 773, june 2005.

[26] C. Klumpner and F. Blaabjerg. Using reverse blocking igbts in power converters for adjustable speed drives. In *Industry Applications Conference, 2003. 38th IAS Annual Meeting. Conference Record of the*, volume 3, pages 1516–1523 vol.3, Oct. 2003.

[27] M. Takei, T. Naito, and K. Ueno. Reverse blocking igbt for matrix converter with ultra-thin wafer technology. *Circuits, Devices and Systems, IEE Proceedings* -, 151(3):243–247, June 2004.

[28] M. Vellvehi, J.L. Galvez, X. Perpina, X. Jorda, P. Godignon, and J. Millan. Trench isolation technique for reverse blocking igbt using boron nitride doping wafers. In *Power Electronics and Applications, 2009. EPE '09. 13th European Conference on*, pages 1–5, Sept. 2009.

[29] A.; Fujimoto S. Takei, M.; Odaka. Application technologies of reverse-blocking igbt. *Fuji Electric Journal*, 75(8), June 2002.

[30] P. J. Grbovic, F. Gruson, N. Idir, and P. Le Moigne. Turn-on performance of reverse blocking igbt (rb-igbt) and optimization using advanced gate driver. In *Power Electronics, IEEE Transactions on : Accepted for future publication*, volume PP, pages 1–1, 2009.

[31] N. Mohan, T. Undeland, and W.P. Robbins. *Power Electronics; Converters, applications and Design*. John Wiley and Sons, Inc., third edition, 2003.

[32] M. Takei, Y. Harada, and K. Ueno. 600 v-igbt with reverse blocking capability. In *Power Semiconductor Devices and ICs, 2001. ISPSD '01. Proceedings of the 13th International Symposium on*, pages 413–416, 2001.

[33] A. Garces and M. Molinas. High frequency wind energy conversion from the ocean. In *Power Electronics Conference (IPEC), 2010 International*, pages 2056 –2061, june 2010.

[34] N. Mohan. *Advanced Electric Drives*. Mnpere, 2001.

[35] P. Nielsen. *The Matrix Converter for an Inductive Motor Drive*. PhD thesis, Aalborg University, 1996.

[36] J. Mahlein, M. Bruckmann, and M. Braun. Passive protection strategy for a drive system with a matrix converter and an induction machine. *Industrial Electronics, IEEE Transactions on*, 49(2):297 –303, april 2002.

[37] K. You and F. Rahman. Over-voltage protection using power zener diode for matrix converter and matrix-z-source converter. In *Power Electronics and Drive Systems, 2009. PEDS 2009. International Conference on*, pages 193 –197, 2009.

[38] L. Empringham, L. de Lillo, P.W. Wheeler, and J.C. Clare. Matrix converter protection for more electric aircraft applications. In *IEEE Industrial Electronics, IECON 2006 - 32nd Annual Conference on*, pages 2564 –2568, 2006.

[39] A.M. Trzynadlowski. *Introduction to Modern Power Electronics*. John Wiley and Sons, Inc., second edition, 2010.

[40] P. Nielsen, F. Blaabjerg, and J.K. Pedersen. New protection issues of a matrix converter: design considerations for adjustable-speed drives. *Industry Applications, IEEE Transactions on*, 35(5):1150 –1161, sep/oct 1999.

[41] V. Benda, J. Gowar, and D.A Grant. *Power semiconductor devices: theory and applications*. John Wiley and Sons, Inc., second edition, 1999.

[42] A.I Pressman, K.H Billings, and T. Morey. *Switching Power Supply Design*. The McGraw-Hill Companies, third edition, 2009.

[43] J. Andreu, J.M. De Diego, I.M. de Alegria, I. Kortabarria, J.L. Martin, and S. Ceballos. New protection circuit for high-speed switching and start-up of a practical matrix converter. *Industrial Electronics, IEEE Transactions on*, 55(8):3100 –3114, aug. 2008.

[44] J-K. Kang, H. Hara, E. Yamamoto, and E. Watanabe. Analysis and evaluation of bi-directional power switch losses for matrix converter drive. In *Industry Applications Conference, 2002. 37th IAS Annual Meeting. Conference Record of the*, 2002.

[45] A.R. Garces and M. Molinas. Investigation and losses comparison of a reduced matrix converter for off-shore turbines. *5th IET International Conference on Power Electronics, Machines and Drives, PEMD*, April 2010.

Appendix A

Simulation parameters

PM generator

Type	Sinusoidal voltage source
Resistance	0.041239Ω
Inductance	$10.50{\cdot}10^{-3}H$

Table A.1: PM generator data

Clamp circuit

Resistance	100Ω
Capacitor	$300{\cdot}10^{-6}F$

Table A.2: Clamp circuit data

HF transformer

Type	Single-phase transformer
Resistance primary winding	0.01Ω
Resistance secondary winding	0.01Ω
Leakage inductance primary winding	$1.7090{\cdot}10^{-6}H$
Leakage inductance secondary winding	$1.7090{\cdot}10^{-6}H$
Magnetizing inductance seen from primary winding	0.0036H
Number of turns of the primary winding	1
Number of turns of the secondary winding	1

Table A.3: HF transformer data

Appendix B

Loss calculation method

To calculate the losses in the reduced matrix converter it is necessary with four different measurements for each bi-directional switch in order to decide which category the losses belong to. These categories are conduction losses, reverse recovery losses of the intrinsic diode portion and turn on and turn off losses of the IGBT portion.

Two of the four aforementioned measurements needed for each switch are the voltage between collector and emitter, and the current in the collector in the instance *t*. These values are calculated with the RMC model in PSIM, and the information is then sent to a Dynamic Link Library (DLL) file. Since PSIM sends the information to the DLL-file for each time step *dt* it takes, it is already stored information about the two other measurements needed: the voltage and current from the time step precedent to *t*, i.e. *t-dt*. Thereafter, the c++ code in the DLL-file classifies loss category by comparing the measurements from *t-dt* and *t*. It can then calculate the losses and store them for the next time steps in such a way that the total losses within each category can be summarized in the end.

The loss calculations in the DLL-file are based on the equations from [2], which is characterized for a RB-IGBT (600V/200A). Conduction losses are calculated as for a conventional IGBT, with the equation for power dissipation.

$$P_{cond} = V_{ce} \cdot I_c \tag{B.1}$$

V_{ce}: voltage between collector and emitter, I_c: collector current

Where V_{ce} is calculated as follows, according to [45]:

$$V_{ce} = A + B \cdot I_c + C \cdot I_c^2 \tag{B.2}$$

Where $A = 22.789, B = 28.536, C = -32.091$ are extracted from [2]

The turn on, turn off and reverse recovery energy losses are calculated with equation (B.3), and are as well as the conduction losses a function of the voltage across the RB-IGBT and the current flowing through it.

$$E = k_1 \cdot I_c^2 + k_2 \cdot I_c \tag{B.3}$$

E: energy loss in MJ, k_1 and k_2: constants characterized for each loss category.

In [2] k_1 and k_2 is defined for each loss category as follows:

Turn on loss:

$$k_1 = (8.14 \times 10^{-12}) \cdot V_{ce}^2 + (1.78 \times 10^{-7}) \cdot V_{ce} \tag{B.4}$$

$$k_2 = (2.78 \times 10^{-7}) \cdot V_{ce}^2 + (1.32 \times 10^{-5}) \cdot V_{ce} \tag{B.5}$$

Turn off loss:

$$k_1 = (4.77 \times 10^{-8}) \cdot V_{ce} + (4.92 \times 10^{-5}) \tag{B.6}$$

$$k_2 = (-2.98 \times 10^{-9}) \cdot V_{ce}^2 + (2.11 \times 10^{-4}) \cdot V_{ce} \tag{B.7}$$

Reverse recovery loss:

$$k_1 = (-5.66 \times 10^{-11}) \cdot V_{ce}^2 + (-1.82 \times 10^{-7}) \cdot V_{ce} \tag{B.8}$$

$$k_2 = (3.73 \times 10^{-9}) \cdot V_{ce}^2 + (9.35 \times 10^{-5}) \cdot V_{ce} \tag{B.9}$$

The turn on, turn off and reverse recovery losses have to be converted to the same unity as the conduction losses, in that way it is possible to compare them. The conversion is done with equation (B.10).

$$E = \frac{dW_{loss}}{dt} \Rightarrow dW_{loss} = Edt \tag{B.10}$$

dW: the instantaneous power dissipated in the time period dt, E: the energy dissipated.

Until now the instantaneous power losses for all of the four groups is calculated. To obtain the average power loss, independent of the total time period which is simulated in PSIM, the instantaneous losses have to be averaged, this is done by dividing each loss category with the time period for sinusoidal input 0.02s, as in (B.11).

$$W_{loss} = \frac{\sum dW_{loss}}{T_p} = \frac{\int Edt}{T_p} \tag{B.11}$$

W_{loss}: average power loss within one category, T_p:total time period sinusoidal input.

Appendix C

Related papers

During the work with the specialization project a paper was accepted for the conference ISIE 2010 in Bari, Italy and presented orally July 2010. The paper had the title "Operation features of a reduced matrix converter for offshore wind power". Later an invitation to submit a modified version of the paper to the special section devoted to ISIE 2010 in IEEE Transaction on Industrial Electronics was recevied. This paper has the title "Characterization of a Reduced Matrix Converter for Offshore Wind Power" and is still under revising. Both papers are included and can be found at the following pages.

Operation Features of a Reduced Matrix Converter for Offshore Wind Power

Mari Røed Hanssen, Alejandro Garces Ruiz, Marta Molinas
Department of Electrical Engineering
NTNU
Trondheim, Norway
Email: mariroed@stud.ntnu.no

***Abstract*—The reduced matrix converter (RMC) implemented in offshore wind power conversion system is investigated in this paper. The RMC is built with 6 bi-directional switches, and the losses produced by these switches are compared under different conditions. Each bi-directional switch is made up by two RB-IGBTs in antiparallel, and it is studied how the special structure of the RB-IGBT will affect the total losses of the switch. The entire offshore wind power conversion system is modeled in PSIM. The first conversion stage after the wind turbine is direct ac-ac conversion by the reduced matrix converter. Thereafter a high frequency square wave voltage is fed into a transformer. Due to the high frequency, the transformer will have reduced weight, which is an important aspect of the lightweight and compact component requirements for offshore wind turbine installations. After the transformer the second conversion stage is carried out. This is done by a full-bridge converter where the output is dc voltage, for enabling series connection of wind turbines in dc. The study is aimed at the achievement of an energy efficient converter, with high power density and reliability.**

I. Introduction

The oceans cover approximately two thirds of the earth surface, and will be a great resource for generating energy from renewable sources in the future. The wind conditions in the open ocean is better than on land because the wind velocity is 30 to 40 % higher, and the wind is also more steady and less turbulent [1]. However, challenges in offshore wind power are more severe than in onshore wind power: the components have to be compact, lightweight and highly reliable. According to [2], for distances longer than 55-70 km, high voltage DC transmission to shore will be a cheaper and more efficient solution than high voltage ac transmission . The proposed conversion system in this paper is based on a long transmission line with HVDC.

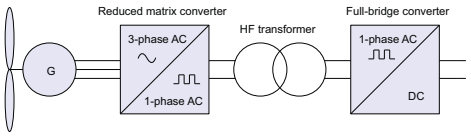

Fig. 1. The offshore wind power conversion system

The wind power conversion system discussed in this paper and depicted in figure 1, is build up with direct ac-ac conversion, where the ac output from the converter is rectified in order to obtain a dc voltage. The dc voltage is the output from the nacelle of the wind turbine, and is connected in series with the dc outputs from the other turbines in order to increase the voltage to a suitable level for high DC voltage transmission to on-shore. The direct ac-ac conversion makes it possible to omit the bulky dc-link capacitor and with high frequency voltage the weight of the transformer can be reduced [3].

Power losses are an important issue when it comes to conversion of energy. In this paper the losses generated by the bi-directional switches of ac/ac converter will be investigated by a simulation model in PSIM. There are several topolgies for bi-directional switches, where two of them is depicted in figure 2(b) and (c). In this paper the newly developed bidirectional switch with two reverse blocking IGBTs (RB-IGBT) connected in antiparallel will be investigated. In [4] it is shown how changing the design of the bi-directional switch from the conventional with two IGBts with antiparalleled diodes to the new one with two RB-IGBTs in antiparallel can reduce the total losses.

II. The converter topology

The reduced matrix converter discussed in this paper is a direct ac-ac converter with 3-phase sinusoidal wave as input and 1-phase high frequency square wave as output, see figure 2(a). The switches are controlled by a modified version of standard pulse width modulation (PWM) [3]. The RMC consist of six bi-directional switches, which are different from the

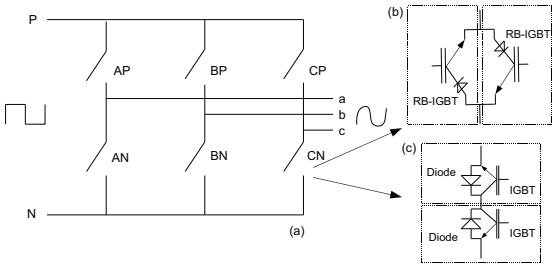

Fig. 2. (a) Reduced matrix converter with bi-directional switches, either as in (b) or as in (c)

standard IGBTs with freewheeling diodes because they are able to block the same voltages of both polarities. This special attribute of the bi-directional switch is necessary when both the output and the input of the converter is ac.

A. Reverse blocking IGBT

The RB-IGBT used in a bi-directional switch has a structure similar to another version of the IGBT, the non-punch-through IGBT (NPT-IGBT). The NPT-IGBT can also sustain blocking voltages of both polarities, but it has a high leakage current in reverse bias which is generated due to the severe roughness remaining after the mechanical dicing process. To prevent this leakage current, the RB-IGBT has an extra isolation layer made by extending the bottom p^+-region to include the vertical dicing sides of the device. The p^+-isolation region together with the n^--drift region constitute what can best be characterized as an intrinsic diode of the device [5]. The vertical cross section of the structure of one of the half cells of a RB-IGBT is depicted in figure 3(a). This design of a RB-IGBT is named isolation type, and is the one which are open for commercial use [6].

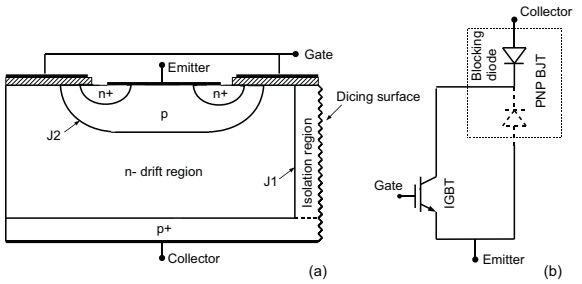

Fig. 3. (a) Vertical cross section of the structure of a half cell, and (b) equivalent circuit of the RB-IGBT

B. Operation of the RB-IGBT

In an equivalent circuit of the RB-IGBT, the intrinsic diode can be extracted from the model. It will then appear in series connection with the IGBT portion of the transistor, and together with the diode drawn with a dashed line the intrinsic diode also constitutes the bipolar junction transistor portion of the device, see figure 3(b). Even if the intrinsic diode appears as an external part to the rest of the model, it is important to remember that the diode "does not exist physically in the switch module" [5].

The operation of the intrinsic diode in the RB-IGBT demonstrates that the diode does not operate as a conventional, external diode. The intrinsic diode is dependent on the off and on-state of the RB-IGBT: even if the diode is forward biased it cannot conduct when the RB-IGBT is turned off, and when the diode is reverse biased it does not have to be forward biased to start to conduct; it is enough that the RB-IGBT is switched on, so that the voltage across the element goes to zero.

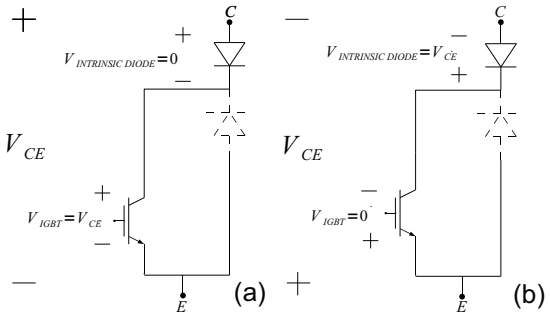

Fig. 4. (a) RB-IGBT is forward biased, (b) RB-IGBT is reverse biased

In figure 4 there is depicted two situations in which the RB-IGBT is in off state. In (a) the RB-IGBT is forward biased, and the voltage will be blocked by junction 2 (J2), see figure 3(a). The RB-IGBT operates like a conventional IGBT, and all the collector emitter voltage will be across the IGBT portion of the RB-IGBT. The intrinsic diode has no special function in this case, since a conventional IGBT can withstand high positive voltages. If the IGBT switches under this condition it will constitute a hard switching. In (b) the RB-IGBT is in reverse bias, and junction 1 (J1) in figure 3(a), i.e. the intrinsic diode, will block the voltage. The result is zero voltage across the IGBT portion of the RB-IGBT, because the intrinsic diode withstands all the negative collector emitter voltage alone. If the IGBT switches under this condition it will constitute a soft switching.

C. Losses in the RB-IGBT

The losses generated in a RB-IGBT can be divided into two categories: the conduction losses and the switching losses. While the switching losses in a conventional IGBT are generated due to the hard switching of the device, the RB-IGBT can either have a hard or soft switching transient. The hard switching occurs when the RB-IGBT operates as an IGBT, i.e. that the device is forward biased before switching it on or after switching it off. The natural soft switching feature of the RB-IGBT is a special attribute of the device. The soft switching occurs when the RB-IGBT is reverse biased so that all the collector emitter voltage is across the intrinsic diode portion of the device, as in figure 4(b). When the RB-IGBT is turned on, the voltage across the IGBT portion is constant zero, while the voltage transient of the intrinsic diode change from V_{ce} to zero in a finite time. This generates what is called reverse recovery losses in the intrinsic diode of the RB-IGBT. In a conventional diode the reverse recovery losses is connected to the turn off period of the device, but for the intrinsic diode these losses are generated both by turn on and turn off.

In [4] simulation methods to calculate losses for a RB-IGBT (600V/200A) have been suggested. In the loss characteristics reported, it has been measured that reverse recovery losses of the intrinsic diode are lower than turn on and turn off losses of the IGBT portion of the device.

III. Operation of the reduced matrix converter

The entire model of the offshore wind power conversion system is investigated by a simulation model built in PSIM. While the power flow in a power generating system normally is from the generator to the grid side, the power flow in this model will be in the opposite direction for simulation purposes. The reason is that the generator is replaced with a motor. The motor is of type squirrel cage induction machine, and delivers the power to the input of the reduced matrix converter, which from now will be the sinusoidal 3-phase side. The voltage from the square wave output is fed into a high frequency transformer which further is transformed into dc voltage by the full-bridge converter. The dc grid is modeled as a dc voltage source.

A. Switching scheme

Figure 5 shows the modified carrier based PWM algorithm which is used to modulate the switches of the reduced matrix converter and the full-bridge converter [9]. In order to generate switching signals for the full-bridge converter, its associated carrier signal is compared with zero: when the carrier is greater than zero the switches which generate positive voltage signals are turned on, and when the carrier is lower than zero the switches which generate negative voltage signals are turned on. The carrier of the full-bridge (carrier F-B) is a triangular signal as in equation 1 with a phase angel that can be varied. The path of the reference signals for phase a,b and c in the reduced matrix converter depends on the position of carrier F-B compared to the zero x-axis. If carrier F-B is greater than zero, the reference signals will be multiplied with $+1$ and thus continue as normal, on the other hand, if carrier F-B is lower than zero, the reference signals of the RMC will be multiplied with -1, and thus be inverted. Further, the reference signals for each phase a, b and c are compared with the carrier of the RMC, a triangular signal as in equation 2, in order to turn on or off the bi-directional switches. The reference signals for each phase follow equation 3 with a constant frequency of 50 Hz.

$$y_{R-B}\left(t\right) = 1 - \frac{2}{\pi} \cdot arccos(sin(2 \cdot \pi \cdot f \cdot t - \theta)) \quad (1)$$

$$y_{RMC}\left(t\right) = 1 - \frac{2}{\pi} \cdot arccos(sin(2 \cdot \pi \cdot f \cdot t)) \quad (2)$$

θ is the phase angle between carrier F-B and carrier RMC.

$$x_{RMC}\left(t\right) = m_a \cdot sin(2 \cdot \pi \cdot f \cdot t + \varphi) \quad (3)$$

Where φ is 0° for phase a, 120° for phase b and -120° for phase c, m_a is the amplitude.

In [3] the special switching pattern based on PWM for the reduced matrix converter is explained more thoroughly.

B. Modulation characteristics

The modulation curve is a function of the voltage ratio, presented at the y-axis, and modulation amplitude ratio, presented at the x-axis. The voltage ratio is found by dividing the peak line to line output voltage to the peak input voltage. The curve is made by trying different modulation amplitudes in the model in PSIM, which means by changing the amplitude of the reference signal, while the carrier has constant amplitude equal to one.

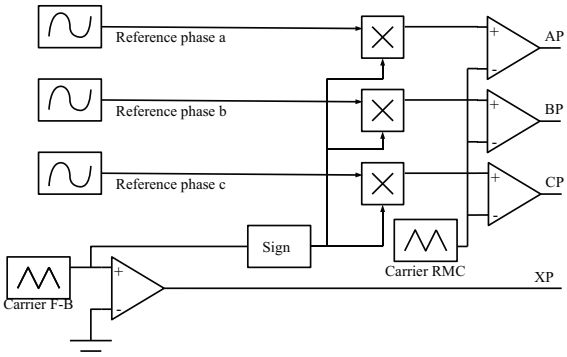

Fig. 5. Switching of the RMC and full-bridge converter

The result in figure 6 shows a curve which is linear until the modulation amplitude ratio reaches 1. From amplitude equal to 1 it is overmodulated, and the curve is no longer linear. After 1.2 the output line to line voltage stop increasing, see figure 8, and that is the reason why the modulation amplitude curve is straight from that time on.

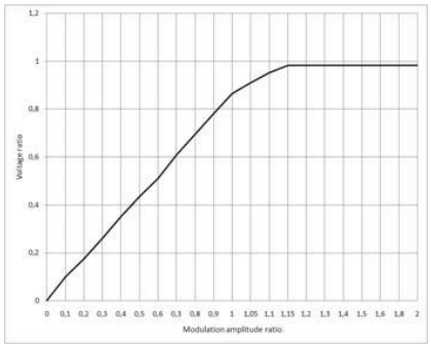

Fig. 6. Modulation characteristic for RMC

The reason to the overmodulated system can be explained by the definition of modulation amplitude ratio m_a.

$$m_a = \frac{V_{reference}}{V_{carrier}} \quad (4)$$

Where $V_{reference}$ is the peak amplitude of the reference signal, and $V_{carrier}$ is the peak value of the carrier signal.

When the amplitude of the sinusoidal reference signal is greater than the amplitude of the triangular carrier signal, there will be a period where the reference signal is higher than the carrier signal. Then the reference signal will cross the carrier signal in the same height on the triangular curve for each time it is inverted, see figure 7, this result in a switch duty ratio which is constant for each period of the carrier signal in this

specific time period. The consequence is that the output pulses after a short time will be generated with the same time interval, the sinusoidal output stops increasing and the top of it is cut right over with a straight line; the signal is overmodulated. The signal will continue being overmodulated until the reference signal again is lower than the carrier. Figure 8 shows how the line to line voltage of the output acts when the converter is overmodulated and the amplitude modulation ratio is equal to 1.5, the red line is the sinusoidal curve which represents the pulses when they are fed into a second-order low pass filter, and figure 9 shows the distorted current.

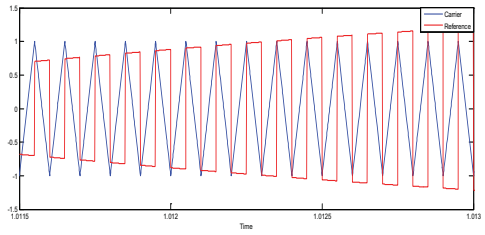

Fig. 7. Carrier and reference signal with $m_a = 1.5$

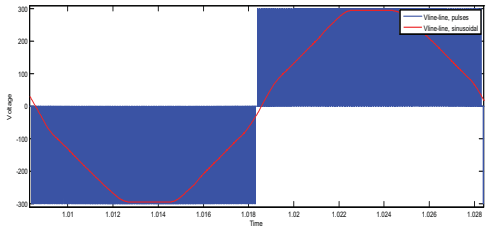

Fig. 8. Line to line voltage output with $m_a = 1.5$

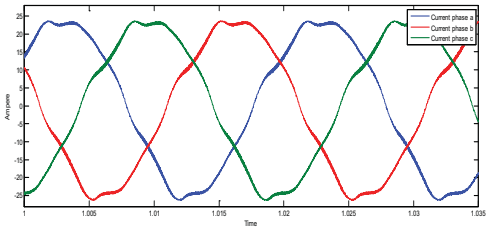

Fig. 9. Current output with $m_a = 1.5$

IV. Loss model for the reduced matrix converter

To calculate the losses in the reduced matrix converter it is necessary with four different measurements for each bidirectional switch in order to decide which category the losses belong to. These categories are conduction losses, reverse recovery losses of the intrinsic diode and turn on or turn off losses of the bidirectional switch.

Two of the four aforementioned measurements needed for each switch are the voltage between collector and emitter, and the current in the collector in the instance *t*. These values are calculated with the RMC model in PSIM, and the information is then sent to a Dynamic Link Library (DLL) file. Since PSIM sends the information to the DLL-file for each time step *dt* it takes, it is already stored information about the two other measurements needed: the voltage and current from the time step precedent to *t*, i.e. *t-dt*. Thereafter, the code in the DLL-file classifies loss category by comparing the measurements from *t-dt* and *t*. It can then calculate the losses and store them for the next time steps in such a way that the total losses within each category can be summarized in the end.

The calculations in the DLL-file are based on the equations from [4], which is characterized for a RB-IGBT (600V/200A). Conduction losses are calculated as for a conventional IGBT, with the equation for power dissipation.

$$P_{cond} = V_{ce} \cdot I_c \tag{5}$$

V_{ce}: voltage between collector and emitter, I_c: collector current

Where V_{ce} is calculated as follows:

$$V_{ce} = A + B \cdot I_c + C \cdot I_c^2 \tag{6}$$

Where $A = 22.789, B = 28.536, C = -32.091$ are extracted from [4]

The turn on, turn off and reverse recovery energy losses are calculated with equation (7), and are as well as the conduction losses a function of the voltage across the transistor and the current flowing through it.

$$E = k_1 \cdot I_c^2 + k_2 \cdot I_c \tag{7}$$

E: energy loss in MJ, k_1 and k_2: constants characterized for each loss category.

In [4] k_1 and k_2 is defined for each category as follows:

Turn on loss:

$$k_1 = (8.14 \times 10^{-12}) \cdot V_{ce}^2 + (1.78 \times 10^{-7}) \cdot V_{ce} \tag{8}$$

$$k_2 = (2.78 \times 10^{-7}) \cdot V_{ce}^2 + (1.32 \times 10^{-5}) \cdot V_{ce} \tag{9}$$

Turn off loss:

$$k_1 = (4.77 \times 10^{-8}) \cdot V_{ce} + (4.92 \times 10^{-5}) \tag{10}$$

$$k_2 = (-2.98 \times 10^{-9}) \cdot V_{ce}^2 + (2.11 \times 10^{-4}) \cdot V_{ce} \tag{11}$$

Reverse recovery loss:

$$k_1 = (-5.66 \times 10^{-11}) \cdot V_{ce}^2 + (-1.82 \times 10^{-7}) \cdot V_{ce} \tag{12}$$

$$k_2 = (3.73 \times 10^{-9}) \cdot V_{ce}^2 + (9.35 \times 10^{-5}) \cdot V_{ce} \tag{13}$$

The turn on, turn off and reverse recovery losses have to be converted to the same unity as the conduction losses so they can be easily compared, then the instantaneous power losses within all of the four groups is obtained. In order to calculate the average power loss, the instantaneous losses have to be averaged, this is done by dividing each loss category with the total simulated time period.

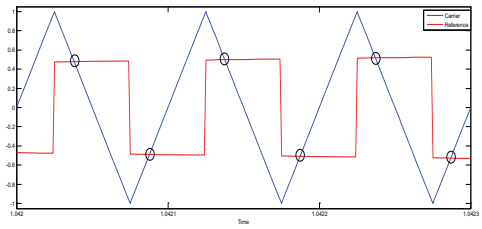

Fig. 10. Case 1: Switching actions, F-B carrier frequency=10 kHz, angel=90

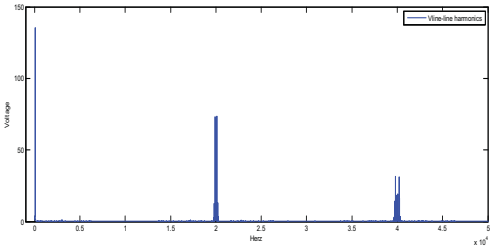

Fig. 11. Case 1: $V_{line-line}$-harmonics in range from 0 to 50 kHz

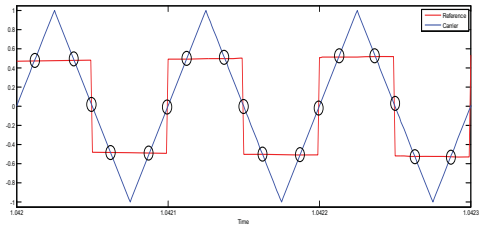

Fig. 12. Case 2: Switching actions, F-B carrier frequency=10 kHz, angle=0

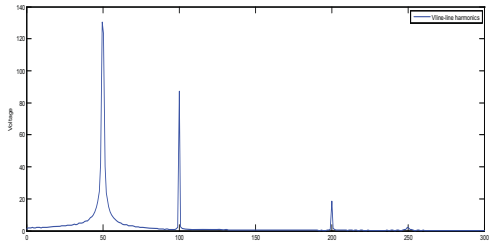

Fig. 13. Case 2: $V_{line-line}$-harmonics in range from 0 to 300 Hz

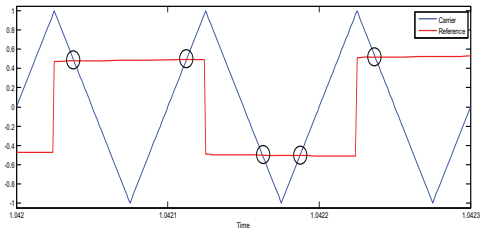

Fig. 14. Case 3: Switching actions, F-B carrier frequency 5 kHz, angle=45

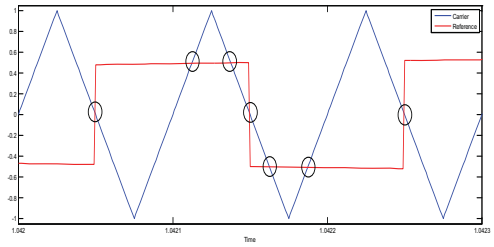

Fig. 15. Case 4: Switching actions, F-B carrier frequency 5 kHz, angle=90

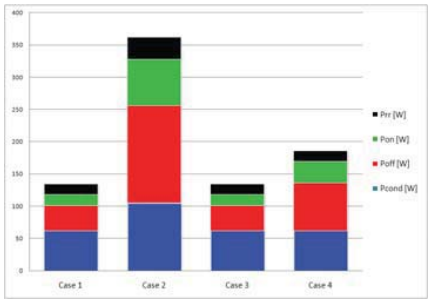

Fig. 16. Total losses for case 1, 2, 3 and 4

1) Switching conditions for Reduced Matrix Converter: The switching conditions are tested in two different situations. In situation 1 the system is tested with same carrier frequencies for both converters, and in situation 2 the system is tested with different carrier frequencies, respectively 10 kHz in the RMC and 5 kHz in the full-bridge. In both situations the phase angle between the carriers is varied in order to obtain an optimal and a non-optimal condition. In total there will be four cases, where case 1 and 2 represent situation 1, and case 3 and 4 represent situation 2. Case 1 and 3 give the optimal conditions which have less switching actions and generate less losses and harmonics at low frequencies. Case 2 and 4 give the non-optimal condition.

Case 1, i.e. the result which gives optimal conditions is obtained with phase angle of 90 degrees. The number of switching actions are on a minimum, represented by the circles in figure 10, and the harmonics produced by the three phase ac voltage pulses, see figure 11, are of high frequencies which do not affect the system. In situation 1 the conduction losses varies with different phase angle between the carrier frequencies. The reason is that the squirrel cage motor is not an ideal voltage source, and therefore is affected by the harmonics produced by the voltage pulses in the input to the RMC. Case 2 produce low frequency harmonics, see figure 13, this affects the three-phase current generated by the motor. The current will be distorted and therefore not follow a sinusoidal path

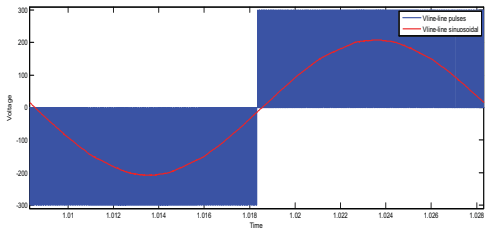

Fig. 17. Output from RMC - voltage line to line, pulses and the corresponding sinusoidal wave

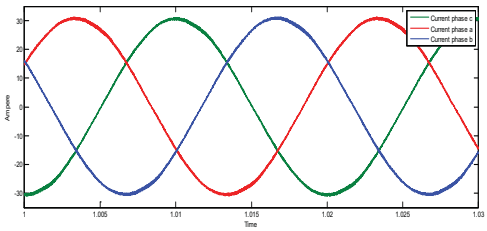

Fig. 18. Output from RMC - three phase current

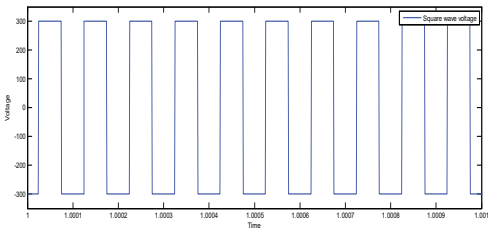

Fig. 19. Input to RMC - square wave voltage

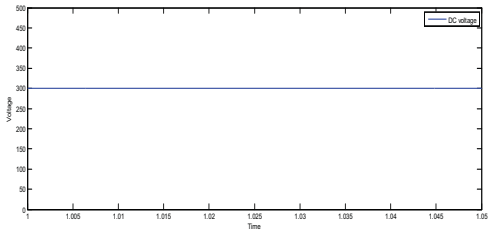

Fig. 20. Input to full-bridge - dc voltage

with constant amplitude. For that reason the rms-value of the current is higher than normal, and the conduction losses are increased. In figure 12 the circles represent the number of switching actions for case 2. The number of switching actions, and thus the switching losses, are on a maximum when the phase angle is 0 degrees. The total losses generated for each case in the reduced matrix converter can be seen in figure 16, where column one represent case 1, and column 2 represent case 2.

In situation 2 case 3 gives the optimal condition when the carrier frequencies for the RMC and the F-B are different. Figure 14 shows the switching actions for phase angle of 45 degrees. However, in case 3 there are more result which gives the same amount of losses, these are all phase angles of $45 \cdot n$ where $n = 0, 1, 2, 3...$, and the losses generated in the RMC is shown in column 3, figure 16. Case 4 gives the worst condition which is given for phase angles of $90 \cdot n$ where $n = 0, 1, 2, 3....$ The loss generation in the RMC is given in column 4, figure 16, and the switching actions are depicted in figure 15.

V. Simulation Results

The simulation results for the voltages and currents are obtained for the system operating with optimal conditions. I.e. when the carrier frequencies of both the RMC and the full-bridge are the same (10 kHz), the phase angle between the carriers is $\frac{\pi}{2}$, the modulation amplitude ratio is equal to 0.866, and the frequency of the reference signal is 50 Hz. Figure 17 to 20 shows the result.

VI. Conclusion

In this paper the reduced matrix converter implemented in an offshore wind power conversion system is studied. The RMC consist of 6 bi-directional switches, where each switch is made up of 2 RB-IGBTs in antiparallel. The RB-IGBT has a special structure, which contributes to reduce the total losses. The reason is the natural soft switching feature of the device, which occurs when the RB-IGBT is reverse biased either before turn on or after turn off. The intrinsic diode portion of the device will then withstand the blocking voltage, and all the negative collector emitter voltage will be across the intrinsic diode. By the switching action the generation of losses is in the intrinsic diode, and the loss will be reverse recovery loss.

The loss model has been implemented in PSIM, and impacts on the losses generated in the switches of the reduced matrix converter were investigated for two different situations; one with carrier frequency of both converters equal to 10 kHz, the other with two different carrier frequencies, respectively 10 kHz for the RMC and 5 kHz for the full-bridge. In both situations the phase angle between the carriers was varied in order to find the optimal condition for the system with lowest losses and the non-optimal condition with highest losses. The optimal condition found for each situation gave the same amount of losses, but the result were obtained for different phase angles in the two situations. In situation 1 the optimal condition was obtained for phase angle of 90 degrees, while in situation 2 the best result were given for all phase angles equal to $45 \cdot n$ where $n = 0, 1, 2, 3...$

In situation 1 the result was special beacuse it was observed that changing the phase angle gave impacts on the conduction losses. Since there are always three switches turned on in the reduced matrix converter, the conduction losses should be constant and unaffected of the change of the phase angle. However, the reason was that the squirrel cage machine which is

not an ideal voltage source, was sensitive for the low frequency harmonics produced by the three phase voltage pulses in the input of the RMC. The three-phase current from the machine was by that reason distorted, and did not follow a sinusoidal path with constant amplitude, but rather a curve which resulted in a higher rms-value of the current. Thus, the conduction losses were increased. Additionally, the switching losses were also increased due to increased number of switching actions. The non-optimal condition for situation 2 were given for phase angles equal to $90 \cdot n$, where $n = 0, 1, 2, 3...$

The next step of this research is the extraction of losses characteristics of one leg of the reduced matrix converter by measurements with the modulation.

REFERENCES

[1] M.R. Patel, "Wind and Solar Power Systems; Design, Analysis and Operation", second edition, Taylor & Francis Group.

[2] N. Negra, J. Todorovic, T. Ackermann, "Loss evaluation of hvac and hvdc transmission for large offshore wind farms", *ELSEVIER Electric Power System Research*, Science Direct, no. 76, pp. 916927, 2005.

[3] A.B. Mogstad, M.Molinas, "Power Collection and Integration on the Electrical Grid from Offshore Wind Parks", *NORPIE/2008, Nordic Workshop on Power and Industrial Electronics*, June 9-11, 2008.

[4] A. Odaka, J. Itoh, I. Sato, H. Ohguchi, H. Kodachi, N. Eguchi, H. Umida, "Analysis of loss and junction temperature in power semiconductors of the matrix converter using simple simulation methods", *Industry Applications Conference*, 2004. 39th IAS Annual Meeting. Conference Record of the 2004 IEEE Volume 2, 2004 Pages:850 - 855 vol.2.

[5] P.J. Grbovic, F. Gruson, N. Idir, P. Le Moigne, "Turn-on Performance of Reverse Blocking IGBT (RB-IGBT) and Optimization Using Advance Gate Driver", *Power Electronics*, IEEE Transactions on : Accepted for future publication Volume PP, Forthcoming, 2009 Pages:1 - 1.

[6] M. Vellvehi, J.L. Galvez, X. Perpiña, X. Jordà, P. Godignon, J. Millán, "Trench isolation technique for Reverse Blocking IGBT using Boron Nitride doping wafers", *Power Electronics and Applications*, 2009. EPE '09. 13th European Conference on 8-10 Sept. 2009 Pages:1 - 5.

[7] A. Garces and M. Molinas "Electrical conversion system for offshore wind turbines based on high frequency ac link", *IX International Conference and Exhibition of Renewal Energy and Ecological Vehicles EVER2009*, March 2009.

[8] A. Garces and M. Molinas "Cluster interconnection of offshore wind farms using a direct high frequency link on Large-Scale Integration of Wind Power into Power Systems as well as on Transmission", *Networks for Offshore Wind Farms*, October 2009.

[9] A. Garces and M. Molinas "Investigation and losses comparison of a reduced matrix converter for off-shore turbines", *5th IET International Conference on Power Electronics, Machines and Drives, PEMD*, April 2010.

Characterization of a Reduced Matrix Converter for Offshore Wind Power

Mari Røed Hanssen, Alejandro Garces Ruiz, Marta Molinas
Department of Electrical Engineering
NTNU
Trondheim, Norway
Email: mariroed@stud.ntnu.no

***Abstract*—The reduced matrix converter (RMC) implemented in an offshore wind power conversion system is investigated in this paper. The RMC built with 6 bi-directional switches, is thoroughly investigated to characterize the losses under different conditions. Each bi-directional switch is made up by two RB-IGBTs in antiparallel, and the impact of the special structure of the RB-IGBT on the total losses is studied. The offshore wind power conversion system is modeled in PSIM with the RMC as the first conversion stage after the wind turbine. Thereafter a high frequency square wave voltage is fed into a transformer. Due to the high frequency, the transformer will have reduced weight, which is an important aspect of the lightweight and compact component requirements for offshore wind turbine installations. After the transformer the second conversion stage is carried out. This is done by a full-bridge converter where the output is dc voltage, for enabling series connection of wind turbines in dc, with HVDC transmission to shore. The study is aimed at the achievement of an energy efficient converter, with high power density and reliability.**

I. Introduction

The oceans cover approximately two thirds of the earth surface, and will be a great resource for generating energy from renewable sources in the future. The wind conditions in the open ocean is better than on land because the wind velocity is 30 to 40 % higher, and the wind is also more steady and less turbulent [1]. However, challenges in offshore wind power are more severe than in onshore wind power, which is reflected in the high increment of the costs. Operation and maintenance of the wind park is one of the issues that contribute to the high costs [2], where the maintenance is constricted by the accessibility to the offshore wind parks; because while the accessibility to onshore wind farms are assumed to be close to 100 %, some offshore wind parks has experienced an accessibility below 70 % [3] because of the harsh weather conditions. During winter time when the wind is strong and the turbines can deliver the highest amount of electricity, the accessibility has an even greater impact on the costs, due to lost revenue if the turbines suffer from downtime.

In this paper it will be focused on one of the solutions to improve the maintenance conditions of offshore wind farms, i.e. by increasing the reliability of the components. The development of the direct drive concept with permanent magnet generator is one step in the right direction. Since the PM generator can rotate with the same speed as the wind speed, the gearbox is redundant in the system [4]. This is an advantage because the gearbox has a high failure rate and is considered as one of the most crucial components of the wind turbine [5]. Siemens and Vestas, the two largest manufacturers of offshore wind turbine already offer this concept to their customers.

To follow the tendency of the market, the direct drive concept is implemented in the wind energy conversion system discussed in this paper, see figure 1 c). The system in a) represent the conventional WECS today [6], and b) represent the WECS discussed in [7] which was first presented in [8]. The solution in b) and c) has improvements compared to the solution in a) since the reduced matrix converter perform direct ac-ac conversion which makes it possible to omit one of the less reliable components of the power electronics part [10]; the bulky DC link capacitor which is needed in the back to back converter. In addition, the high frequency voltage in the output of the RMC decreases the size of the transformer compared to a) where the step-up transformer is designed for low frequencies [9]. The result in c) is a WECS which is more compact, lightweight and reliable than the systems of b) and c).

Power losses are an important issue when it comes to conversion of energy. In this paper the losses generated by the bi-directional switches of ac/ac converter will be investigated

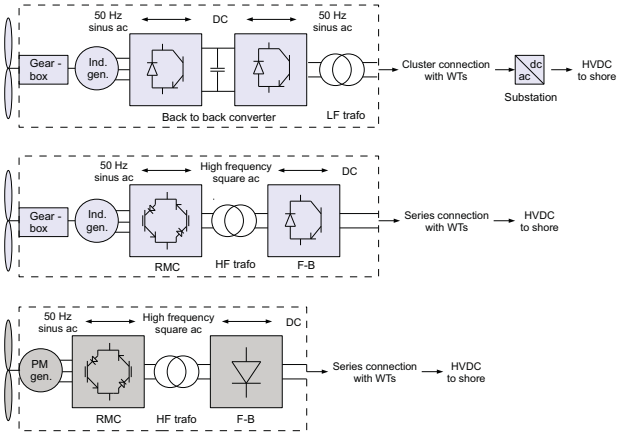

Fig. 1. The offshore wind power conversion system

by a simulation model in PSIM. There are several topologies for bi-directional switches, where two of them is depicted in figure 2(b) and (c) [11]. In this paper the newly developed bidirectional switch with two reverse blocking IGBTs (RB-IGBT) connected in antiparallel will be investigated. In [12] it is shown how changing the design of the bi-directional switch from the conventional with two IGBTs with antiparalleled diodes to the new one with two RB-IGBTs in antiparallel can reduce the total losses.

II. The converter topology

The reduced matrix converter discussed in this paper is a direct ac-ac converter with 3-phase low frequency sinusoidal wave as input and 1-phase high frequency square wave as output, see figure 2(a). The RMC consist of six bi-directional switches which are controlled by a modified version of standard pulse width modulation (PWM) [8]. The PWM can either be carrier based or space vector modulation. In order to protect the converter against overvoltages and overcurrents a clamp circuit is connected between the input and the output of the RMC.

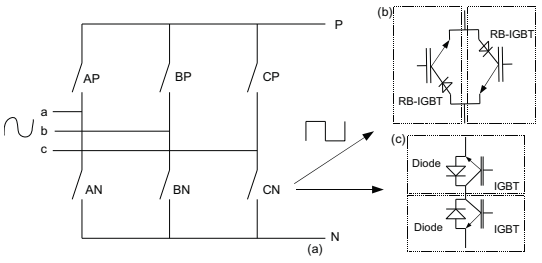

Fig. 2. (a) Reduced matrix converter with bi-directional switches, either as in (b) or as in (c)

A. Bidirectional switches

The bidirectional switches are different from the standard IGBTs with freewheeling diodes because they are able to block voltages of both polarities and allow current in both directions. This special attribute of the bi-directional switch is necessary when both the output and the input of the converter is ac. The RB-IGBT used in a bi-directional switch has a structure similar to another version of the IGBT, the non-punch-through IGBT (NPT-IGBT) [13]. The NPT-IGBT can also sustain blocking voltages of both polarities, but it has a high leakage current in reverse bias which is generated due to the severe roughness remaining after the mechanical dicing process. To prevent this leakage current, the RB-IGBT has an extra isolation layer made by extending the bottom p^+-region to include the vertical dicing sides of the device. The p^+-isolation region together with the n^--drift region constitute what can best be characterized as an intrinsic diode of the device [14]. The vertical cross section of the structure of one of the half cells of a RB-IGBT is depicted in figure 3(a). This design of a RB-IGBT is named isolation type, and is the one which are open for commercial use [15].

In an equivalent circuit of the RB-IGBT, the intrinsic diode can be extracted from the model. It will then appear in series connection with the IGBT portion of the transistor, and together with the diode drawn with a dashed line the intrinsic diode also constitutes the bipolar junction transistor portion of the device, see figure 3(b). Even if the intrinsic diode appears as an external part to the rest of the model, it is important to remember that the diode "does not exist physically in the switch module" [14].

The operation of the intrinsic diode in the RB-IGBT demonstrates that the diode does not operate as a conventional, external diode. The intrinsic diode is dependent on the off and on-state of the RB-IGBT: even if the diode is forward biased it cannot conduct when the RB-IGBT is turned off, and when the diode is reverse biased it does not have to be forward biased to start to conduct; it is enough that the RB-IGBT is switched on, so that the voltage across the element goes to zero.

B. Clamp circuit

Like the matrix converter [16], the RMC needs to have a protection scheme to avoid destruction of the semiconductor devices when there is a fault or operation mode that causes overvoltage or overcurrent. This is because none of the converters provide a freewheeling path, such as the diodes of the three-phase voltage source converter do when the IGBTs are turned off in an emergency shutdown. Since both the MC and the RMC are made up of bi-directional switches and are direct ac-ac converters, the same strategy of protection can be used.

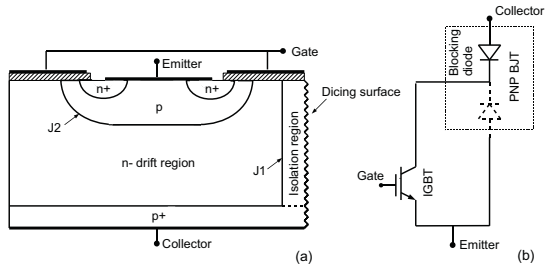

Fig. 3. (a) Vertical cross section of the structure of a half cell, and (b) equivalent circuit of the RB-IGBT

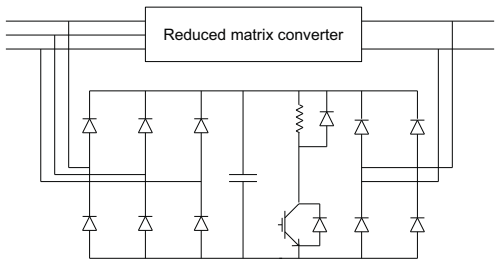

Fig. 4. Clamp circuit connected to output and input of RMC

There are already various topologies of protection schemes that have been proposed for the matrix converter the last years. Among these can be mentioned power zener diodes [17] and varistors [18], however they are only designed for low power devices.

The solution which suits the RMC best is the clamp circuit presented in [19]-[21] and depicted in figure 4. It is developed for high power applications, and can provide freewheeling path in emergency shutdown of the switches and protection against $L_{leakage}\frac{di}{dt}$ in the transformer. The clamp is connected to the input and output by two rectifier bridges consisting of in total 10 diodes. In [23] a version of the clamp is suggested where 6 diodes are replaced by the series diodes of the bi-directional switch in figure 2 c). However, since the RMC proposed in this paper is built up by bi-directional switches with RB-IGBTs, this scheme is inconvenient.

In addition to the two rectifier bridges, the clamp circuit consists of a capacitor and a braking chopper with IGBT and resistor. When the voltage in the input or output of the RMC is higher than V_{clamp}, the clamp circuit is activated and the capacitor will protect the converter by absorbing the excess energy. In the moment the capacitor exceeds a specified voltage level, the IGBT is turned on so that the resistor discharge the capacitor until it has decreased to its original voltage level and the IGBT turns off. The dissipative resistor is of great importance in the circuit, because the clamp circuit operates not only during faults, but also in stationary state. This is because the leakage inductance in the transformer causes overvoltage in the output of the RMC every time a switch is turned off. According to [24] the clamp circuit with dissipative resistor is 10-100 times more compact than the one with only a capacitor.

III. Operation of the reduced matrix converter

The reduced matrix converter can be operated either as a current source converter or voltage source converter. Due to the results from [22] where it is proved that voltage source operation of the converter generates lowest losses, it is decided to concentrate on that operation mode. In the wind energy conversion system, the task of the RMC is to modulate the frequency and amplitude of the input voltage in such a way that the current in the generator fits the requirements of the torque. In the output of the RMC modulate the voltage so that it is a square wave voltage with high frequency, which is fed into the transformer and then further to the full-bridge rectifier.

A. Carrier based modulation

The carrier based pulse width modulation of the RMC is performed in a similar way as explained in [7]; a high frequency triangular carrier signal is compared with a low frequency sinusoidal reference signal, and the reference signal is inverted for the negative periods of the square-wave ouput, i.e. when the carrier of the square wave is negative [8]. However, two modifications is performed and will be described further. The first one is that now the full-bridge converter only consists of diodes. They are non-controllable semi-conductors,

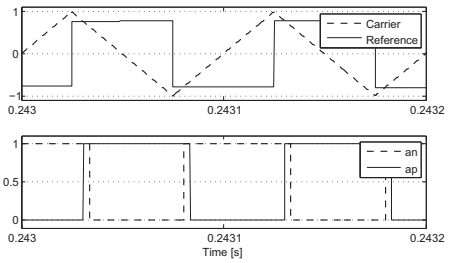

Fig. 5. Overlapping of the switches of one leg

which means that it is not possible to modulate the square wave voltage through this converter anymore. The solution has been to implement the modulation of the square wave signal in the PWM of the RMC. Then it will be possible to modulate the frequency of both the square wave and the sinusoidal voltage with the PWM of the RMC.

The second modification is made regarding the switching characteristic of the RB-IGBTs, which are no longer assumed to be ideal devices. The consequence will be that the switches in one leg will not switch on and off perfectly synchronous. This means that during a short time period it is possible that both the negative and the positive switch in one leg are open or closed simultaneously. There are several ways to avoid the problems this could cause, and the solution depends on whether the output side of the converter is mainly inductive or capacitive. The standard method is to implement a deadtime period where both switches are open simultaneously. However, this gives only good results when the output circuit is mainly capacitive, like in a conventional voltage source inverter where it is important to avoid a short-circuit of the DC-link capacitor.

In the proposed system a transformer is connected to the output side of the reduced matrix converter, and the output circuit is mainly inductive. It is therefore not recommended to have any sudden interruptions of the current through it, which could cause dangerous over-voltage. This will occur when the transformer is open-circuited and both switches of one leg are open simultaneously. Therefore is overlapping of the switches introduced as a solution; for every time the phase current change between the positive and negative switch, the gate signal which turns off the outgoing switch is delayed compared with the gate signal which turns on the incoming switch, so that both switches are closed and lead a current in a short time period. This will lead to a short circuit of the transformer, which is a harmless operation mode. In figure 5 the turn on and turn off of the positive and negative switch of leg a is depicted.

B. Space vector modulation

The space vector modulation of the RMC is performed as in [22] except that here the two modifications explained above in the section about CBM are taken into account; the modulation of both the sinusoidal input and the square wave output is implemented in the SVM of the RMC, as well as the

overlapping of the switches. The rotating vector V_s in equation (1), where V_a, V_b and V_c are the sinusoidal phase voltages of the input, is to be achieved by using the active vectors and zero vectors given in (2) and (3). Due to the transformer in the converter output, the system allows operation where both converter sides are short circuited. There are therefore 6 more zero vectors than usual.

$$\vec{V}_s = \frac{2}{3}\left(V_a + V_b \cdot e^{j2\pi/3} + V_c \cdot e^{-j2\pi/3}\right) \tag{1}$$

$$A_s = \{(ap, bn, cn), (ap, bp, cn), (an, bp, cn), (an, bp, cp), (an, bn, cp), (ap, bn, cp)\} \tag{2}$$

$$Z_s = \{(ap, bp, cp), (an, bn, cn), (ap, an, bp, cn), (ap, an, bn, cn), (ap, bp, cn, cp), (an, bp, bn, cp), (ap, bp, cp, cn), (an, bn, cp, cn)\} \tag{3}$$

The method to achieve the required V_s is similar to that of the conventional voltage source inverter (VSI), but it has to be considered that while the conventional VSI has a constant DC output, the RMC has a DC output which changes in polarity. Figure 6 depicts the situation of V_s, drawn with continuous line when it is in sector 0 and has the adjacent active vectors $\vec{V}_{pnn}$ and $\vec{V}_{ppn}$. These active vectors together with the zero vectors would be enough to generate the reference for V_s in a VSR, but for the RMC it will only contribute to the positive half of the square wave output. In order to generate the negative half of the square wave, sector 3 in the opposite side of the circle has to be used. V_s drawn with stippled line will however generate the same reference point for the sinusoidal input as the V_s drawn with a continuous line.

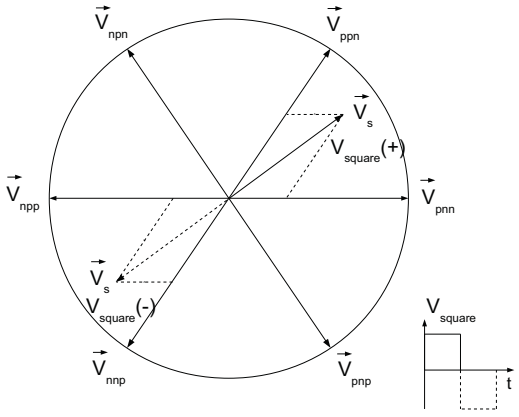

Fig. 6. Space vector modulation

C. Modulation characteristics

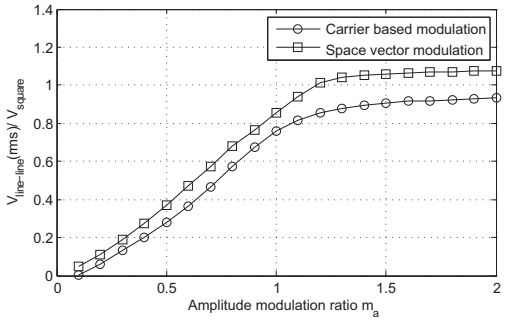

Fig. 7. Modulation characteristic

IV. Losses in the RMC

The losses in the RMC are generated due to the operation of the RB-IGBTs and can be divided into two categories: the conduction losses and the switching losses. While the switching losses in a conventional IGBT are generated due to the hard switching of the device, the RB-IGBT can either have a hard or soft switching transient.

The hard switching occurs when the RB-IGBT operates as an IGBT, i.e. that the device is forward biased before switching it on or after switching it off. When the RB-IGBT is forward biased the voltage will be blocked by junction 2 (J2), see figure 3(a). The RB-IGBT operates like a conventional IGBT, and all the collector emitter voltage will be across the IGBT portion of the RB-IGBT, as depicted in figure 8. The intrinsic diode has no special function in this case, since a conventional IGBT can withstand high positive voltages. Switching under this condition generates either turn on or turn off losses in the IGBT portion of the RB-IGBT.

The natural soft switching feature of the RB-IGBT is a special attribute of the device. The soft switching occurs when the RB-IGBT is reverse biased and junction 1 (J1) in figure 3(a), i.e. the intrinsic diode, blocks the voltage. The result is zero voltage across the IGBT portion of the RB-IGBT, because the intrinsic diode withstands all the negative collector emitter voltage alone, as depicted in figure 8(b). When the RB-IGBT is turned on, the voltage across the IGBT portion is constant zero, while the voltage transient of the intrinsic diode change from V_{ce} to zero in a finite time. This generates what is called reverse recovery losses in the intrinsic diode portion of the

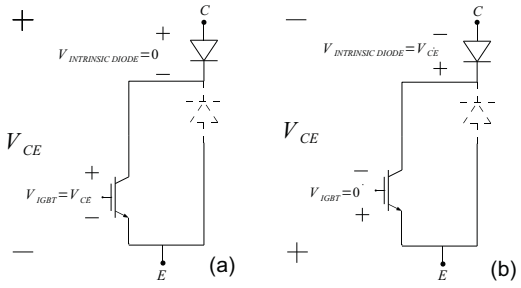

Fig. 8. (a) RB-IGBT is forward biased, (b) RB-IGBT is reverse biased

RB-IGBT. In a conventional diode the reverse recovery losses is connected to the turn off period of the device, but for the intrinsic diode these losses are generated both by turn on and turn off.

In [12] simulation methods to calculate losses for a RB-IGBT (600V/200A) have been suggested. In the loss characteristics reported, it has been measured that reverse recovery losses of the intrinsic diode are lower than turn on and turn off losses of the IGBT portion of the device.

A. Loss model for the reduced matrix converter

To calculate the losses in the reduced matrix converter in PSIM it is necessary with four different measurements for each bidirectional switch in order to decide which category the losses belong to. These categories are conduction losses, reverse recovery losses of the intrinsic diode portion and turn on or turn off losses of the IGBT portion in the RB-IGBT.

Two of the four aforementioned measurements needed for each switch are the voltage between collector and emitter, and the current in the collector in the instance *t*. These values are calculated with the RMC model in PSIM, and the information is then sent to a Dynamic Link Library (DLL) file. Since PSIM sends the information to the DLL-file for each time step *dt* it takes, it is already stored information of the two other measurements needed: the voltage and current from the time step precedent to *t*, i.e. *t-dt*. Thereafter, the code in the DLL-file classifies loss category by comparing the measurements from *t-dt* and *t*. It can then calculate the losses and store them for the next time steps in such a way that the total losses within each category can be summarized in the end.

The calculations in the DLL-file are based on the equations from [12], which is characterized for a RB-IGBT (600V/200A). Conduction losses are calculated as for a conventional IGBT, with the equation for power dissipation.

$$P_{cond} = V_{ce} \cdot I_c \tag{4}$$

V_{ce}: voltage between collector and emitter, I_c: collector current

Where V_{ce} is calculated as follows:

$$V_{ce} = A + B \cdot I_c + C \cdot I_c^2 \tag{5}$$

Where $A = 22.789, B = 28.536, C = -32.091$ are extracted from [12]

The turn on, turn off and reverse recovery energy losses are calculated with equation (6), and are as well as the conduction losses a function of the voltage across the transistor and the current flowing through it.

$$E = k_1 \cdot I_c^2 + k_2 \cdot I_c \tag{6}$$

E: energy loss in MJ, k_1 and k_2: constants characterized for each loss category.

In [12] k_1 and k_2 is defined for each category as follows:

Turn on loss:

$$k_1 = (8.14 \times 10^{-12}) \cdot V_{ce}^2 + (1.78 \times 10^{-7}) \cdot V_{ce} \tag{7}$$

$$k_2 = (2.78 \times 10^{-7}) \cdot V_{ce}^2 + (1.32 \times 10^{-5}) \cdot V_{ce} \tag{8}$$

Turn off loss:

$$k_1 = (4.77 \times 10^{-8}) \cdot V_{ce} + (4.92 \times 10^{-5}) \tag{9}$$

$$k_2 = (-2.98 \times 10^{-9}) \cdot V_{ce}^2 + (2.11 \times 10^{-4}) \cdot V_{ce} \tag{10}$$

Reverse recovery loss:

$$k_1 = (-5.66 \times 10^{-11}) \cdot V_{ce}^2 + (-1.82 \times 10^{-7}) \cdot V_{ce} \tag{11}$$

$$k_2 = (3.73 \times 10^{-9}) \cdot V_{ce}^2 + (9.35 \times 10^{-5}) \cdot V_{ce} \tag{12}$$

B. Impact of modulation technique

As the results in [7] demonstrated, the losses in the RMC will vary when there is a change in the parameters of the modulation technique. It showed that it is important to keep the number of switching actions at a minimum while avoiding a decrease in the quality of the voltage and current waveform.

This study explore more thoroughly the switching conditions of carrier based modulation and it also include a loss study of the more complicated modulation technique, space vector modulation described in part III-B, to compare and see if there are differences in the loss generation. The loss model of [12] is used to calculated the losses in PSIM.

1) Carrier based modulation: For the carrier based modulation there are two parameters which are varied. The first one is the carrier frequency of the square wave, where there is decided to look at 4 different cases, respectively with frequency 10kHz, 5kHz, 2.5kHz and 1kHz. For all 4 cases the carrier frequency of the sinusoidal wave is kept at 10 kHz. The second parameter to be varied is the displacement angle between the carrier of the square wave and the carrier of the sinusoidal wave. It is important to notice that for each case the carrier of the square wave is displaced with an angle increasing from 0 to 180 degrees while the carrier of the sinusoidal wave is the reference. As explained in part III-A the waveform of reference signal of the sinusoidal wave is dependent of the carrier of the square wave in such a way that it is inverted for every time the carrier of the square wave is lower than zero. Thus by a displacement of the carrier of the square wave or a change in its frequency, the reference signal will be modified accordingly. The results of the total losses are depicted in figure 9-12.

As there can be seen from the figures there is a relation between the ratio of the two carrier frequencies and the number of times the curve is repeated along the x-axis. The case where the carrier frequency of the square wave is 5 kHz is chosen as an example. 10 kHz divided by 5 kHz is 2, which is also the number of times the curve is repeated along the x-axis. The same relation yields for the three other cases, where the ratio is 1 for frequency 10 kHz, 4 for frequency 2.5 kHz and 10 for frequency 1 kHz, and the curve is repeated accordingly. This pattern can be explained by returning to the case where the carrier frequency of the square wave is 5 kHz which gives a ratio of 2. Figure 13 depicts the displacement of the reference signal in two situations which according to figure 11 gives the lowest losses for this case. In order to distinguish the situations from each other, the reference drawn in blue

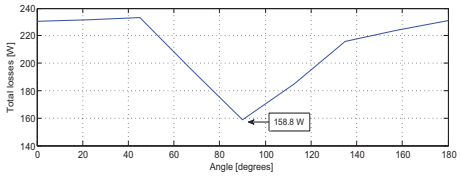

Fig. 9. Total losses as a function of phase displacement, frequency 10 kHz for CBM

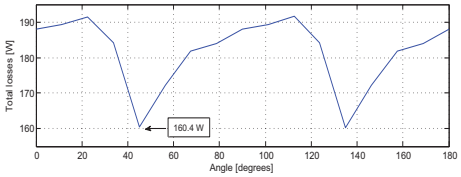

Fig. 10. Total losses as a function of phase displacement, frequency 5 kHz for CBM

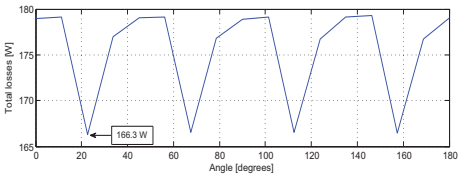

Fig. 11. Total losses as a function of phase displacement, frequency 2.5 kHz for CBM

has two different amplitudes, where the curve with the large amplitude represent the reference when the displacement angle is 45 degrees, and the curve with small amplitude represent the reference with displacement angle of 135 degrees. The red curve is the carrier signal of the sinusoidal wave. The figure shows that the positive periods of the reference signal with displacement angle of 45 degrees cross the carrier signal in the same points as the negative periods of the reference signal with displacement angle of 135 degrees, and the negative periods of the reference signal with displacement angle of 45 degrees cross the carrier signal in the same points as the positive periods of the reference signal with displacement angle of 135 degrees. The two situations has therefore exactly the same amount of switching losses which indicates that for every 90 degrees of an arbitrary displacement angle, the losses will be equal, and thus the curve is repeated.

The optimal condition which produces fewer losses is the case where both carrier frequencies are the same, i.e. 10 kHz, and the displacement angle is 90 degrees.

2) Space vector modulation: The SVM has limitations regarding the operational parameters which make it difficult to perform a similar study of the impacts from the frequency and phase displacement as CBM provide. With the modulation method explained in III-B the square wave frequency will always be half of the switching frequency of the sinusoidal wave. Simulations is performed to find the relation between the

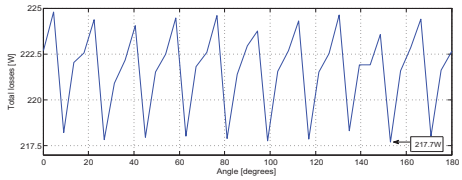

Fig. 12. Total losses as a function of phase displacement, frequency 1 kHz for CBM

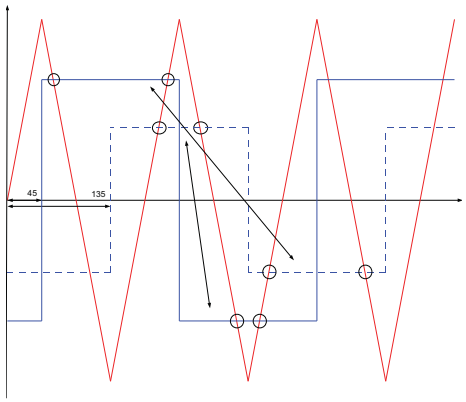

Fig. 13. Reference displaced with angles of 45 and 135 degrees for CBM

switching frequency and the total losses, the result is showed in figure. As depicted, the total losses decrease approximately linearly from 10 kHz and until the switching frequency reaches 2 kHz, then the losses suddenly increase again. The reason is that the phase currents are highly distorted, and this is reflected in the rms value of the current; the rms value increase from 15 A for switching frequency 10 kHz to 33 A for frequency of 1 kHz. The effect of this is higher conduction losses. Actually the conduction losses increase gradually from 10 kHz to 2 kHz, however since the switching losses decrease with a higher rate, the total losses decrease.

Even if the case where the switching frequency is 10 kHz generates higher losses than other frequencies, it is decided to use this for further comparisons with the optimal case from carrier based modulation since high switching frequencies lead to fewer harmonic.

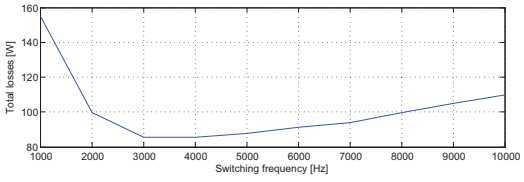

Fig. 14. Total losses as a function of switching frequency for SVM

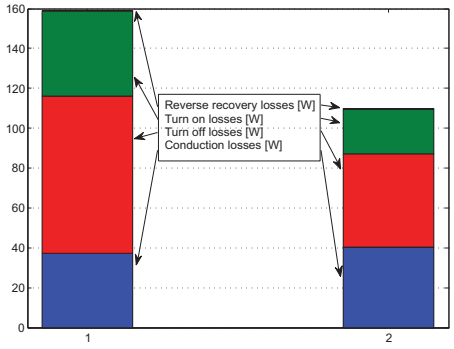

Fig. 15. Loss distribution for 1) CBM and 2) SVM

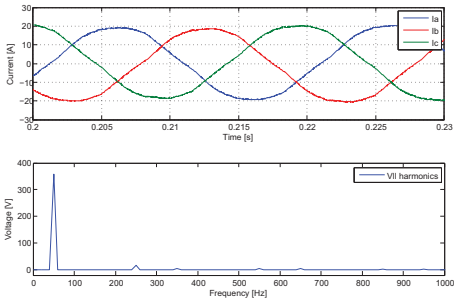

Fig. 16. CBM phase currents and $V_{linetoline}$ harmonics

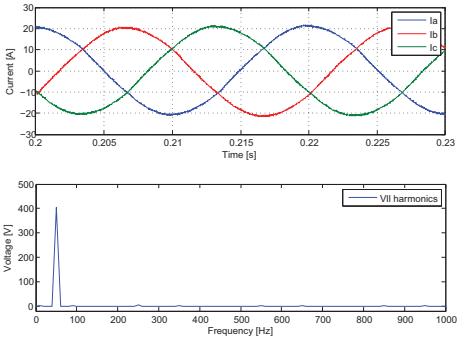

Fig. 17. SVM phase currents and $V_{linetoline}$ harmonics

V. Discussion

The bars of figure 15 shows the distribution of losses in 1) Carrier based modulation and 2) Space vector modulation with switching frequencies 10 kHz. Both modulation techniques give almost the same amount of conduction losses; however the switching losses appear to be quite different. The turn on and turn off losses of CBM are nearly doubled compared to SVM, while the reverse recovery losses in both situations are close to zero. The low switching losses of SVM can be explained with the fact that the transition between the switching states is more efficient and require less switching

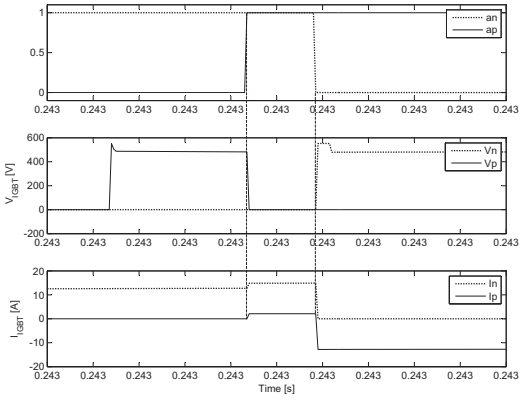

Fig. 18. Voltage and current waveform in switching

actions than CBM, both because there are more zero vectors available and also because it is easier to control which zero vector will be utilized.

Another remarkable point with the distribution of the switching losses is that compared to the results obtained with CBM in [7] the reverse recovery losses are close to absent, while the turn off losses have increased drastically. The reasons for this are 1) due to the modifications in the modulation where overlapping of the switches is introduced as a method to avoid open-circuit of the transformer, and 2) due to the $L_{leakage}\frac{di}{dt}$ of the transformer which appears every time a switch is turned off. Figure 18 depicts the voltage and current waveform when CBM is used to modulate the switches.

When the positive switch turns on, the voltage across it decreases to zero. The current through the switch is at the same time only increasing slightly to contribute to the short circuit current in the leg due to the overlapping of the switches, and will thus not immediately start to lead the phase current. Therefore, instead of calculating the switching loss with the negative directed phase current through the switch, it will be calculated with the short circuit current which is both smaller and in the opposite direction of the phase current. This is the reason why there is a turn on loss instead of a reverse recovery loss, since a switch which has a positive applied voltage in the instant before it is turned on and starts to lead a positive directed current generates turn on losses. However, without the overlapping the switch would have started to lead a negative directed current, and that would have generated reverse recovery losses. Due to the short circuit current the reverse recovery losses are decreased to almost zero compared with the result in [7], and the turn on losses are lower than they normally would be since the short circuit current is much lower than the phase current. The instant before the negative switch turns off, the switch leads both the positive directed phase current and the short-circuit current. This, in addition to the overvoltage which appears due to the turn off of the switch result in an increase in the turn off losses compared to an ideal situation where both overlapping of the switches and

leakage inductance in the transformer could be omitted.

REFERENCES

[1] M.R. Patel, "Wind and Solar Power Systems; Design, Analysis and Operation", second edition, Taylor & Francis Group.

[2] F. Besnard, M. Patriksson, A.Wojciechowski, A.-B. Strömberg, and L. Bertling, "An Optimization Framework for Opportunistic Maintenance of Offshore Wind Power System", *Proc. IEEE Power Tech Conf., Bucharest, Romania* , 2009.

[3] S. Vestgaard, "Offshore Technology/Operation and Maintenance accessibility", *Proc. Copenhagen Offshore Wind 05*, 2005.

[4] H. Li, Z. Chen and H. Polinder, "Optimization of Multibrid Permanent-Magnet Wind Generator Systems", *IEEE Transaction on Energy Conversion*, vol. 24, no. 1, pp. 82-92, 2009.

[5] W. Musial, S. Butterfield and B. McNiff, "Improving wind turbine gearbox reliability", *European Wind Energy Conference, Milan, Italy*, 2007.

[6] Z. Chen, J. M. Guerrero and F. Blaabjerg, "A Review of the State of the Art of Power Electronics for Wind Turbines", *IEEE Transaction on Power Electronics*, vol. 24, no. 8, pp. 1859-1875, 2009.

[7] M.R. Hanssen, A. Garces and M. Molinas, "Operation Features of a Reduced Matrix Converter for Offshore Wind Power", *2010 IEEE International Symposium on Industrial Electronics (ISIE)*, July 2010.

[8] A.B. Mogstad, M.Molinas, "Power Collection and Integration on the Electrical Grid from Offshore Wind Parks", *NORPIE/2008, Nordic Workshop on Power and Industrial Electronics*, June 9-11, 2008.

[9] J. C. Fothergill, P. W. Devine and P. W. Lefley, "A Novel Prototype Design for a Transformer for High Voltage, High Frequency, High Power Use", *IEEE Transactions on Power Delivery*, vol. 16, no. 1, pp. 89-98, 2001.

[10] C. Rodriguez and G.A.J Amaratunga, "Long-Lifetime Power Inverter for Photovoltaic AC Modules", *IEEE Transactions on Power Electronics*, vol. 55, no. 7, pp. 2593-2601 2008.

[11] C. Klumpner and F. Blaabjerg, "Using Reverse-Blocking IGBTs in Power Converters for Adjustable-Speed Drives", *IEEE Transactions on Industry Applications*, vol. 42, no. 3, pp. 807-816, 2006.

[12] A. Odaka, J. Itoh, I. Sato, H. Ohguchi, H. Kodachi, N. Eguchi, H. Umida, "Analysis of loss and junction temperature in power semiconductors of the matrix converter using simple simulation methods", *Industry Applications Conference, 2004. 39th IAS Annual Meeting*, Conference Record of the 2004 IEEE vol. 2, pp. 850 - 855.

[13] M. Takei, T. Naito and K. Ueno, "Reverse blocking IGBT for matrix converter with ultra-thin wafer technology", *IEE Proceedings - Circuits, Devices and Systems*, vol. 151, no.3, pp. 243-247, 2004.

[14] P.J. Grbovic, F. Gruson, N. Idir, P. Le Moigne, "Turn-on Performance of Reverse Blocking IGBT (RB-IGBT) and Optimization Using Advance Gate Driver", *IEEE Transactions on Power Electronics*, vol. 25, no.4, pp. 970-980, April 2010.

[15] M. Vellvehi, J.L. Galvez, X. Perpiña, X. Jordà, P. Godignon, J. Millán, "Trench isolation technique for Reverse Blocking IGBT using Boron Nitride doping wafers", *Power Electronics and Applications, 2009. EPE '09. 13th European Conference*, pp. 1 - 5, September 2009.

[16] P.W. Wheeler, J. Rodriguez, J.C. Clare, L. Empringham and A. Weinstein, "Matrix converters: a technology review ", *IEEE Transactions on Industrial Electronics*, vol. 3, pp. 1936-1941, 2000.

[17] K. You and F. Rahman, "Over-voltage protection using power Zener diode for matrix converter and matrix-Z-source converter", *International Conference on Power Electronics and Drive Systems, PEDS*, 2009.

[18] J. Mahlein, M. Bruckmann and M. Braun, "Passive protection strategy for a drive system with a matrix converter and an induction machine", *IEEE Transactions on Power Electronics*, vol. 49, no. 2, pp. 297-303, 2002.

[19] A. Garces and M. Molinas, "High frequency wind energy conversion from the ocean", *2010 International Power Electronics Conference (IPEC)*, 2010.

[20] S. J. Itoh, A.I. Odaka, H. Ohguchi, H. Kodachi and N. Eguchi, "A novel approach to practical matrix converter motor drive system with reverse blocking IGBT ", *IEEE Transactions on Power Electronics*, vol. 20, no. 6, pp. 1256 - 1363, 2005.

[21] J. Andreu, J.M. De Diego, I.M. de Alegria, I. Kortabarria, J.L. Martin and S. Ceballos, "New Protection Circuit for High-Speed Switching and Start-Up of a Practical Matrix Converter", *IEEE Transactions on Industrial Electronics*, vol. 55, no. 8, pp. 3100-3114, 2008.

[22] A. Garces and M. Molinas, "Impact of operation principle on the losses of a reduced matrix converter for offshore wind parks", *2010 IEEE International Symposium on Industrial Electronics (ISIE)*, 2010.

[23] P.Nielsen, F. Blaabjerg and J.K Pedersen, "New protection issues of a matrix converter: design considerations for adjustable-speed drives", *IEEE Transactions on Industry Applications*, vol. 35, no. 5, pp. 1150-1161, 1999.

[24] C. Klumpner and F. Blaabjerg, "Short term braking capability during power interruptions for integrated matrix converter-motor drives", *IEEE Transactions on Power Electronics*, vol. 19, no. 2, pp. 303-311, 2004.